Attenuation Models for Material Characterization

A Thesis
Presented to
The Academic Faculty

by

Johannes Maess

In Partial Fulfillment
of the Requirements for the Degree
Master of Science in
Engineering Science and Mechanics

School of Civil and Environmental Engineering
Georgia Institute of Technology
November 2004

Attenuation Models for Material Characterization

Approved:

Dr. Laurence J. Jacobs, Chairman

Dr. Jianmin Qu

Dr. Reginald DesRoches

Date Approved: October 22, 2004

Acknowledgements

I would like to thank Prof. Laurence J. Jacobs for all his advice and support I received from him during my year at Georgia Tech, and especially for his help concerning my research. It was always a lot of fun working together with him.

I would like to express my thanks to Prof. Jianmin Qu, who gave me helpful hints and developed ideas to support my research, and to Prof. Reginald DesRoches.

My special thanks go to Dr. Jin-Yeon Kim for being a great help in answering my questions concerning the detailed theory of this thesis.

I am very grateful to Prof. Lothar Gaul from the University of Stuttgart, who made my year at Georgia Tech possible. Furthermore I want to thank the DAAD (German Academic Exchange Service) for the financial support.

Furthermore, I want to extend my gratitude to my colleagues at the Lab for their support and the good time we had together.

Table of Contents

List of Tables

List of Figures

List of Symbols or Abbreviations

$\|\ \ \|$	magnitude
α	longitudinal wave number
$\alpha_{L,T}$	attenuation coefficient
β	transversal wave number
γ	scattering cross section
δ_{ij}	Kronecker delta
ϵ_{ij}	strain tensor
κ	bulk modulus
λ, μ	Lamé constants
ν	Poisson's ratio
ω	angular frequency
$\boldsymbol{\psi}$	displacement potential
ϕ	azimuthal angle
θ	polar angle
ρ	density
σ_{ji}	stress tensor
φ	displacement potential
a	radius of the scatterer
a_i,b_i	amplitude
A_i,B_i	scattering amplitudes
c_L	phase velocity of a longitudinal wave
c_T	phase velocity of a shear wave
C_{ijkl}, c_{ij}	stiffness tensor
$\mathbf{d}$	direction of particle motion
R	distance

E_d	energy density
E	Young's modulus
$\mathbf{f}$	body force
f	frequency
f_I	volume fraction of the inclusions
G,g_{im}	Green's function
h_n	spherical Hankel function of order n
i	imaginary unit
j_n	spherical Bessel function of order n
$\mathbf{p}$	direction of wave propagation
P_n	Legendre polynomial of order n
P^s	scattered power
p	pressure
$\mathbf{t}$	traction
$\mathbf{r}$	observation point
$\mathbf{r}'$	point on the scatterer
$\hat{\mathbf{r}}_I$	direction of the incident wave
t	time
$\mathbf{u}$	displacement
Re	real part of a complex number
Im	imaginary part of a complex number

Summary

Ultrasonic attenuation is a useful tool in characterizing the damage state of different materials. The attenuation coefficients for the incident longitudinal and transverse waves are both derived from the scattering cross section of the material. Scattering cross section is defined as the ratio of the scattered energy to the incident energy. The incident wave field can be scattered at inclusions, voids and material defects; there is also grain boundary scattering in polycrystalline materials. For accurate material characterization, it is important to distinguish between the different types of scattering and to relate the attenuation to its appropriate source. This study first solves the single scatterer problem using both the Born approximation (for complex scatterer shapes and for anisotropic scatterers), and an exact solution (in cases where it is necessary to provide an accurate description of the viscoelastic behavior of the surrounding effective medium). Multiple scattering effects are investigated by a differential self-consistent scheme and a self-consistent scheme. Both multiple scattering approaches are applicable for each single scatterer solution. The differential self-consistent scheme describes the scattering cross section dependent on the volume fraction of the scatterers, and is restricted to low volume fractions and materials, where the surrounding material is clearly distinguished from the inclusions. The self-consistent scheme is applicable to high volume fractions of inclusions as well as to polycrystalline materials, where the distinction between surrounding material and inclusions is not possible.

CHAPTER 1

Introduction

One goal of nondestructive evaluation (NDE) and testing (NDT) is to find a relationship between a property (or properties) of a propagating ultrasonic wave and the damage state of the material under consideration. Ultrasonic attenuation has proven to be one of these properties. By comparing measurements to a theoretical model, one can draw conclusions about the damage state of a candidate material component. Attenuation is a potential predictor of damage because the attenuation coefficient depends on material properties, such as its microstructure or the presence of material defects. The objective of the current study is to develop a theoretical model which can predict the attenuation coefficients of a given material based on the scattering properties of a propagating ultrasonic wave. Note that a description of flaw detection measurements and analysis can be found in Thompson [43].

Previous researchers have developed several approaches to relate the attenuation coefficient of an ultrasonic wave to the damage state of different types of materials. In general, the ultrasonic attenuation is caused by scattering effects which occur at material inhomogeneities. In this context, inhomogeneity means a mismatch in the impedance of the material along the propagation direction of the ultrasonic wave. This mismatch can be caused by voids or cracks in a damaged material, in composite materials by a change in the material properties between matrix and inclusions, and in polycrystalline materials by the changing orientation of the single grains. In the latter case, the impedance mismatch is due to the anisotropic elastic properties of the single (individual) crystals. The scattering at the boundaries between the single crystals is denoted as grain boundary scattering, and it is inherent in any polycrystalline

material. Single scattering refers to the situation in which only the attenuation generated by one single inhomogeneity is taken into account, multiple scattering denotes models which include scattering effects from many inhomogeneities, and in parts, interactions between the different scatterers. To describe the damage state accurately, a multiple scattering approach must be developed.

The single scatterer problem can be solved in several ways. The two approaches taken in this study are the Born approximation (see for example Gubernatis et al. [20]) and the exact solution, which was first developed by Einspruch et al. [12] for an incident longitudinal wave and a spherical fluid obstacle, by Ying et al. [52] for an incident longitudinal wave and an elastic obstacle, and by Einspruch et al. [13] for an incident transverse wave and an elastic obstacle. The advantage of the Born approximation is its simplicity, especially for the treatment of different scatterer shapes. The application of the Born approximation to scatterers of different sizes, shapes and orientations is shown in Section 3.1. On the other hand, the Born approximation has poor accuracy if the impedance mismatch is large, thus its application is limited to composite materials where the impedance difference between the matrix material and the inclusions is not significant, and to the grain boundary scattering in polycrystalline materials. The exact solution is used to describe the scattering due to voids and cracks, as well as for composite materials with strongly different material properties of the matrix and the inclusion. In Section 3.3, the exact solution is applied to spherical scatterers and the differences in the near- and far-field solutions are emphasized at the example of the scattered power. In Section 3.4, the results of the Born approximation and of the exact solution are compared with regard to the most important aspects. A special development for crack-like shaped two-dimensional scatterers can be found in Gubernatis et al. [22]. Both single scatterer approaches can be applied to any of the multiple scattering models.

The methods used to derive theoretical models relating the ultrasonic attenuation to the damage state include the finite element method, used for example in Yeh et al. [51], a tensor based approach described by Yang et al. [49] and methods relating

the attenuation caused by just one scatterer to the multiple scatterer situation. In this study, the latter method is used. It can be classified furthermore into the model of Waterman and Truell introduced by Waterman et al. [47], a differential self-consistent scheme applied by Littles et al. [31] and a self-consistent scheme which is described by Sabina et al. [39]. All of these methods are treated in the present research, giving a theoretical basis for the development of attenuation models. Results of the model of Waterman and Truell and the differential self-consistent scheme are compared in Section 4.2.2. The model developed by Waterman and Truell and the differential self-consistent method are restricted to composite materials with a low volume fraction of inclusions and materials containing voids or cracks and can thus not be applied to the grain boundary scattering. The self-consistent scheme on the other hand is valid for high volume fractions of inclusions and is not based upon a clear distinction between the matrix material and the inclusions, making this a suitable approach for the analysis of grain boundary scattering.

The multiple scattering methods yield different descriptions of the ultrasonic attenuation. The differential self-consistent scheme describes the attenuation in terms of the scattering cross section which depends on the volume fraction of the inhomogeneities. The scattering cross section is defined as the ratio of the energy scattered per unit time by the inhomogeneities to the energy of the incident wave per unit time and unit area which is analogous to the definition of the scattering cross section as the ratio of the scattered power to the intensity of the incident wave. The differential self-consistent scheme gives solutions for the longitudinal and transverse scattering cross sections, which are obtained independently from each other. Relationships for the derivation of the attenuation coefficient from the scattering cross section are given in Section 4.2. The model developed by Waterman and Truell and the self-consistent scheme directly provide the attenuation coefficients of the longitudinal and transverse waves.

Attenuation models have been developed for a variety of materials. Sayers et al. [41] investigate ultrasonic attenuation in porous media, and research concerning wave

propagation and attenuation in cement-based materials can be found in Becker [7]. Polycrystalline materials are treated by Stanke et al. [42], and applications to composite materials are made by Kim et al. [29].

In polycrystalline materials, a characterization of the material state is already possible before the material is severely damaged, i.e. before the formation of cracks. This is due to the fact that grain boundary scattering and thus attenuation depend on the shape and the orientation of the scatterer. Under load and during life time, the grains will elongate and align in a preferred orientation which causes a change in the grain boundary scattering. The influence of a texture on ultrasonic attenuation is analyzed by Turner [44], while Ahmed et al. [4] describe the influence of elongated grains on the attenuation. One of the difficulties is therefore to relate the change in the ultrasonic attenuation to its source, which can be either the change in the grain structure or the development of material defects like cracks.

CHAPTER 2

Theoretical background

This chapter provides a brief introduction to the fundamentals of wave propagation in elastic solids. There are a number of comprehensive books on wave propagation theory, for example Bedford et al. [8], Achenbach [2] and Graff [17].

2.1 Wave propagation

2.1.1 Linear elasticity and equation of motion

In elasticity, the traction t_i on a plane $n_i x_i = d$ is given by

$$t_i = \sigma_{ji} n_j, \tag{2.1}$$

where σ_{ji} is the stress tensor. The balance of linear momentum for a body with volume V and surface S can be expressed as

$$\int_S \sigma_{kl} n_k \mathrm{d}S + \int_V \rho f_l \mathrm{d}V = \int_V \rho \ddot{u}_l \mathrm{d}V, \tag{2.2}$$

with ρ representing the material mass density and f_i the body force. Gauss' theorem applied to Equation 2.2 leads to

$$\int_V (\sigma_{kl,k} + \rho f_l - \rho \ddot{u}_l) \mathrm{d}V = 0. \tag{2.3}$$

Equation 2.3 has to be fulfilled for any arbitrary volume V of the body, and therefore the stress equations of motion become

$$\sigma_{kl,k} + \rho f_l = \rho \ddot{u}_l. \tag{2.4}$$

It is often more efficient to have the equations of motion given solely in terms of the displacement, u_i (as opposed to Equation 2.4, which has terms of stress σ_{ij} and

displacement u_i). This can be achieved by applying Hooke's law for a homogeneous, isotropic and linear elastic medium, which is given by

$$\sigma_{ij} = \lambda \epsilon_{kk} \delta_{ij} + 2\mu \epsilon_{ij}, \tag{2.5}$$

where ϵ_{ij} is the strain tensor, related to the displacement u_i by

$$\epsilon_{ij} = \frac{1}{2}(u_{i,j} + u_{j,i}), \tag{2.6}$$

and μ and λ are the Lamé constants. Plugging Equation 2.6 into Equation 2.5 and subsequently into Equation 2.4 leads to Navier's equations of motion

$$\mu u_{i,jj} + (\lambda + \mu) u_{j,ji} = \rho \ddot{u}_i \tag{2.7}$$

$$\mu \nabla^2 \mathbf{u} + (\lambda + \mu) \nabla \nabla \cdot \mathbf{u} = \rho \ddot{\mathbf{u}}. \tag{2.8}$$

Note that in this development, body forces $\mathbf{f}$ are neglected. Solving Equation 2.8, however, is difficult, because it is a coupled partial differential equation (PDE). The Helmholtz decomposition

$$\mathbf{u} = \nabla \varphi + \nabla \times \boldsymbol{\psi}, \tag{2.9}$$

provides a convenient way to uncouple these equations. Equation 2.9 represents the three components of displacement u with the four functions φ, ψ_1, ψ_2 and ψ_3. To guarantee the uniqueness of the solution, an additional constraint

$$\nabla \cdot \boldsymbol{\psi} = 0 \tag{2.10}$$

is introduced. Substitution of equation Equation 2.9 (Helmholtz decomposition) into the displacement equations of motion (Equation 2.8) leads to two uncoupled wave equations expressed in terms of the displacement potentials φ and $\boldsymbol{\psi}$

$$\nabla^2 \varphi = \frac{1}{c_{\mathrm{L}}^2} \ddot{\varphi}, \qquad \nabla^2 \boldsymbol{\psi} = \frac{1}{c_{\mathrm{T}}^2} \ddot{\boldsymbol{\psi}}, \tag{2.11}$$

whereas (will be shown later) c_L represents the wave speed of the longitudinal wave and c_T the wave speed of the vertically and horizontally polarized (transverse) shear waves,

$$c_{\mathrm{L}}^2 = \frac{\lambda + 2\mu}{\rho}, \qquad c_{\mathrm{T}}^2 = \frac{\mu}{\rho}. \tag{2.12}$$

It always holds $c_L > c_T$. Both wave speed equations are expressed in terms of material properties density ρ and the Lamé constants μ and λ. A relationship to material properties Young's modulus E and Poisson's ratio ν is given by

$$\lambda = \frac{E\nu}{(1+\nu)(1-2\nu)}, \tag{2.13}$$

$$\mu = \frac{E}{2(1+\nu)}. \tag{2.14}$$

In analogy to the wave speed, one defines the longitudinal and the transverse wave numbers as

$$\alpha = \frac{\omega}{c_{\mathrm{L}}}, \qquad \beta = \frac{\omega}{c_{\mathrm{T}}}. \tag{2.15}$$

2.1.2 Wave phenomena

Wave phenomena discussed in this section are based on the plane wave assumption, i.e. assuming a wave with constant properties (ϵ, σ, u) on a plane perpendicular to its direction of propagation $\mathbf{p}$. Equation 2.16 shows the mathematical representation of a plane wave,

$$\mathbf{u} = f(\mathbf{x} \cdot \mathbf{p} - ct)\mathbf{d}, \tag{2.16}$$

where $\mathbf{d}$ is the unit vector defining the direction of particle motion, and c is either the longitudinal wave speed c_L or the transverse wave speed c_T. By substituting Equation 2.16 into Equation 2.8, one obtains

$$(\mu - \rho c^2)\mathbf{d} + (\lambda + \mu)(\mathbf{p} \cdot \mathbf{d})\mathbf{p} = 0. \tag{2.17}$$

Since $\mathbf{p}$ are two different unit vectors, it can immediately be seen that the two possible solutions that form the basis of wave propagation are either $\mathbf{d} = \pm\mathbf{p}$ or $\mathbf{p} \cdot \mathbf{d} = 0$:

- $\mathbf{d} = \pm\mathbf{p}$ leads to $\mathbf{p} \cdot \mathbf{d} = \pm 1$ and yields with Equation 2.17, $c = c_{\mathrm{L}}$ (see Equation 2.12). Since $\mathbf{d}$ and $\mathbf{p}$ are linearly dependent, this represents a particle movement in the direction of propagation — a longitudinal or P-wave.

- $\mathbf{p} \cdot \mathbf{d} = 0$ yields with Equation 2.17, $c = c_{\mathrm{T}}$ (see Equation 2.12). Now the direction of motion is normal to the direction of propagation, and the wave is called a transverse wave. If a two dimensional plane of propagation is considered (for example, the $(x_1 - x_2)-$plane), a wave with an in-plane displacement

(in the $(x_1 - x_2)-$plane) is called an SV-wave (vertically polarized), while a wave with out-of-plane displacement (in the x_3 direction) is called an SH-wave (horizontally polarized).

In an unbounded, homogeneous, isotropic material, transverse and longitudinal wave speeds are independent of frequency — they are nondispersive.

2.1.2.1 Reflections of P and SV-waves

The wave types derived so far propagate independently in an infinite media. As soon as a finite media in the direction of propagation is considered, reflections and coupling will occur. A incident P-wave (SV-wave), which is reflected at a stress free boundary ($\sigma_{22} = 0$ and $\sigma_{21} = 0$) normally consists of both, a P-wave (SV-wave) and a SV-wave (P-wave). Figure 2.1 shows the reflections of an incident P and SV-wave.

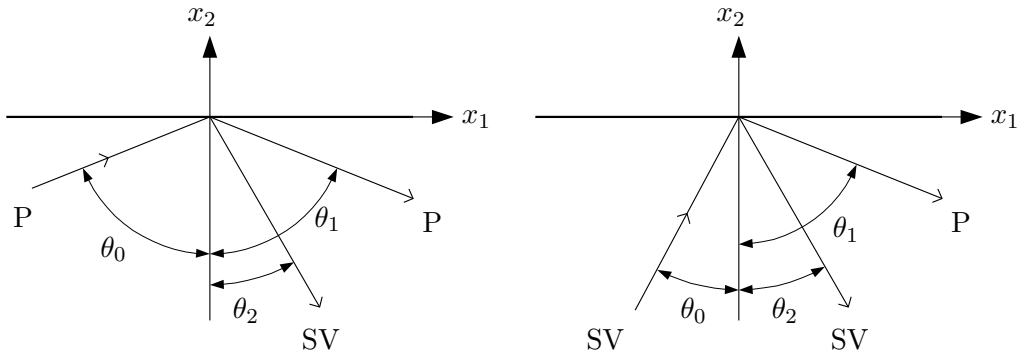

(a) Reflection of a P-wave (b) Reflection of a SV-wave

Figure 2.1: Wave reflections

The effect of a single incident wave-type producing two different waves (after reflection from a boundary) is called mode conversion. The displacement field of a harmonic wave in the $(x_1 - x_2)-$plane (propagating in infinite media, plane-strain case) can be expressed as

$$\mathbf{u}^{(n)} = A_n \mathbf{d}^{(n)} e^{ik_n(x_1 p_1^{(n)} + x_2 p_2^{(n)} - c_n t)}, \tag{2.18}$$

whereas n denotes the wave (longitudinal or transverse), $k_n = \frac{\omega}{c_n}$ is called the wavenumber of wave n and the respective wave speeds are c_n. Using these definitions, and noting that the angular frequency ω is equal for the incident and reflected

waves, it is possible to determine the relationship between the angle of the incident and the angles of the reflected waves (see Table 2.1).

Table 2.1: Angle relations for reflection on a stressfree surface

incident θ_0	reflected P θ_1	reflected SV θ_2
P	$\theta_1 = \theta_0$	$\sin\theta_2 = (c_T/c_L)\sin\theta_0$
SV	$\sin\theta_1 = (c_L/c_T)\sin\theta_0$	$\theta_2 = \theta_0$

Exceptions of mode conversion are the normal incidence with $\theta_0 = 0$ — in this case, the waves are reflected as themselves, and if the angle θ_0 is greater than a critical angle,

$$\theta_{cr} = \arcsin\frac{c_{\mathrm{T}}}{c_{\mathrm{L}}}; \tag{2.19}$$

then only a SV-wave is reflected. The P-wave portion of the reflected signal degenerates into a surface wave (Raleigh wave), traveling along the surface and exponentially decreasing in amplitude with increasing depth.

2.2 Attenuation

There are several attenuation mechanisms that are briefly introduced and their underlying physics are explained.

Attenuation is usually incorporated in the framework previously discussed by the introduction of a complex wave number, k (equivalent to a complex wave speed and complex material constants). The complex wavenumber k^* is defined as

$$k^* = \frac{\omega}{c_{\mathrm{L}}} = k' + ik'' \tag{2.20}$$

In the example of a plane, harmonic, one-dimensional wave (derived from Equation 2.16), the displacement field is given by

$$u(x,t) = f(k^*x - \omega t) = e^{i(k^*x - \omega t)} \tag{2.21}$$

The influence of the attenuation coefficient is more obvious if Equation 2.21 is written as

$$u(x,t) = e^{-k''\omega x}e^{i(k'x-\omega t)} \quad \text{for} \quad x \geqq 0 \tag{2.22}$$

Note that non-geometric attenuation is intrinsically linked to wave-velocity dispersion by the Kramers-Kronig relationship that is derived from the causality condition that the output strain cannot precede the input stress in any physical material (Molyneux [32]). This is obvious, for example, if the dispersion relation is modified in accordance to Equation 2.20,

$$c_{\mathrm{L}} = \frac{\omega}{k^*} = \frac{\omega}{k' + ik''} \tag{2.23}$$

where $k'' \equiv \alpha_{\mathrm{att}}$ denotes the attenuation coefficient and k' the real part of the wavenumber. It is clear that the (now complex) wavespeed depends on the frequency, therefore dispersion is found. This means, waves of different frequencies travel with different velocities.

2.2.1 Viscoelastic media

General elasticity theory assumes that a material stores energy without dissipation during deformation. But many materials (e.g. polymers, composites, and cement-based materials) dissipate some stored energy. Such materials are called viscoelastic, because they combine the properties of an elastic solid and a viscous liquid. Stress in a viscoelastic material is a function of strain and the derivative of strain over time (Achenbach [2], Rose [38]). If these functions are linearly dependent on the strain and their derivatives, the material is called linearly viscoelastic. Viscoelastic material behavior leads to attenuation that is also known as material absorption. Material absorption in viscoelastic materials is commonly assumed to be linearly dependent on frequency within the ultrasonic frequency range (Rose [38]).

2.2.2 Geometric spreading

The spreading of an ultrasonic wave attenuates the initial wave amplitude, and this attenuation effect is independent of frequency. Geometric attenuation depends on the wave mode and the geometry of the investigated elastic body. Surface (Rayleigh) waves, for example, are attenuated by $1/\sqrt{r}$, where r is the propagation distance.

Plane longitudinal wave amplitudes are attenuated by $1/r$, where r is the distance to the (point) source. This attenuation type is intrinsic to the wave equation. In a strict sense, geometric spreading is not counted to attenuation.

2.2.3 Scattering

Scattering attenuation in heterogeneous materials is caused by wave scattering at material (different phases) interfaces, mode conversion between longitudinal and transverse (shear) waves at these interfaces and diffraction effects (see also Section 2.1.2).

Different domains are distinguished that have different approximations for the frequency dependence of the scattering attenuation coefficient, depending on the ratio of wavelength λ to size of the scatterer B.

The attenuation coefficient introduced in Equation 2.20 leads to attenuation of the initial wave amplitude with initial amplitude A_0 with distance z

$$A(\lambda, z, B) = A_0 e^{-\alpha(\lambda,B)z}. \tag{2.24}$$

This coefficient is a function of the wavelength λ and the scatterer size B. It is the sum of the coefficients of the individual attenuation mechanism, absorption α_a and scattering α_s

$$\alpha(\lambda, B) = \alpha_a(\lambda) + \alpha_s(\lambda, B). \tag{2.25}$$

The absorption coefficient is defined as follows

$$\alpha_a(\lambda) = \frac{C_a}{\lambda} \tag{2.26}$$

where C_a is a medium constant.

The scattering coefficient α_s in Equation 2.25 depends on the domain [23]. In the Rayleigh domain, when the wavelength is much longer than scatterer size, the following functional form is found

$$\alpha_s(\lambda, B) = \frac{C_r * B^3}{\lambda^4} \quad \text{for } \lambda >> B$$

In the stochastic domain, with wavelength of the order of the scatterer size, the following functional form is found

$$\alpha_s(\lambda, B) = \frac{C_s * B}{\lambda^2} \quad \text{for } \lambda \approx B$$

In the geometric domain, when the wavelength is much smaller than scatterer size, the following functional form is found

$$\alpha_d(\lambda, B) = \frac{C_d}{B} \quad \text{for } \lambda << B$$

Note that the functional forms of the scattering coefficients given in the equations above are rough approximations. Their accuracy depends on the specific case under consideration, and on the method used to solve the scattering problem. Especially the transition between the different domains is a very rough estimate and depends strongly on the configuration of the scattering problem. On the other hand, some methods are just applicable to one of the domains described above.

The purpose of this work is to relate the damage state of a material to its attenuation coefficient. In general, geometric spreading does not depend on the material properties and can thus not be used as a measure for the material state. Scattering is found to be the attenuation mechanism which strongly depends on the material properties and the damage state, so the focus of this research will be on scattering attenuation. In the special case of grain boundary scattering in polycrystalline materials overlaid on scattering effects by inclusions, cracks and voids, the viscoelastic attenuation is also of interest. The difficulty is then to distinguish between the viscoelastic attenuation, which depends on the microstructure of the material, and the attenuation caused by

scattering in the damaged material. Note in this context, that a viscoelastic media is described by complex material properties, leading to complex wavenumbers with their imaginary parts describing the attenuation coefficients.

CHAPTER 3

Single scatterer solutions

This chapter considers two approaches for the solution of the single scatterer problem. The first approach is the Born approximation, a method first developed in physics dealing with the scattering of light at small particles. The second approach yields an exact solution to the single scattering problem.

3.1 The Born approximation

The Born approximation is based on a Green's function approach, leading to an integral equation describing the scattered wave field. In order to avoid a volume integration, the Born approximation is in general coupled with the far-field approximation, leading to simple expressions characterizing the properties of the scattered wave.

3.1.1 Scattering at spherical obstacles in liquids

In this section a simplified model is developed for a first principle understanding of scattering problems. Two useful simplifications are possible when examining an incident ultrasonic wave in a liquid that is scattered by a spherical, hydrostatically compressible obstacle. First, shear waves can not occur in liquids, so mode conversion is not possible. Second, a sphere has a simple geometry, with symmetric geometric properties. This section calculates the scattered pressure field using the Green's function theory and the Born approximation. This approach is available in a number of books and papers, for example in Kino [30] and in Gubernatis et al. [20].

3.1.1.1 General scattering theory

The scattering situation illustrated in Figure 3.1 is valid for the Born approximation approach as well as for the exact solution approach, and for scatterers of arbitrary shape. The incident wave propagates in the $+\mathbf{z}$ direction, while the direction of the scattered wave is defined by the polar angle θ and the azimuthal angle ϕ. The vector $\mathbf{r}$ describes the observation point outside the scattering object, and $\mathbf{r}'$ depicts a point on the surface of the scatterer. Furthermore, V' is the volume of the scatterer and S' is its surface.

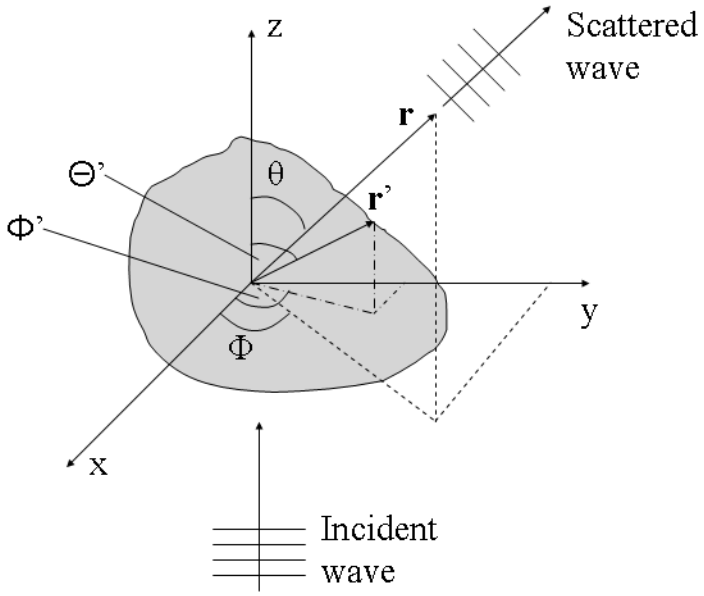

Figure 3.1: Illustration of the scattering problem.

The scattering problem is solved by using a surface integral formulation in combination with Green's function theory. If the potential φ and its normal gradient $\nabla\varphi \cdot \mathbf{n}$ are known on a surface S, the potential at any other point due to excitation of this surface is given by

$$\varphi_{\mathrm{s}}(x,y,z) = \int_S (\varphi \nabla' G - G \nabla' \varphi) \cdot \mathbf{n} \mathrm{d}S'. \tag{3.1}$$

The primed coordinate system denotes the source coordinates, in this case any point on the surface of the sphere, and the integration is carried out over the surface of the scatterer. In Equation 3.1, $\mathbf{n}$ is the outward unit vector normal to the surface of the sphere and G is the free-space Green's function defined as

$$G = \frac{\mathrm{e}^{-ikR}}{4\pi R} \tag{3.2}$$

with

$$R = \sqrt{(x-x')^2 + (y-y')^2 + (z-z')^2}. \tag{3.3}$$

If the potential of the incident wave is denoted by φ^{i}, the total potential in the presence of the scatterer is

$$\varphi = \varphi^{\mathrm{i}} + \varphi^{\mathrm{s}} \tag{3.4}$$

where φ^{s} is the potential of the scattered wave. Knowing the total potential on the surface of the sphere, it is possible to determine the total potential at any other point by combining Equation 3.1 and Equation 3.4 as

$$\varphi = \varphi^{\mathrm{i}} + \int_S (\varphi \nabla' G - G \nabla' \varphi) \cdot \mathbf{n} \mathrm{d}S'. \tag{3.5}$$

Equation 3.1 can be written as a volume integral formulation. Together with the relationship $p = \omega^2 \rho_{\mathrm{M}} \varphi$, Equation 3.1 can be written in terms of the pressure inside the scatterer as

$$p_{\mathrm{s}}(x,y,z) = \int_S \Big(p \nabla' G - \frac{\rho_{\mathrm{M}}}{\rho_{\mathrm{I}}} G \nabla' p \Big) \cdot \mathbf{n} \mathrm{d}S' \tag{3.6}$$

where ρ_{M} and ρ_{I} are the densities outside of and inside the scatterer (the inclusion). The area outside of the scatterer is denoted as the matrix. By employing Gauss' integral theorem, it is finally possible to express the scattered pressure as

$$p^{\mathrm{s}}(x,y,z) = \int_V \Big[\Big(1 - \frac{\rho_{\mathrm{M}}}{\rho_{\mathrm{I}}} \Big) \nabla' p \cdot \nabla' G - k^2 p G \Big(1 - \frac{\kappa_{\mathrm{M}}}{\kappa_{\mathrm{I}}} \Big) \Big] \mathrm{d}V' \tag{3.7}$$

which is sometimes referred to as the scattering theorem. Note that $k^2 = \omega^2 \rho_{\mathrm{M}} / 3\kappa_{\mathrm{M}}$ is the wavenumber of the surrounding liquid, while κ_{M} and κ_{I} are the bulk modulus of the liquid and the scatterer.

3.1.1.2 Born approximation

Solving Equation 3.7 for the scattered pressure is not easy, because the total pressure p (p consists of the incident and the scattered waves) must be known inside the scatterer. As a simplification, the Born approximation makes the assumption that the pressure inside the scatterer equals the pressure of the unperturbed incident wave, i.e. $p = p^{\mathrm{i}}$ on the right hand side of Equation 3.7.

Other methods (besides the Born approximation) can be used to solve the scattering problem described in Equation 3.7. Among these methods are the quasistatic approximation described by Gubernatis et al. [18] and the Keller approximation, which can be found in Stanke et al. [42]. Each of this approaches has its advantages — for example the Keller approximation can be used for high frequencies in the geometric domain. The advantage of the Born approximation is its simplicity, especially its applicability to several different scatterer shapes.

On the other hand, there are restrictions to the Born approximation:

- The wavelength of the incident wave must be large when compared to the dimension of the scatterer (Rayleigh domain).
- The differences in the elastic constants between the scatterer and the surrounding media can not be too great.

If these assumptions are not met, the accuracy of the Born approximation is rather poor. However, if these conditions are met, it is possible to converge to the exact solution by an iterative process when the scattered pressure calculated with the Born approximation is used together with the incident pressure as the pressure on the right hand side of Equation 3.7.

Furthermore, the accuracy of the Born approximation depends on the direction of the scattered wave. In general, the Born approximation works better for backward scattering, than for forward scattering. The exact forward scattering direction is defined

by $\theta = 0$, and the exact backward scattering direction by $\theta = \pi$, see Figure 3.1.

The scattered pressure on a sphere of radius $R = 0.1$ m (the absolute value together with the real and imaginary parts) for an incident plane wave propagating in the $\mathbf{x}$ direction with

$$p^{\mathrm{i}} = a_i \mathrm{e}^{-ikx'} \tag{3.8}$$

is shown in Figure 3.2. The time dependency $\mathrm{e}^{i\omega t}$ is omitted in Equation 3.8. In Figure 3.2, the scattered pressure is plotted in dependence on the polar angle θ and the azimuthal angle ϕ (both in radians) for the case $a_i = 1$. The density and the bulk modulus of the inclusion are 1/10 th of the density and the bulk modulus of the liquid. The radius of the scatterer is $a = 6.5\mu$m, and the observation point is at a distance of $R = 0.1$ m from the center of the inclusion, so that $R \gg a$ holds. The results in the left column of Figure 3.2 are for the Rayleigh regime — wavelength of the incident wave $\lambda = 1 \cdot 10^{-3}$ m, so $\lambda \gg a$. In contrast, the right column of Figure 3.2 shows the results for the stochastic regime — the wavelength approaches the radius of the sphere — this is the case where the Born approximation is no longer accurate. That the Born approximation is not applicable in the stochastic regime is evidenced by the fact that the shape of the scattered pressure in the stochastic regime is much more complicated than in the Rayleigh regime. Taking this shape of the scattered pressure as a criteria for the transition between the Rayleigh and stochastic regimes (and thus a way to identify the limit for the applicability of the Born approximation), it is possible to show that for a wavelength below approximately $3 \cdot 10^{-5}$ m, the assumptions for the application of the Born approximation are satisfied.

Figure 3.2 also makes it possible to distinguish between forward and backward scattering. Since the incident wave is now propagating in the $+\mathbf{x}$ direction, (and not in $+\mathbf{z}$ direction as in Figure 3.1), the backward scattering area is determined by $-\pi/2 < \phi < \pi/2$, whereas the forward scattering region is defined by $\pi/2 < \phi < 3\pi/2$. It is obvious that the scattered pressure is symmetric with respect to both angles. If the azimuthal angle, ϕ, equals $\pi/2$ or $3\pi/2$, then the scattered pressure is independent of the polar angle θ.

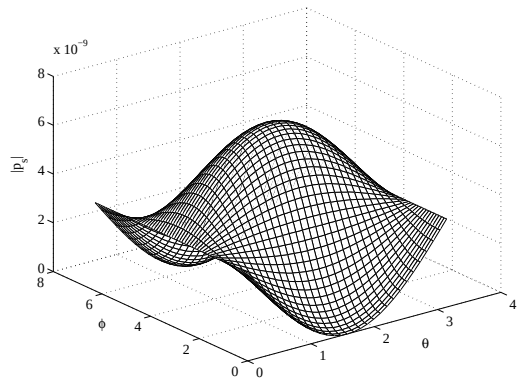

(a) Absolute value of scattered pressure for $\lambda \gg a$

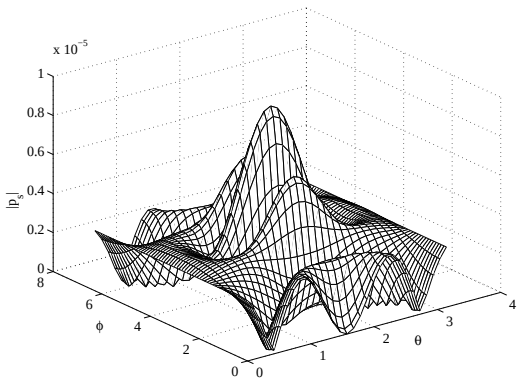

(b) Absolute value of scattered pressure for $\lambda \simeq a$

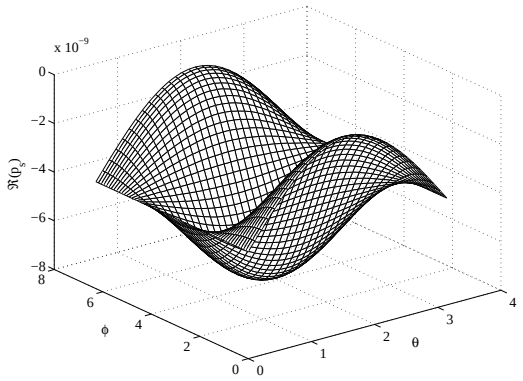

(c) Real part of scattered pressure for $\lambda \gg a$

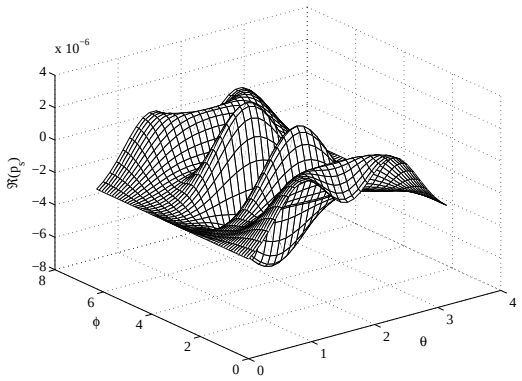

(d) Real part of scattered pressure for $\lambda \simeq a$

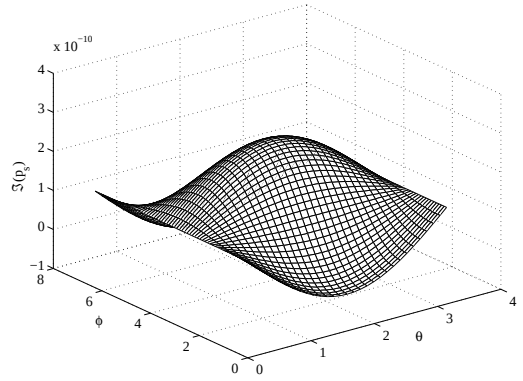

(e) Imaginary part of scattered pressure for $\lambda \gg a$

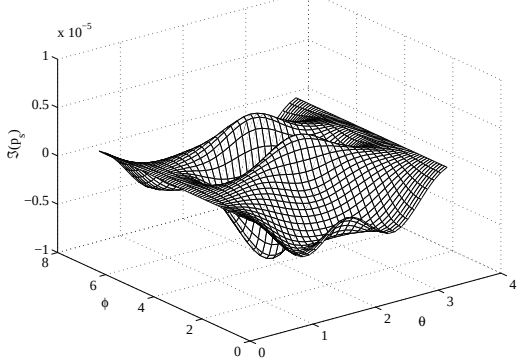

(f) Imaginary part of scattered pressure for $\lambda \simeq a$

Figure 3.2: Scattered pressure at a spherical inclusion in a liquid media.

The amplitude of the scattered pressure has to be treated with care. It can not be used as an attribute which is directly related to the attenuation coefficient of a material with inclusions, since it is subjected to geometric spreading and therefore dependent on the propagation distance between the scatterer and the observation point. Thus, to find a measure of the influence of the inclusion on the attenuation of the incident wave, it is necessary to balance this effect. It will be shown that integrating the scattered pressure over the area in order to determine the scattered intensity (or energy) makes it possible to obtain a result which is independent of the observation point (propagation distance).

3.1.2 Scattering of elastic inclusions in solids

In this section, the aforementioned model is extended to the case of a single inclusion in a solid matrix. This means, that during the scattering process, mode conversion occurs, and therefore for the incident wave being purely longitudinal, the scattered wave consists of a longitudinal and a transverse part. On the other hand, a purely transverse incident wave results in scattered longitudinal and transverse waves. The approach taken here is similar to the development in the paper of Gubernatis et al. [19].

In the following, the standard tensor index convention is used, so repeated indices imply summation, and differentiation with respect to the ith coordinated is denoted with the subscript $_{,i}$. The differential scattering cross section is the sought quantity to describe the scattering and it is defined as

$$\frac{\mathrm{d}\gamma(\omega)}{\mathrm{d}\Omega} = \lim_{r\to\infty} \frac{\langle r^2 \hat{r}_i \sigma^{\mathrm{s}}_{ij} \dot{u}^{\mathrm{s}}_j \rangle}{\langle I^{\mathrm{i}} \rangle} \tag{3.9}$$

where the angular brackets denote time averaging and $\mathrm{d}\Omega$ is the differential element of the solid angle. I^{i} is the intensity of the incident wave. From the differential scattering cross section, the scattering cross section — which is directly related to the attenuation — can be determined by integration over $\mathrm{d}\Omega$.

Clearly, the determination of the scattering cross section and the attenuation coefficient requires the calculation of the scattered stress field σ_{ij}^{s} and the scattered displacement field u_j^{s}. By extending Equation 3.7 to the case where the elastic properties of the surrounding material are isotropic, the total displacement field as a sum of the incident displacement field u_m^i and the scattered displacement field u_m^s is found as

$$u_m = u_m^{\mathrm{i}} + \delta\rho\omega^2 \int_{V_2} g_{im} u_i \mathrm{d}V + \delta C_{ijkl} \int_{V_2} g_{im} u_{k,jl} \mathrm{d}V - \delta C_{ijkl} \int_{S_2} g_{im} n_j u_{k,l} \mathrm{d}S \quad (3.10)$$

where the Green's function is now defined as (Gubernatis et al. [19])

$$g_{ij} = \frac{1}{4\pi\rho\omega^2}\left[\beta^2 \frac{\mathrm{e}^{i\beta R}}{R}\delta_{ij} - \frac{\partial}{\partial x_i}\frac{\partial}{\partial x_j}\left(\frac{\mathrm{e}^{i\alpha R}}{R} - \frac{\mathrm{e}^{i\beta R}}{R}\right)\right] \quad (3.11)$$

and its derivative is given by

$$g_{ij,k} = \frac{1}{4\pi\rho\omega^2}\left[\beta^2 \frac{\partial}{\partial x_k}\frac{\mathrm{e}^{i\beta R}}{R}\delta_{ij} - \frac{\partial}{\partial x_i}\frac{\partial}{\partial x_j}\frac{\partial}{\partial x_k}\left(\frac{\mathrm{e}^{i\alpha R}}{R} - \frac{\mathrm{e}^{i\beta R}}{R}\right)\right]. \quad (3.12)$$

To solve the scattering problem, the far-field approximation is made, that is the scattered displacement and stress fields are calculated for the case $R \to \infty$. The basic scattering equation is obtained from Equation 3.10 as

$$u_i(\mathbf{r}) = u_i^{\mathrm{i}}(\mathbf{r}) + \delta\rho\omega^2 \int_{V_2} g_{im}(\mathbf{r}-\mathbf{r}') u_m(\mathbf{r})' \mathrm{d}V' + \delta C_{jklm} \int_{V_2} g_{ij,k}(\mathbf{r}-\mathbf{r}') u_{l,m'}(\mathbf{r}'). \quad (3.13)$$

The scattered displacement field in the limit $r \to \infty$ is then

$$u_i^{\mathrm{s}} \sim \hat{r}_i \hat{r}_j f_j(\alpha)\left[\frac{\mathrm{e}^{i\alpha r}}{r}\right] + (\delta_{ij} - \hat{r}_i\hat{r}_j) f_j(\beta)\left[\frac{\mathrm{e}^{i\beta r}}{r}\right], \quad (3.14)$$

where the following approximations are used in the far-field:

$$\begin{aligned}
&R^{-1} \sim r^{-1} \\
&R \sim r - (\mathbf{r}' \cdot \mathbf{r}) \\
&\frac{\partial}{\partial x_i}\frac{\mathrm{e}^{ikR}}{R} \sim ik\frac{\mathrm{e}^{ikr}}{r}\hat{r}_i \mathrm{e}^{-i\mathbf{k}\cdot\mathbf{r}'} \\
&\frac{\partial}{\partial x_i}\frac{\partial}{\partial x_j}\frac{\mathrm{e}^{ikR}}{R} \sim (ik)^2\frac{\mathrm{e}^{ikr}}{r}\hat{r}_i\hat{r}_j \mathrm{e}^{-i\mathbf{k}\cdot\mathbf{r}'} \\
&\frac{\partial}{\partial x_i}\frac{\partial}{\partial x_j}\frac{\partial}{\partial x_k}\frac{\mathrm{e}^{ikR}}{R} \sim (ik)^3\frac{\mathrm{e}^{ikr}}{r}\hat{r}_i\hat{r}_j\hat{r}_k \mathrm{e}^{-i\mathbf{k}\cdot\mathbf{r}'}.
\end{aligned} \quad (3.15)$$

The scattered stress field is obtained as

$$\sigma_{ij}^{\mathrm{s}} \sim i\lambda\alpha\frac{\mathrm{e}^{i\alpha r}}{r}A_k\hat{r}_k\delta_{ij} + i\mu\left[\alpha\frac{\mathrm{e}^{i\alpha r}}{r}\left(A_i\hat{r}_j + A_j\hat{r}_i\right) + \beta\frac{\mathrm{e}^{i\beta r}}{r}\left(B_i\hat{r}_j + B_j\hat{r}_i\right)\right]. \tag{3.16}$$

Hereby, the symbol $\sim$ denotes asymptotic equality and

$$f_i(k) = \frac{k^2}{4\pi\rho\omega^2}\Big(\delta\rho\omega^2\int\limits_{V_2} u_i\mathrm{e}^{-i\mathbf{k}\cdot\mathbf{r'}}\mathrm{d}V' + ik\hat{r}_j\delta C_{ijkl}\int\limits_{V_2}\varepsilon_{kl}\mathrm{e}^{-i\mathbf{k}\cdot\mathbf{r'}}\mathrm{d}V'\Big) \tag{3.17}$$

is called the f vector. In Equations 3.14, 3.16 and 3.17, r_i is the vector from the origin of the coordinate system to the observation point and $\mathbf{k}$ is the wavenumber vector defined as $\mathbf{k} = k\hat{r}_i$ with k being α or β for longitudinal and shear waves, respectively, and $\hat{r}_i$ is the unit vector defining the direction of the propagating wave. The difference in the elastic constants between the matrix and the inclusion is expressed by $\delta\lambda = \lambda_{\mathrm{I}} - \lambda_{\mathrm{M}}$ and $\delta\mu = \mu_{\mathrm{I}} - \mu_{\mathrm{M}}$, whereas the difference in density is $\delta\rho = \rho_{\mathrm{I}} - \rho_{\mathrm{M}}$.

From Equation 3.14 it is possible to define a longitudinal scattering amplitude A_i and a transverse scattering amplitude B_i as

$$A_i(\theta,\phi) = \hat{r}_i\hat{r}_j f_j(\alpha), \qquad B_i(\theta,\phi) = (\delta_{ij} - \hat{r}_i\hat{r}_j)f_j(\beta). \tag{3.18}$$

Finally, one obtains by combining Equation 3.14 and Equation 3.16 and by taking the limit $r \to \infty$ for the nominator on the right side of Equation 3.9

$$\lim_{r\to\infty}\langle r^2\hat{r}_i\sigma_{ij}^{\mathrm{s}}\dot{u}_j^{\mathrm{s}}\rangle = -\frac{1}{2}\omega\left[\alpha(\lambda+2\mu)|A_i|^2 + \beta\mu|B_i|^2\right]. \tag{3.19}$$

If not declared otherwise, λ, μ and ρ are the Lamé constants and the density of the matrix material.

The plane-wave displacement field of the incident wave travelling in $+\mathbf{z}$ direction is

$$u_i^{\mathrm{i}} = a_i\mathrm{e}^{i(\alpha z-\omega t)} + b_i\mathrm{e}^{i(\beta z-\omega t)}. \tag{3.20}$$

and the time-averaged intensity of the incident wave is found to be

$$\langle I^{\mathrm{i}}\rangle = -\frac{1}{2}\omega\left[\alpha(\lambda+2\mu)|a_i|^2 + \beta\mu|b_i|^2\right]. \tag{3.21}$$

With Equation 3.19 and Equation 3.21, it is possible to express the differential scattering cross section from Equation 3.9 as

$$\frac{\mathrm{d}\gamma(\omega)}{\mathrm{d}\Omega} = \frac{\alpha(\lambda+2\mu)|A_i|^2 + \beta\mu|B_i|^2}{\alpha(\lambda+2\mu)|a_i|^2 + \beta\mu|b_i|^2}, \tag{3.22}$$

where a_i and b_i are the longitudinal and transverse amplitude vectors of the incident wave. The wavenumbers and the Lamé constants in Equation 3.22 are in general the ones of the matrix material. The total scattering cross section is defined as the integral of the differential scattering cross section over the differential element of solid angle $\mathrm{d}\Omega = \sin\theta \mathrm{d}\theta\mathrm{d}\phi$.

If the incident wave is purely longitudinal ($b_i = 0$) with

$$u_i^{\mathrm{i}} = \hat{a}_i \mathrm{e}^{i\alpha z'}, \tag{3.23}$$

where $\hat{a}_i$ is the unit vector in $\mathbf{z}$ direction, Equation 3.22 simplifies to

$$\frac{\mathrm{d}\gamma(\omega)}{\mathrm{d}\Omega} = \left[\frac{|A_i|}{|a_i|}\right]^2 + \frac{\alpha}{\beta}\left[\frac{|B_i|}{|a_i|}\right]^2. \tag{3.24}$$

For brevity, the time dependency $\mathrm{e}^{-i\omega t}$ is omitted in Equation 3.24 and in the following equations.

If the incident wave is a purely transverse wave polarized in $\mathbf{x}$ direction ($a_i = 0$), namely

$$u_i^{\mathrm{i}} = \hat{b}_i \mathrm{e}^{i\beta z'} \tag{3.25}$$

with $\hat{b}_i$ denoting the unit vector in the $\mathbf{x}$ direction, the differential cross section is

$$\frac{\mathrm{d}\gamma(\omega)}{\mathrm{d}\Omega} = \frac{\beta}{\alpha}\left[\frac{|A_i|}{|b_i|}\right]^2 + \left[\frac{|B_i|}{|b_i|}\right]^2. \tag{3.26}$$

These formulae allow the calculation of the scattering cross section of arbitrarily shaped inclusions in isotropic materials. For some shapes like spheres and ellipsoids,

it is possible to find easier equations. Gubernatis et al. [20] rewrite Equation 3.24 as

$$\begin{aligned}\frac{\mathrm{d}\gamma}{\mathrm{d}\Omega} &= \frac{\beta\alpha^3}{(4\pi)^2}\Big(\frac{\delta\rho\sin\theta\cos\phi}{\rho} - \frac{\delta\lambda + 2\delta\mu(\cos\theta)^2}{\lambda+2\mu}\Big)^2 |S(\alpha,\alpha)|^2 \\ &\quad + \frac{\alpha\beta^3}{(4\pi)^2}\Big(\frac{2\alpha\delta\mu\cos\theta\sin\theta}{\beta\mu} - \frac{\delta\rho\sin\theta}{\rho}\Big)^2 |S(\alpha,\beta)|^2 \\ &\equiv \frac{\mathrm{d}\gamma_{\mathrm{L}}}{\mathrm{d}\Omega} + \frac{\alpha}{\beta}\frac{\mathrm{d}\gamma_{\mathrm{T}}}{\mathrm{d}\Omega} \end{aligned} \tag{3.27}$$

where for the incident wave propagating in the $+\mathbf{z}$ direction, the shape factor is defined as

$$S(p,q) = \int_V \mathrm{e}^{i(p\hat{z} - q\hat{r})\cdot\mathbf{r}'}\mathrm{d}V' \tag{3.28}$$

with p and q being either α or β. The first term on the right-hand side of Equation 3.27 is called longitudinal differential cross section (caused by the scattered longitudinal wave), the second term is the transverse differential cross section (caused by the scattered transverse wave).

Analog to Equation 3.27 for the incident wave being purely longitudinal, it is also possible for the case of a purely transverse incident wave polarized in the $\mathbf{x}$ direction to derive the differential scattering cross section from Equation 3.26 as

$$\begin{aligned}\frac{\mathrm{d}\gamma}{\mathrm{d}\Omega} &= \frac{\alpha^4}{(4\pi)^2}\Big(\frac{\delta\rho\cos\theta}{\rho} - \frac{\delta\mu}{\lambda+2\mu}\frac{\beta}{\alpha}\sin\theta\cos\phi\Big)^2 |S(\beta,\alpha)|^2 \\ &\quad + \frac{\beta^4}{(4\pi)^2}\Big[\Big(-\frac{\delta\rho\sin\phi}{\rho} + \frac{\delta\mu\sin\phi\cos\theta}{\mu}\Big) \\ &\quad + \Big(\frac{\delta\rho\cos\theta\cos\phi}{\rho} - \frac{\delta\mu\cos2\theta\cos\phi}{\mu}\Big)^2\Big] |S(\alpha,\beta)|^2 \\ &\equiv \frac{\beta}{\alpha}\frac{\mathrm{d}\gamma_{\mathrm{L}}}{\mathrm{d}\Omega} + \frac{\mathrm{d}\gamma_{\mathrm{T}}}{\mathrm{d}\Omega}. \end{aligned} \tag{3.29}$$

The shape factor has the same form as for the incident longitudinal wave and is defined in Equation 3.28.

Now consider the case of an incident transverse plane wave, which is right circularly polarized and defined as

$$\mathbf{u}^i = \Big(\sqrt{2}\Big)^{-1}(\hat{x} + i\hat{y})\,\mathrm{e}^{i\beta z} \tag{3.30}$$

where $\hat{x}$ and $\hat{y}$ are unit vectors in the $\mathbf{x}$ and $\mathbf{y}$ direction. The total scattering cross section is then given by

$$\frac{\mathrm{d}\gamma}{\mathrm{d}\Omega} = \frac{\beta}{\alpha}\frac{\mathrm{d}\gamma_{\mathrm{L}}}{\mathrm{d}\Omega} + \frac{\mathrm{d}\gamma^{+}}{\mathrm{d}\Omega} + \frac{\mathrm{d}\gamma^{-}}{\mathrm{d}\Omega} \tag{3.31}$$

where the longitudinal scattering cross section $d\gamma_L/d\Omega$, the right circularly polarized scattering cross section $d\gamma^+/d\Omega$ and the left circularly polarized scattering cross section $d\gamma^-/d\Omega$ are determined by

$$\begin{aligned}
\frac{\mathrm{d}\gamma_{\mathrm{L}}}{\mathrm{d}\Omega} &= \alpha^4 \left(\frac{\delta\rho}{\rho}\sin\theta - \frac{\beta}{\alpha}\frac{\delta\mu}{\lambda+2\mu}\sin 2\theta \right)^2 |S(\beta,\alpha)|^2 \\
\frac{\mathrm{d}\gamma^{+}}{\mathrm{d}\Omega} &= \beta^4 \left(\frac{\delta\rho}{\rho}\frac{1+\cos\theta}{2} - \frac{\delta\mu}{\mu}\frac{\cos\theta+\cos 2\theta}{2} \right)^2 |S(\beta,\beta)|^2 \\
\frac{\mathrm{d}\gamma^{-}}{\mathrm{d}\Omega} &= \beta^4 \left(\frac{\delta\rho}{\rho}\frac{\cos\theta-1}{2} + \frac{\delta\mu}{\mu}\frac{\cos\theta-\cos 2\theta}{2} \right)^2 |S(\beta,\beta)|^2
\end{aligned} \tag{3.32}$$

and the shape factor is again defined in Equation 3.28.

The shape factor contains all the information about the shape of the scatterer, and for the case of a spherical scatterer Equation 3.28 can be simplified to

$$S = 4\pi a^3 \frac{\sin(a\Delta k) - a\Delta k\cos(a\Delta k)}{(a\Delta k)^3} \tag{3.33}$$

where a is the radius of the scatterer, $\Delta k = |\mathbf{\Delta k}|$ with $\mathbf{\Delta k} = p\hat{z} - q\hat{r}$. p and q are again either α or β, depending on the type of the incident and the scattered wave.

Similarly, the shape factor for an ellipsoidal inclusion is given by

$$S = 4\pi a_1 a_2 a_3 \frac{\sin(\Delta K) - \Delta K\cos(\Delta K)}{(\Delta K)^3} \tag{3.34}$$

with $\Delta K = \sqrt{\Delta k_1^2 a_1^2 + \Delta k_2^2 a_2^2 + \Delta k_3^2 a_3^2}$ and Δk_i is the projection of $\mathbf{\Delta k}$ onto the $\mathbf{x_i}$ axis. The axes of the ellipsoid, a_1,a_2 and a_3 are aligned along the $\mathbf{x}$,$\mathbf{y}$ and $\mathbf{z}$ directions.

The scattered displacement and stress fields in Equations 3.14 and 3.16 can be easily calculated by expressing the f vector from Equation 3.17 in terms of the shape factor. This gives for the incident longitudinal wave

$$f_i(k) = \frac{k^2}{4\pi\rho\omega^2}\left[(\delta\rho\omega^2 - 2\alpha k\delta\mu\cos\theta)\hat{a}_i - \alpha k\delta\lambda\hat{r}_i\right] S(\alpha,k) \tag{3.35}$$

and for the incident transverse wave

$$f_i(k) = \frac{k^2}{4\pi\rho\omega^2}\left[(\delta\rho\omega^2 - \beta k\delta\mu\cos\theta)\hat{b}_i - k\beta\delta\mu\hat{r}_1\hat{b}_1\delta_{1,3}\right]S(\beta,k). \tag{3.36}$$

Computationally, Equations 3.35 and 3.36 have the big advantage that no volume integration is necessary to determine the scattered stress and displacement fields. Compared to the calculation of the f vector by the use of Equation 3.17, the computation time is decreased significantly while the accuracy remains unchanged. Thus it is very convenient to use the non-integral form of the shape factor for all computations whenever it is possible to find such an expression for the corresponding scatterer shape.

3.2 Results for single scattering

In the following figures, the differential scattering cross sections for an aluminum inclusion in titanium are plotted. The material properties of aluminum and titanium are summarized in Table 3.1.

Table 3.1: Wavespeeds and material properties for aluminum and titanium.

material	$\rho[\frac{kg}{m^3}]$	$c_{\mathrm{L}}\ [\frac{m}{s}]$	$c_{\mathrm{T}}\ [\frac{m}{s}]$	$E[GPA]$	ν	$\lambda[GPa]$	$\mu[GPa]$
titanium	4500	6070	3130	116.3	0.32	77.6	44.1
aluminum	2700	6570	3150	72.4	0.35	63	26.8

3.2.1 Differential scattering cross section

Figure 3.3 shows the total, longitudinal and transverse differential scattering cross section for a spherical aluminum inclusion in titanium. The incident wave is longitudinal in the left column and transverse in the right column. The differential scattering cross section is plotted in dependence of the scattering angle θ (in radians) and the normalized longitudinal wave number $a\alpha$. The amplitude of the differential cross section is normalized, thus only its shape is relevant. Note that the value of $a\alpha = 6$ corresponds to the ratio $a/\lambda \simeq 1$. Compared to the exact solution, which can be

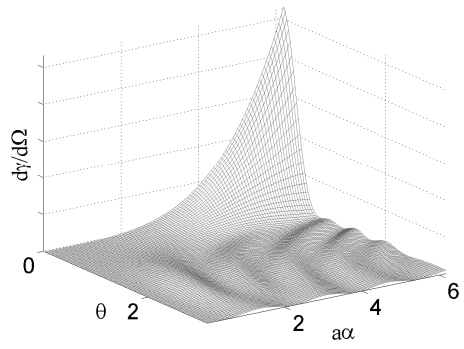

(a) Total differential scattering cross section for incident longitudinal wave

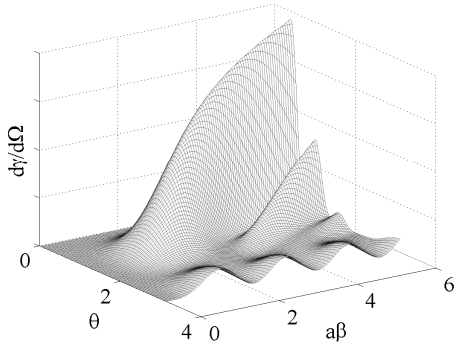

(b) Total differential scattering cross section for incident transverse wave

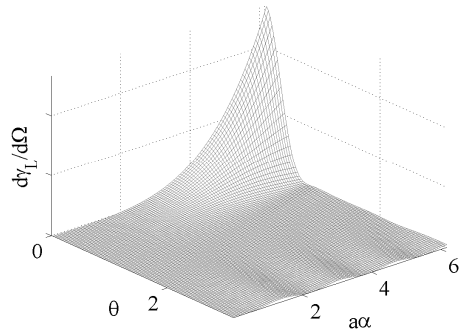

(c) Longitudinal differential scattering cross section for incident longitudinal wave

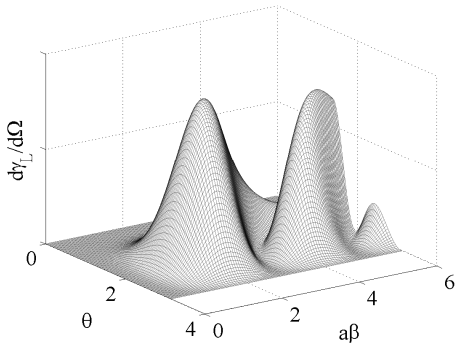

(d) Longitudinal differential scattering cross section for incident transverse wave

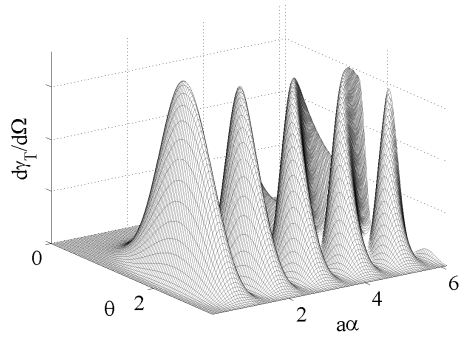

(e) Transverse differential scattering cross section for incident longitudinal wave

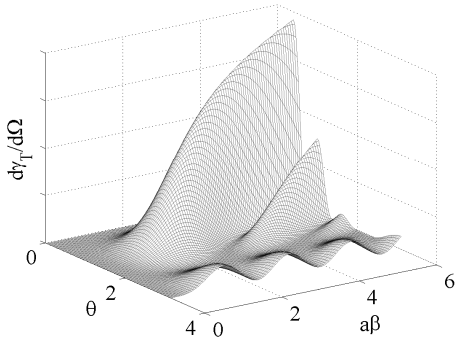

(f) Transverse differential scattering cross section for incident transverse wave

Figure 3.3: Differential scattering cross sections for a spherical inclusion.

found in Ying et al. [52], the result by using the Born approximation and the far-field approximation $R \to \infty$ is very accurate for the incident longitudinal wave for all values of θ. For this case the procedure developed by Gubernatis et al. [20] is useful, which is due to the facts that for the plotted frequency range the wavelength λ is of the same dimension as the radius of the sphere or less, and that the material properties of titanium and aluminum are comparable. If the incident wave is transverse, the Born approximation gives more precise results for the backward scattering direction ($\theta > \pi/2$) than for the forward scattering direction.

In Figure 3.4 the differential scattering cross sections for the right circularly polarized incident transverse wave are shown. A comparison to the exact result can be found in Gubernatis et al. [20]. Similar to the above cases for the incident longitudinal and the incident transverse wave polarized in $\mathbf{x}$ direction, the agreement of the Born approximation with the exact solution is satisfactory for $0 \leq \beta a \leq 1/2$ and $\pi/2 \leq \theta \leq \pi$, whereas the agreement is rather poor in the remaining domain.

3.2.2 Scattering cross section

The scattering cross section is calculated from the differential scattering cross section by the integration

$$\gamma = \int_0^{2\pi} \int_0^{\pi} \frac{\mathrm{d}\gamma}{\mathrm{d}\Omega} \sin\theta \mathrm{d}\theta \mathrm{d}\phi. \tag{3.37}$$

Therefore, the scattering cross section depends on the frequency of the incident wave, the diameter (or in general the volume) of the scatterer, the difference in density and the change in the elastic constants between the inclusion and the matrix. For all other shapes besides spheres, the scattering cross section is furthermore influenced by the orientation of the scatterer. If the observation point is far away from the scatterer, so that the assumption $R \to \infty$ holds, the scattering cross section is independent of the distance between the scattering object and the observation point. The dependency of the scattering cross section on frequency, scatterer size, scatterer shape and scatterer orientation is shown in the following sections.

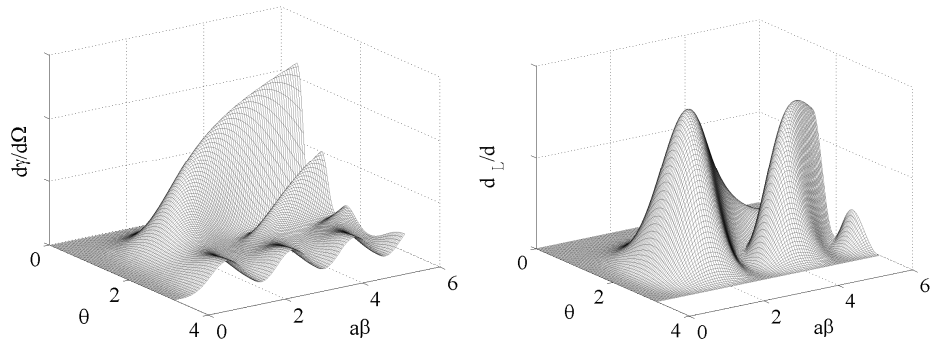

(a) Total differential scattering cross section

(b) Longitudinal differential scattering cross section

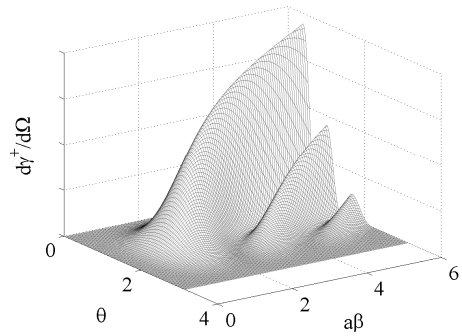

(c) Right circularly polarized differential scattering cross section

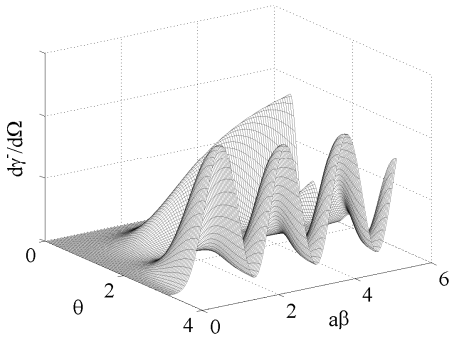

(d) Left circularly polarized differential scattering cross section

Figure 3.4: Differential scattering cross sections for a spherical inclusion and right circularly polarized incident wave.

3.2.2.1 Frequency dependence

The dependence of the scattering cross section normalized to the cross section area of the scatterer πa^2 on the frequency in the Rayleigh regime for an incident longitudinal wave is illustrated in Figure 3.5, where the total, longitudinal and transverse scattering cross sections are shown. Note that the amplitude of the longitudinal scattering cross section is about ten times smaller than the transverse scattering cross section.

For low frequencies with $\alpha a \leq 1$, the scattering cross section is proportional to f^2 which agrees with the result of Kino [42] for the Rayleigh domain. Hence it is possible to conclude that the transition between Rayleigh and stochastic domain occurs for

$\alpha a \simeq 1$.

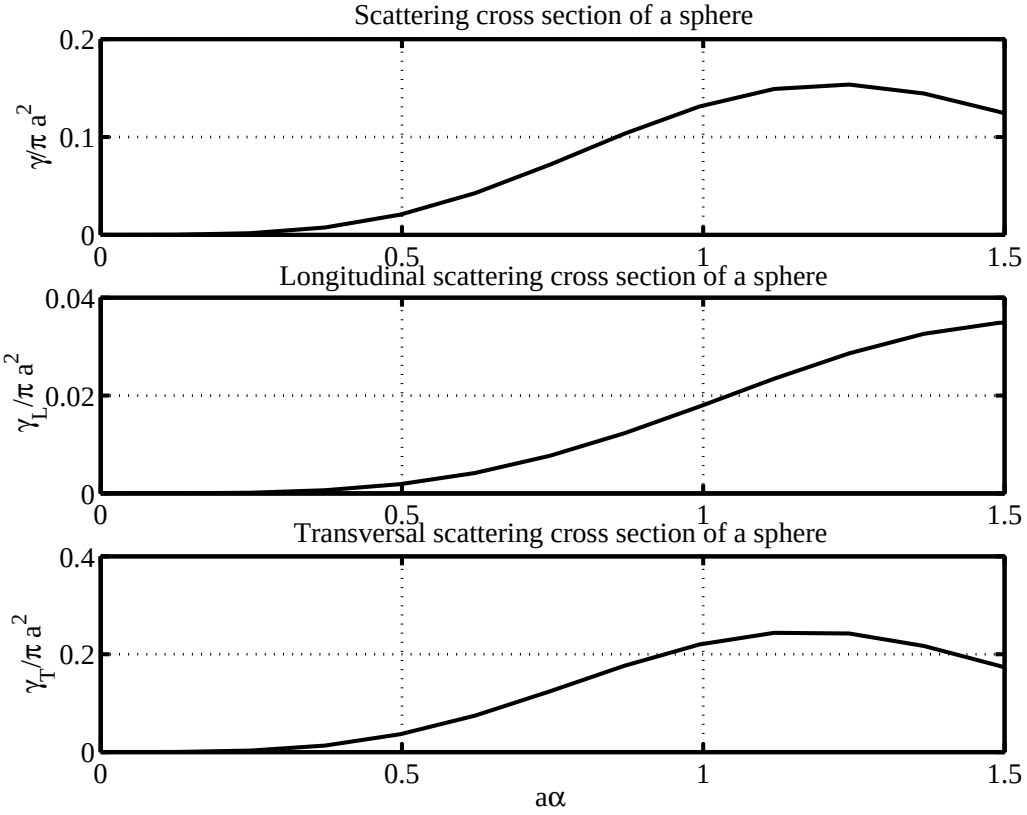

Figure 3.5: Scattering cross section of a single aluminum sphere in titanium for an incident longitudinal wave.

The normalized scattering cross section for an incident transverse wave is plotted in Figure 3.6. Now, the longitudinal cross section is of order 10^{-2} less than the transverse cross section and can therefore be neglected in the total scattering cross section. The change from the Rayleigh to the stochastic regime is here not as obvious as it is for the incident longitudinal wave.

Significant for both the incident longitudinal and transverse wave, is that the scattered longitudinal wave is much weaker than the scattered transverse wave. This means that the mode conversion is stronger for the incident longitudinal wave.

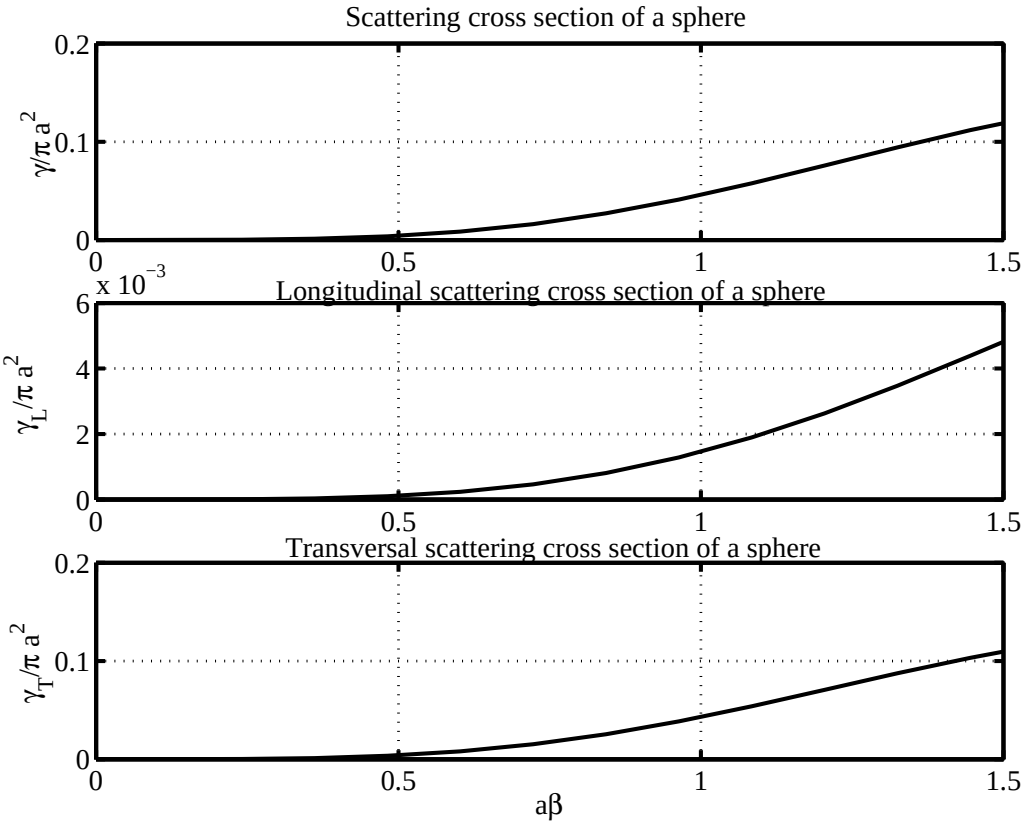

Figure 3.6: Scattering cross section of a single aluminum sphere in titanium for an incident transverse wave.

It should be noted that the frequency for the incident longitudinal wave, f_L, is always approximately twice the frequency of the incident transverse wave, f_T. This is due to the fact, that the ratio between the longitudinal wave speed and the transverse wave speed is from Tab. 3.1 $c_L/c_T \simeq 2$ and thus the ratio of the wavenumbers (for the same frequency) is $\alpha/\beta \simeq 0.5$. The longitudinal and transverse wavelength are than related to the scatterer size to define the Rayleigh domain in which the Born approximation is valid. From Figure 3.5 and Figure 3.6 the limiting value for the applicability of the Born approximation is chosen as $ka = 1$ with k denoting α or β.

3.2.2.2 Dependence on the scatterer size

The normalized scattering cross section $\gamma/\pi a^2$ in Figure 3.5 and 3.6 is independent of the scatterer size. To illustrate that dependence, the scattering cross section

is plotted for varying radii of the sphere at a constant frequency. The frequency is chosen such that for the maximum radius, the wavelength is still larger than the dimension of the scatterer, so it is ensured that all of the considered scattering problems lay in the Rayleigh domain. This means again, that the frequency for the incident longitudinal wave is approximately twice the frequency for the incident transverse wave.

Figure 3.7 shows the dependence of the scattering cross section from the size of the inclusion. The solid lines represent the case of the incident longitudinal wave with the frequency $f_L = 1 \cdot 10^5$ Hz, the dotted line the incident transverse wave with the frequency $f_T = 0.5 \cdot 10^5$ Hz $= 1/2 f_L$, both leading to $ka_{max} \approx 1$, where a_{max} is the maximum radius under consideration.

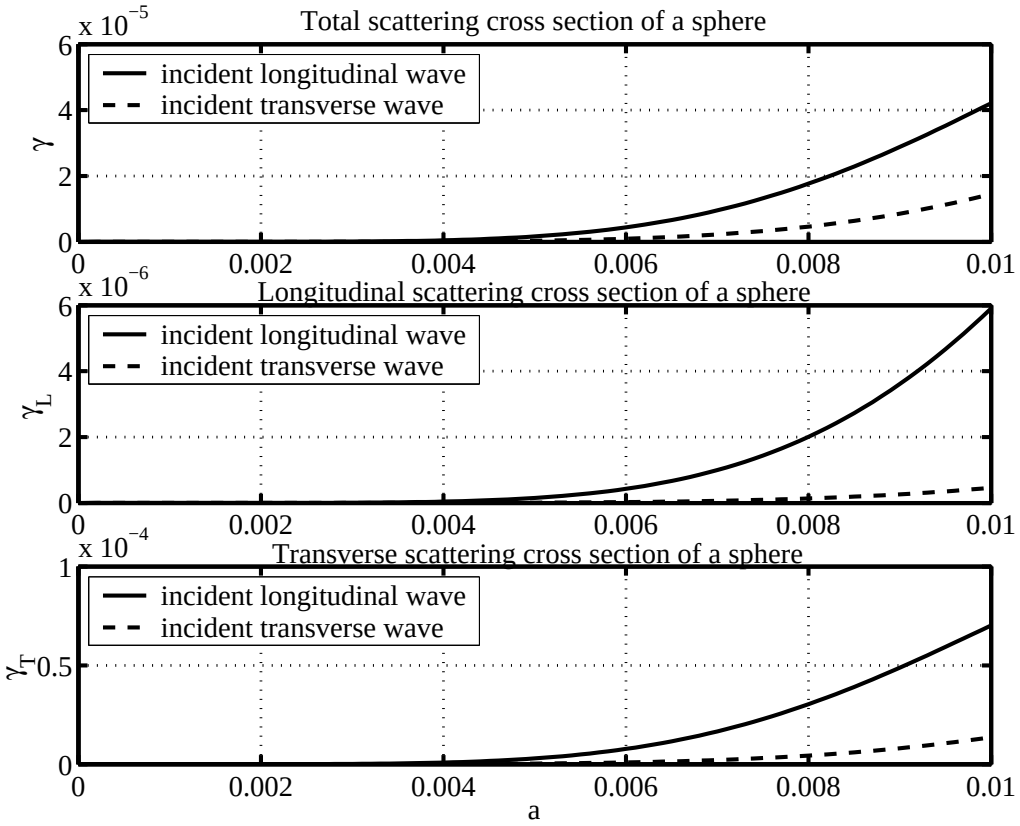

Figure 3.7: Scattering cross sections for a spherical inclusion in dependence of the radius a.

Again, especially for the incident transverse but also for the incident longitudinal wave, the scattered longitudinal wave is very weak and can be neglected in the total scattering cross section. A comparison between the incident transverse and longitudinal wave shows that the scattered wave is much stronger in the latter case.

It is obvious that the scattering cross section depends strongly on the size of the scatterer. If a material contains several inclusions with the size varying more than approximately 50%, it is hard to see any attenuation caused by the smaller inclusions (under the assumption that the scatterers do not influence each other). But also for the case of multiple scattering, this result indicates that it is difficult to distinguish the scattering of a small obstacle in material composed of many and even bigger scatterers, as it is the case for the detection of microcracks in polycrystalline materials.

3.2.2.3 Dependence on the scatterer shape

As mentioned above, the scattering cross section depends (for all kinds of inclusions besides spheres) in addition to frequency and size on the shape of the obstacle in combination with its orientation to the incident wave. This has an influence on the multiple scattering problem in polycrystalline materials with elongated grains which is treated for example by Ahmed [4]. In this chapter, the effect of the scatterer shape and orientation is investigated for a single ellipsoidal inclusion with the axes a_1, a_2 and a_3 aligned along the $\mathbf{x}$, $\mathbf{y}$ and $\mathbf{z}$ directions.

Figure 3.8 shows the total scattering cross section for the incident wave propagating in $+\mathbf{z}$ direction. In the left column, the incident wave is longitudinal and the frequency is $f_L = 1 \cdot 10^5$ Hz, whereas the incident wave is transverse with a frequency of $f_T = 0.5 \cdot 10^5$ Hz in the right column, so for each case, the scattering problem lays in the Rayleigh regime. The procedure is such that in each figure, one of the axes of the ellipsoid is increased from $a_i = 1 \cdot 10^{-5}$ m to $a_i = 1 \cdot 10^{-2}$ m, the other two axes are kept constant at a value of $a_k = 5 \cdot 10^{-3}$ m ($k \neq i$). The solid line belongs to the scattering cross section of the ellipsoid with varying shape, the dotted line is the scattering cross section of a sphere with its radius ranging from $a = 1 \cdot 10^{-5}$ m

to $a = 1 \cdot 10^{-2}$ m. Therefore, all solid and dotted curves cut each other at the radius $a_i = 5 \cdot 10^{-3}$ m, when the ellipsoid is identical to the sphere.

It is obvious that the influence of the shape of the inclusion is rather poor compared to the dependence of the scatterer size, because the scattering cross section increases much more for the circle than it does for ellipsoids. This is in good agreement with the results for multiple scattering found in Ahmed [4].

From Figure 3.8, a slight influence of the direction of the elongation on the scattering cross section can be seen. Comparison of the plots for the elongation along the a_1 and a_2 axis shows that there is no difference at all, that means it does not matter if the ellipsoid is elongated in $\mathbf{x}-$ or $\mathbf{y}-$direction for the incident wave propagating in $\mathbf{z}-$direction. However, when the ellipsoid is elongated in the direction of the a_3 axis, the scattering cross section is slightly smaller than for the elongation along the other two axes. This can be explained by the fact that increasing the value for the a_3 axis does not change the area of the scatterer perpendicular to the incident wave.

To distinguish clearly between the influences of shape and size, another model has been generated in which the volume of the scatterer is constant. It is assumed that always two axes of an ellipsoid with the volume $V = 4\pi a_1 a_2 a_3/3$ are identical, for example $a_1 = a_2 \neq a_3$. Then, if one axis (which is denoted by a_k) is changed, the other ones are given by $a_j = \sqrt{3V/4\pi a_k}$. As can be seen in Figure 3.9, if $a_1 = a_3$ the scattering cross section is the same as for $a_2 = a_3$. These are the cases in which the ellipsoid is elongated along the $\mathbf{y}-$ and $\mathbf{x}-$axis, respectively. If the elongation occurs in the direction of the incident wave, i.e. the $\mathbf{z}-$direction, the scattering cross section is different. This is again due to the fact that in the first two configurations, the scatterer area normal to the incident wave is the same, but it is different in the third case.

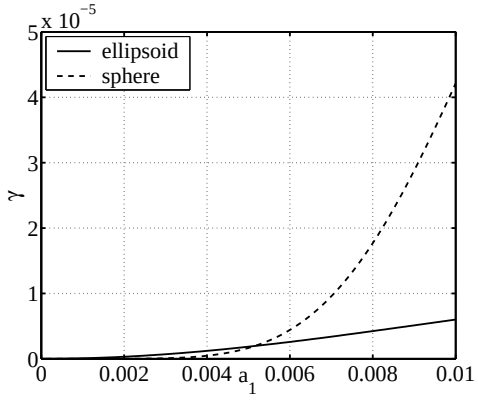

(a) Incident longitudinal wave, a_1 varies, a_2 and a_3 are constant

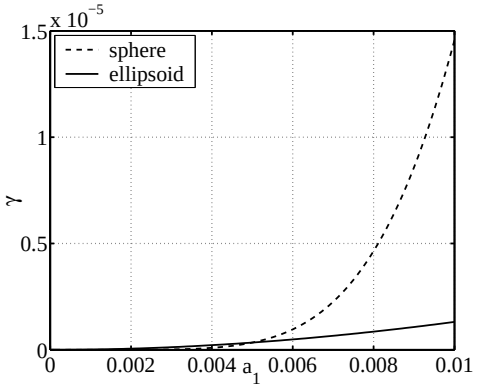

(b) Incident transverse wave, a_1 varies, a_2 and a_3 are constant

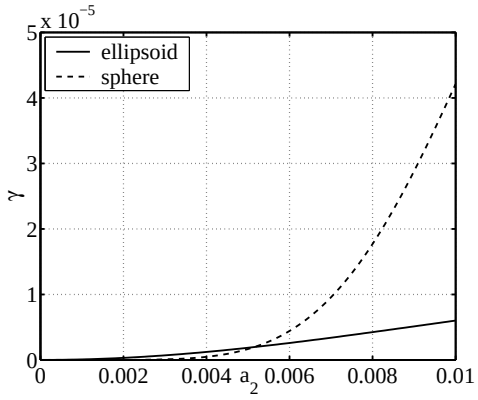

(c) Incident longitudinal wave, a_2 varies, a_1 and a_3 are constant

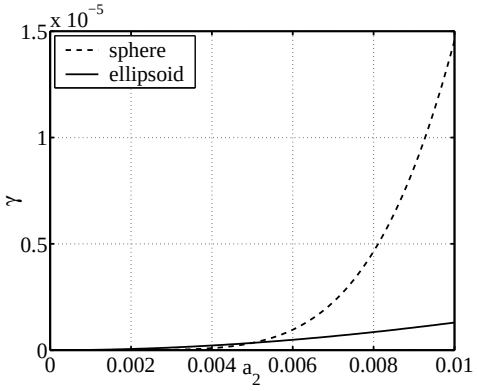

(d) Incident transverse wave, a_2 varies, a_1 and a_3 are constant

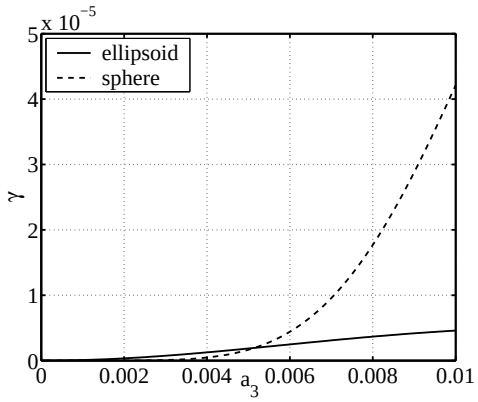

(e) Incident longitudinal wave, a_3 varies, a_1 and a_2 are constant

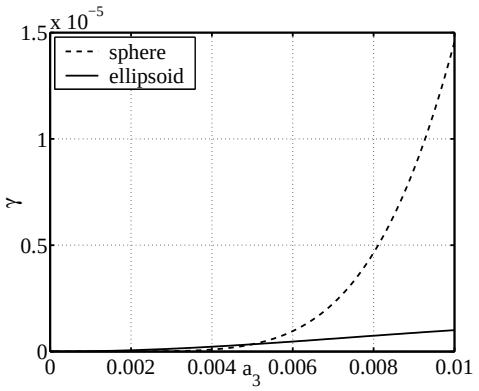

(f) Incident transverse wave, a_3 varies, a_1 and a_2 are constant

Figure 3.8: Total scattering cross sections for an ellipsoidal inclusion.

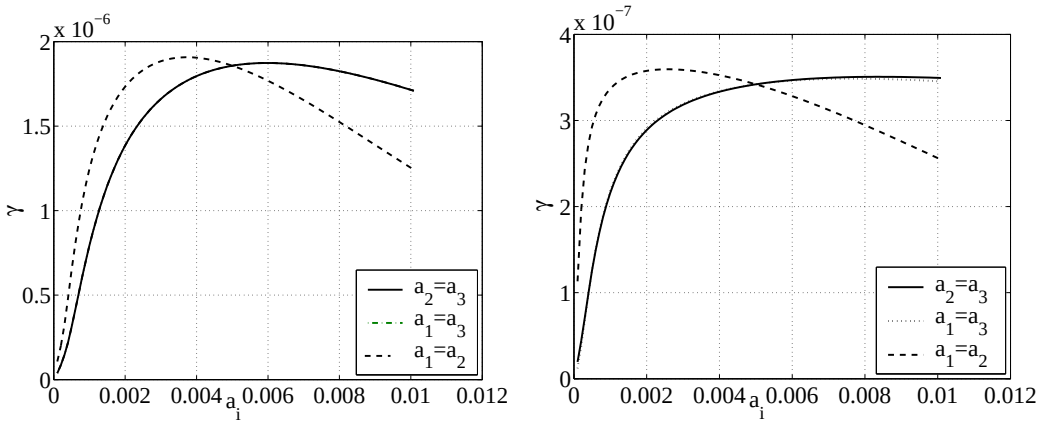

(a) Incident longitudinal wave (b) Incident transverse wave

Figure 3.9: Total scattering cross sections for an ellipsoidal inclusion.

3.2.2.4 Dependence on the scatterer orientation

The scattering problem for the incident wave propagating in an arbitrary direction is solved in Gubernatis [18] by using the quasistatic approximation. In this study, the dependence on the scattering orientation is investigated with the Born approximation.

The influence of the directional orientation of the inclusion to the scattering cross section can be treated in two equivalent ways:

- Keep the direction of the incident wave and rotate the scatterer.
- Change the direction of the incident wave while the inclusion remains in the same position.

The definition of the shape factor in Section 3.1.2 makes it easier to apply the second method.

For propagation in an arbitrary direction, the incident wave is defined as

$$u_i^{\mathrm{i}} = \hat{a}_i^{\mathrm{i}} \mathrm{e}^{i\mathbf{k}^i \cdot \mathbf{r}'} \tag{3.38}$$

where $\hat{\mathbf{a}}^{\mathrm{i}}$ is the amplitude vector and $\mathbf{k}^{\mathrm{i}} = k^{\mathrm{i}}\hat{\mathbf{b}}$ is the incident wave vector. If $\hat{\mathbf{b}}$ is parallel to $\hat{\mathbf{a}}$, the incidence wave is longitudinal, and it is transverse if these vectors

are perpendicular to each other.

Thus, the shape factor has to be modified from Equation 3.28 for the incident wave propagating in $+\mathbf{z}-$direction to the more general case of oblique incidence as

$$S(p,q) = \int_V \mathrm{e}^{i(p\hat{\mathbf{b}^i} - q\hat{r})\cdot\mathbf{r}'} \mathrm{d}V' \tag{3.39}$$

where the unit vector defining the direction of the incidence wave is now given as

$$\hat{\mathbf{b}}^{\mathrm{i}} = \begin{pmatrix} \sin(\theta^{\mathrm{i}})\cos(\phi^{\mathrm{i}}) \\ \sin(\theta^{\mathrm{i}})\sin(\phi^{\mathrm{i}}) \\ \cos(\theta^{\mathrm{i}}) \end{pmatrix}$$

and the supercscript $^{\mathrm{i}}$ denotes the incident wave. The angles θ^{i} and ϕ^{i} are both in the range of $[0; 2\pi]$, if any symmetry of the scatterer is neglected.

By this choice of the direction of the incident wave, the amplitude vector $\hat{\mathbf{a}}^{\mathrm{i}}_L$ for the longitudinal wave and $\hat{\mathbf{a}}^{\mathrm{i}}_T$ for the transverse wave are determined as

$$\hat{\mathbf{a}}^{\mathrm{i}}_L = \begin{pmatrix} \sin(\theta^{\mathrm{i}})\cos(\phi^{\mathrm{i}}) \\ \sin(\theta^{\mathrm{i}})\sin(\phi^{\mathrm{i}}) \\ \cos(\theta^{\mathrm{i}}) \end{pmatrix} \quad , \qquad \hat{\mathbf{a}}^{\mathrm{i}}_T = \begin{pmatrix} -\cos(\theta^{\mathrm{i}})\cos(\phi^{\mathrm{i}}) \\ -\cos(\theta^{\mathrm{i}})\sin(\phi^{\mathrm{i}}) \\ \sin(\theta^{\mathrm{i}}) \end{pmatrix}.$$

In the following an ellipsoidal inclusion is regarded. Then the shape factor is defined for oblique incidence as

$$S = 4\pi a_1 a_2 a_3 \frac{\sin(\Delta K^{\mathrm{i}}) - \Delta K^{\mathrm{i}}\cos(\Delta K^{\mathrm{i}})}{(\Delta K^{\mathrm{i}})^3} \tag{3.40}$$

where ΔK^{i} is given by

$$\Delta K^{\mathrm{i}} = \sqrt{\Delta k_1^{\mathrm{i}^2} a_1^2 + \Delta k_2^{\mathrm{i}^2} a_2^2 + \Delta k_3^{\mathrm{i}^2} a_3^2}$$

For the incident longitudinal wave, the components of $\Delta\mathbf{k}^{\mathbf{i}}$ are defined as

$$\begin{aligned} \Delta k_1^{\mathrm{i}} &= \alpha \sin\theta^{\mathrm{i}} \cos\phi^{\mathrm{i}} - q \sin\theta\cos\phi \\ \Delta k_2^{\mathrm{i}} &= \alpha \sin\theta^{\mathrm{i}} \sin\phi^{\mathrm{i}} - q \sin\theta\sin\phi \\ \Delta k_3^{\mathrm{i}} &= \alpha \cos\theta^{\mathrm{i}} - q\cos\theta \end{aligned} \tag{3.41}$$

and for the incident transverse wave as

$$\begin{aligned} \Delta k_1^{\mathrm{i}} &= \beta \cos\theta^{\mathrm{i}} \cos\phi^{i} - q \sin\theta \cos\phi \\ \Delta k_2^{\mathrm{i}} &= \beta \cos\theta^{\mathrm{i}} \sin\phi^{\mathrm{i}} - q \sin\theta \sin\phi \\ \Delta k_3^{\mathrm{i}} &= -\beta \sin\theta^{\mathrm{i}} - q \cos\theta \end{aligned} \tag{3.42}$$

with q being again either α or β and the a_i being the axes of the ellipsoid.

Furthermore, the f vector is now expressed as

$$f_i(k) = \frac{k^2}{4\pi\rho\omega^2} \left(\delta\rho\omega^2 \hat{a}_i + i\hat{r}_j \delta C_{ijkl} e_{kl}^{\mathrm{i}} \right) S(p,q) \tag{3.43}$$

where e_{ij}^{i} is the amplitude of the strain field caused by the incident wave and is given by

$$e_{ij}^{\mathrm{i}} = \frac{ik}{2} \left(\hat{b}_i \hat{a}_j + \hat{b}_j \hat{a}_i \right). \tag{3.44}$$

Figure 3.10 shows the dependence of the scattering cross section of an ellipsoidal aluminum inclusion with axes $a_1 = 0.01$ m, $a_2 = 0.003$ m and $a_3 = 0.001$ m in titanium on the direction of the incident wave. In the left column, the incident wave is purely longitudinal with a frequency of $f_{\mathrm{L}} = 1 \cdot 10^5$ Hz, and it is purely transverse in the right column with $f_{\mathrm{T}} = 0.5 \cdot 10^5$ Hz, so for all incident waves, the scattering problem lays in the Rayleigh domain. The longitudinal and transverse wave are incident from any possible direction, thus θ^{i} varies between 0 and π, whereas ϕ^{i} varies between 0 and 2π radians.

From Figure 3.10 it is obvious that the directivity pattern of the scattering cross sections shows some symmetry. More precisely, the magnitude of all scattering cross sections repeats after π, for the polar angle θ^{i} as well as for the azimuthal angle ϕ^{i}. This is clear by looking at the shape of the ellipsoid, which contains three planes of symmetry. Hence, changing either θ^{i} or ϕ^{i} by π leads to the same scattering situation, because the incident wave impinges again on the same shape. On the other hand this means that for an arbitrary shaped inclusion without any symmetry, the scattering

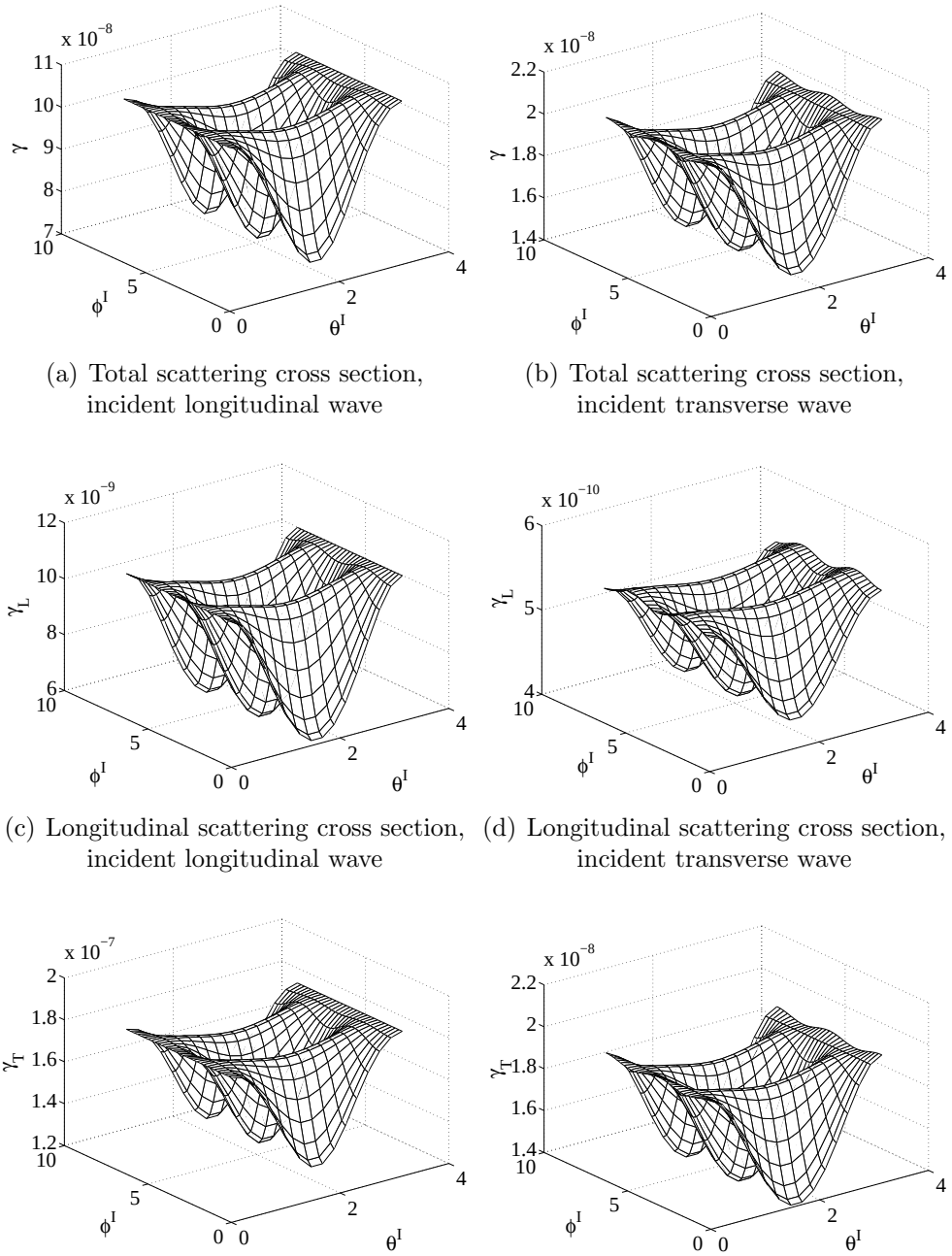

(a) Total scattering cross section, incident longitudinal wave

(b) Total scattering cross section, incident transverse wave

(c) Longitudinal scattering cross section, incident longitudinal wave

(d) Longitudinal scattering cross section, incident transverse wave

(e) Transverse scattering cross section, incident longitudinal wave

(f) Transverse scattering cross section, incident transverse wave

Figure 3.10: Scattering cross sections for an ellipsoidal inclusion with oblique incidence.

cross section has no spatial symmetry either.

For both types of the incident wave, the maxima and minima of the scattering cross section occur for the incident wave propagating in the same direction. Precisely, the maxima are at $\theta^{\mathrm{i}} = 0,\ \pi$, and $\phi^{\mathrm{i}} = 0, \pi, 2\pi$. This corresponds to the incident wave propagating either in $+\mathbf{z}$ or $-\mathbf{z}$ -direction. In these cases, the scatterer area normal to the direction of the incident wave is also maximum, since it is determined by a_1 and a_2. Similarly, the minima of the scattering cross sections are found to be at $\theta^{\mathrm{i}} = \pi/2$, and $\phi^{\mathrm{i}} = 0,\ \pi,\ 2\pi$, for which the incident wave is propagating in $\pm\mathbf{x}-$direction with a minimum normal scatterer area. Furthermore, the directivity dependence is the same for the transverse scattering cross section as it is for the longitudinal scattering cross section.

3.3 Exact solution

The exact solution for the scattering problem at an isotropic sphere takes the form of an infinite harmonic series of spherical vector functions. The derivation of the infinite series and the solution of the boundary problem is either based on wave vector potentials (see Brill [10]) or on the wave displacement field as in Yang [50].

3.3.1 Scattered stress and displacement fields

In terms of an infinite series, it is possible to find the exact solution for the scattering of a plane wave at a spherical, isotropic inclusion. The advantage is, that by taking this approach, the far-field approximation $r \to \infty$ is not necessary, and thus the viscoelastic properties of a lossy medium can be described correctly. The description of the exact solution for the scattered displacement field is found in Eringen [14] and the notation is adopted from Kanaun et al. [24]. In the following sections, the time dependency is always $\mathrm{e}^{-i\omega t}$, but it is suppressed for brevity.

3.3.1.1 Incident longitudinal wave

First, the incident longitudinal wave is treated. Consider the incident wave propagating in $\mathbf{z}-$direction in the form of a series of spherical vector functions

$$\mathbf{u}^{\mathrm{i}} = \mathbf{e}_3 \mathrm{e}^{i\alpha_{\mathrm{eff}} z} = -\frac{1}{\alpha_{\mathrm{eff}}} \sum_{n=0}^{\infty} i^{n+1}(2n+1)\mathbf{L}^1_{0n}(\mathbf{r}) \tag{3.45}$$

with the vector $\mathbf{L}^1_{0n}$ defined as

$$\mathbf{L}^1_{0n} = \mathbf{e}^r \frac{\mathrm{d}j_n(\alpha_{\mathrm{eff}} r)}{\mathrm{d}r} P_n(\cos\theta) + \mathbf{e}^\theta \frac{j_n(\alpha_{\mathrm{eff}} r)}{r} \frac{\mathrm{d}P_n(\cos\theta)}{\mathrm{d}\theta}. \tag{3.46}$$

Here, $P_n(\cos\theta)$ is the Legendre polynomial of order n, and $j_n(z)$ is the spherical Bessel function of order n. The basic vectors of the spherical coordinate system (r, θ, ϕ) in $r-, \theta-$ and $\phi-$direction are denoted with $\mathbf{e}^r$, $\mathbf{e}^\theta$ and $\mathbf{e}^\phi$, while $\mathbf{e}_3$ is the unit vector of the z-axis of the cartesian coordinate system (x, y, z).

In terms of a series of spherical vector functions, the scattered displacement field is

$$\mathbf{u}^{\mathrm{s}} = \sum_{n=0}^{\infty} \left(a_n \mathbf{L}^3_{0n} + b_n \mathbf{N}^3_{0n} \right) \tag{3.47}$$

and the transmitted field inside the inclusion is

$$\mathbf{u}^{\mathrm{t}} = \sum_{n=0}^{\infty} \left(a'_n \mathbf{L}'^1_{0n} + b'_n \mathbf{N}'^1_{0n} \right) \tag{3.48}$$

where the following definitions hold

$$\begin{aligned} \mathbf{L}^3_{0n} &= \mathbf{e}^r \frac{\mathrm{d}h_n(\alpha_{\mathrm{eff}} r)}{\mathrm{d}r} P_n(\cos\theta) + \mathbf{e}^\theta \frac{h_n(\alpha_{\mathrm{eff}} r)}{r} \frac{\mathrm{d}P_n(\cos\theta)}{\mathrm{d}\theta} \\ \mathbf{N}^3_{0n} &= \mathbf{e}^r \frac{n(n+1)}{r} h_n(\beta_{\mathrm{eff}}) P_n(\cos\theta) + \mathbf{e}^\theta \frac{1}{r} \frac{\mathrm{d}}{\mathrm{d}r} \left[r h_n(\beta_{\mathrm{eff}} r) \right] \frac{\mathrm{d}P_n(\cos\theta)}{\mathrm{d}\theta}. \end{aligned} \tag{3.49}$$

In the above equations, $h_n(z)$ are the spherical Hankel functions of the first kind. One obtains $\mathbf{L}'^1_{0n}$ and $\mathbf{N}'^1_{0n}$ from $\mathbf{L}^3_{0n}$ and $\mathbf{N}^3_{0n}$ by replacing $h_n(z)$ with the spherical Bessel function $j_n(z)$. The prime denotes that the wavenumbers of the effective medium, α_{eff} and β_{eff} have to be replaced by the wavenumbers of the material inside the inclusion, α_{I} and β_{I}. The constants a_n, b_n, a'_n and b'_n are found from the boundary conditions on the border of the inclusion. These boundary equations are the continuity of the

total displacement and stress fields outside and inside the inclusion (at $r = a$) and are expressed as

$$u_r^{\mathrm{i}}(a) + u_r^{\mathrm{s}}(a) = u_r^{\mathrm{t}}(a), \qquad u_\theta^{\mathrm{i}}(a) + u_\theta^{\mathrm{s}}(a) = u_\theta^{\mathrm{t}}(a), \tag{3.50}$$

$$\sigma_{rr}^{\mathrm{i}}(a) + \sigma_{rr}^{\mathrm{s}}(a) = \sigma_{rr}^{\mathrm{t}}(a), \qquad \sigma_{r\theta}(a)^{\mathrm{i}} + \sigma_{r\theta}^{\mathrm{s}}(a) = \sigma_{r\theta}^{\mathrm{t}}(a). \tag{3.51}$$

By substituting the components of the displacement vectors and stress tensors into Equation 3.50 and Equation 3.51, four linear algebraic equations for the constants a_n, b_n, a'_n and b'_n are obtained, and the system of equations is given as (see Datta et al. [11])

$$\begin{aligned}
\mathbf{L}_n \begin{bmatrix} a_n \\ b_n \end{bmatrix} - \mathbf{L'}_n \begin{bmatrix} a'_n \\ b'_n \end{bmatrix} &= i^{n+1} \frac{2n+1}{\alpha_{\mathrm{eff}}} \begin{bmatrix} f_1^1(\alpha_{\mathrm{eff}} a) \\ f_3^1(\alpha_{\mathrm{eff}} a) \end{bmatrix} \\
\mathbf{M}_n \begin{bmatrix} a_n \\ b_n \end{bmatrix} - \frac{\mu_{\mathrm{I}}}{\mu_{\mathrm{eff}}} \mathbf{M'}_n \begin{bmatrix} a'_n \\ b'_n \end{bmatrix} &= i^{n+1} \frac{2n+1}{\alpha_{\mathrm{eff}}} \begin{bmatrix} f_5^1(\alpha_{\mathrm{eff}} a) \\ f_7^1(\alpha_{\mathrm{eff}} a) \end{bmatrix}
\end{aligned} \tag{3.52}$$

where the matrices $\mathbf{L}_n$ and $\mathbf{M}_n$ are defined as

$$\mathbf{L}_n = \begin{bmatrix} f_1^2(\alpha_{\mathrm{eff}} a) & f_2^2(\alpha_{\mathrm{eff}} a) \\ f_3^2(\alpha_{\mathrm{eff}} a) & f_4^2(\alpha_{\mathrm{eff}} a) \end{bmatrix}, \qquad \mathbf{M}_n = \begin{bmatrix} f_5^2(\alpha_{\mathrm{eff}} a) & f_6^2(\alpha_{\mathrm{eff}} a) \\ f_7^2(\alpha_{\mathrm{eff}} a) & f_8^2(\alpha_{\mathrm{eff}} a) \end{bmatrix}. \tag{3.53}$$

The radial functions $f_m^i(qr), (m = 1, 2, ..., 8; i = 1, 2)$ are

$$\begin{aligned}
f_1^i(\alpha_{\mathrm{I}} r) &= n y_n^i(\alpha_{\mathrm{I}} r) - \alpha_{\mathrm{I}} r y_{n+1}^i(\alpha_{\mathrm{I}} r), \\
f_2^i(\beta_{\mathrm{I}} r) &= n(n+1) y_n^i(\beta_{\mathrm{I}} r), \\
f_3^i(\alpha_{\mathrm{I}} r) &= y_n^i(\alpha_{\mathrm{I}} r), \\
f_4^i(\beta_{\mathrm{I}} r) &= (n+1) y_n^i(\beta_{\mathrm{I}} r) - \beta_{\mathrm{I}} r y_{n+1}^i(\beta_{\mathrm{I}} r), \\
f_5^1(\alpha_{\mathrm{I}} r) &= \left(n^2 - n - \frac{(\beta_{\mathrm{I}} r)^2}{2} \right) y_n^i(\alpha_{\mathrm{I}} r) + 2\alpha_{\mathrm{I}} r y_{n+1}^i(\alpha_{\mathrm{I}} r), \\
f_6^i(\beta_{\mathrm{I}} r) &= n(n+1) \left[(n-1) y_n^i(\beta_{\mathrm{I}} r) - \beta_{\mathrm{I}} r y_{n+1}^i(\beta_{\mathrm{I}} r) \right], \\
f_7^i(\alpha_{\mathrm{I}} r) &= (n-1) y_n^i(\alpha_{\mathrm{I}} r) - \alpha_{\mathrm{I}} r y_{n+1}^i(\alpha_{\mathrm{I}} r), \\
f_8^i(\beta_{\mathrm{I}} r) &= \left(n^2 - 1 - \frac{(\beta_{\mathrm{I}} r)^2}{2} \right) y_n^i(\beta_{\mathrm{I}} r) + \beta_{\mathrm{I}} r y_{n+1}(\beta_{\mathrm{I}} r)
\end{aligned} \tag{3.54}$$

where the following rules apply:

- The wavenumbers α and β have the subscript $_{\text{eff}}$ if they describe the wave in the effective medium, the subscript $_{\text{I}}$ for the wave inside the inclusion and the subscript $_{\text{M}}$ if the wave is propagating in the matrix material.

- If $i = 1$, the functions $y_n^i(z)$ are the spherical Bessel functions $j_n(z)$, whereas for $i = 2$, the functions $y_n^i(z)$ are the spherical Hankel functions $h_n(z)$.

- The matrices $\mathbf{L}'_n$ and $\mathbf{M}'_n$ are defined by the same Equations 3.53 and 3.54, if the functions $f_m^2(\alpha_{\text{eff}}a)$ and $f_l^2(\beta_{\text{eff}}a)$ are replaced by $f_m^1(\alpha_{\text{I}}a)$ and $f_l^1(\beta_{\text{I}}a)$.

3.3.1.2 Incident transverse wave

Now consider the case of an incident transverse wave propagating in the $\mathbf{z}-$direction. It can be expressed in terms of spherical vector functions as

$$\mathbf{u}^{\text{i}} = \mathbf{e}_1 \mathrm{e}^{i\beta_{\text{eff}}z} = \sum_{n=1}^{\infty} \frac{i^n(2n+1)}{n(n+1)} \left[\mathbf{M}_{01n}^1(\mathbf{r}) - \frac{i}{\beta_{\text{eff}}} \mathbf{N}_{01n}^1(\mathbf{r}) \right] \tag{3.55}$$

where $\mathbf{e}_1$ is its polarization vector in the $\mathbf{x}-$direction and the vectors $\mathbf{M}_{01n}^1$ and $\mathbf{N}_{e1n}^1$ are

$$\begin{aligned} \mathbf{M}_{01n}^1 &= \mathbf{e}^\theta j_n(\beta_{\text{eff}}r) \frac{P_n^1(\cos\theta)}{\sin\theta} \cos\phi - \mathbf{e}^\phi j_n(\beta_{\text{eff}}r) \frac{\mathrm{d}P_n^1(\cos\theta)}{\mathrm{d}\theta} \sin\phi, \\ \mathbf{N}_{e1n}^1 &= \mathbf{e}^r \frac{n(n+1)}{r} j_n(\beta_{\text{eff}}r) P_n^1(\cos\theta)\cos\phi + \\ &\quad \left[\mathbf{e}^\theta \frac{\mathrm{d}P_n^1(\cos\theta)}{\mathrm{d}\theta} \cos\phi - \mathbf{e}^\phi \frac{P_n^1(\cos\theta)}{\sin\theta} \sin\phi \right] \frac{1}{r} \frac{\mathrm{d}}{\mathrm{d}r} \left[r j_n(\beta_{\text{eff}}r) \right] \end{aligned} \tag{3.56}$$

with the first associated Legendre polynomials of order n, P_n^1. The scattered and the transmitted field are now given as

$$\begin{aligned} \mathbf{u}^{\text{s}} &= \sum_{n=1}^{\infty} \left(c_n \mathbf{L}_{e1n}^3 + d_n \mathbf{M}_{o1n}^3 + e_n \mathbf{N}_{e1n}^3 \right), \\ \mathbf{u}^{\text{t}} &= \sum_{n=1}^{\infty} \left(c'_n \mathbf{L}_{e1n}^{1'} + d'_n \mathbf{M}_{o1n}^{1'} + e'_n \mathbf{N}_{e1n}^{1'} \right) \end{aligned} \tag{3.57}$$

where $\mathbf{M}_{01n}^3$ and $\mathbf{N}_{e1n}^3$ are obtained from $\mathbf{M}_{01n}^1$ and $\mathbf{N}_{e1n}^1$ by replacing the functions $j_n(z)$ by $h_n(z)$; and $\mathbf{L}_{e1n}^3$ is given by

$$\begin{aligned} \mathbf{L}_{e1n}^3 &= \mathbf{e}^r \frac{\mathrm{d}}{\mathrm{d}r} \left[h_n(\alpha_{\text{eff}}r) \right] P_n^1(\cos\theta)\cos\phi + \\ &\quad \left[\mathbf{e}^\theta \frac{\mathrm{d}P_n^1(\cos\theta)}{\mathrm{d}\theta} \cos\phi - \mathbf{e}^\phi \frac{P_n^1(\cos\theta)}{\sin\theta} \sin\phi \right] \frac{h_n(\alpha_{\text{eff}}r)}{r}. \end{aligned} \tag{3.58}$$

The functions $\mathbf{L}^{1'}_{e1n}, \mathbf{M}^{1'}_{o1n}$ and $\mathbf{N}^{1'}_{e1n}$ are obtained from $\mathbf{L}^{1}_{e1n}, \mathbf{M}^{1}_{o1n}$ and $\mathbf{N}^{1}_{e1n}$ by changing the arguments $\alpha_{\text{eff}} r$ and $\beta_{\text{eff}} r$ to $\alpha_{\text{I}} r$ and $\beta_{\text{I}} r$.

The scattering coefficients c_n, d_n, e_n and the coefficients for the transmitted field c'_n, d'_n and e'_n in Equation 3.57 have to be determined from the boundary conditions at $r = a$. In addition to the continuity equations for the incident longitudinal wave given in Equations 3.50 and 3.51, the incident transverse wave leads to two more continuity equations

$$u^{\text{s}}_{\phi}(a) + u^{\text{i}}_{\phi}(a) = u^{\text{t}}_{\phi}(a), \quad \sigma^{\text{s}}_{\phi r}(a) + \sigma^{\text{i}}_{\phi r}(a) = \sigma^{\text{t}}_{\phi r}(a). \tag{3.59}$$

In the following steps, the system of equations analog to Equation 3.52 is derived for the notation used in Kanaun et al. [24].

The formulae needed for the calculation of the stress field from the displacement field in spherical coordinates are given by Achenbach [2]. The required equations for the stress field components are

$$\begin{aligned} \sigma_{rr} &= \lambda\varepsilon + 2\mu\frac{\partial u}{\partial r} \\ \sigma_{\phi r} &= \mu\left[\frac{\partial w}{\partial r} + \frac{1}{r\sin\theta}\left(\frac{\partial u}{\partial \phi} - w\sin\theta\right)\right] \\ \sigma_{\theta r} &= \mu\left[\frac{\partial v}{\partial r} + \frac{1}{r}\left(\frac{\partial u}{\partial \theta} - v\right)\right] \end{aligned} \tag{3.60}$$

where u, v, w are the components of the displacement field in the r, θ, ϕ directions and the dilatation ε is given as

$$\varepsilon = \frac{\partial u}{\partial r} + \frac{1}{r}\frac{\partial v}{\partial \theta} + \frac{u}{r} + \frac{1}{r\sin\theta}\left(\frac{\partial w}{\partial \phi} + u\sin\theta + v\cos\theta\right). \tag{3.61}$$

By applying the differential equation for the associated Legendre polynomials, which is for the first associated Legendre polynomials given by (Arfken [6])

$$\frac{\mathrm{d}^2 P^1_n(\cos\theta)}{\mathrm{d}\theta^2} + \frac{\cos\theta}{\sin\theta}\frac{\mathrm{d}P^1_n(\cos\theta)}{\mathrm{d}\theta} - \frac{1}{\sin^2\theta}P^1_n(\cos\theta) = -n(n+1)P^1_n(\cos\theta) \tag{3.62}$$

to the dilatational part of the displacement field, ε is simplified to

$$\begin{aligned} \varepsilon^{\mathrm{i}} &= 0 \\ \varepsilon^{\mathrm{s}} &= -c_n h_n(\alpha_{\mathrm{eff}} r) P_n^1(\cos\theta)\alpha_{\mathrm{eff}}^2 \cos\phi \\ \varepsilon^{\mathrm{t}} &= -c'_n j_n(\alpha_{\mathrm{I}} r) P_n^1(\cos\theta)\alpha_{\mathrm{I}}^2 \cos\phi. \end{aligned} \tag{3.63}$$

With further simplifications and especially the use of the differential equations as well as the recurrence relation for spherical Bessel and Hankel functions found in Abramowitz [1] and given by

$$\begin{aligned} \frac{\mathrm{d}^2 f_n(kr)}{\mathrm{d}(kr)^2} &= -\frac{2n}{(kr)^2} f_n kr + \frac{2}{kr} f_{n+1}(kr) + \frac{n(n+1)}{(kr)^2} f_n(kr) - f_n(kr) \\ \frac{\mathrm{d}f_n(kr)}{\mathrm{d}r} &= \frac{n}{r} f_n(kr) - k f_{n+1}(kr) \end{aligned}$$

where f is either j or h and k any wavenumber, one obtains finally the system of equations

$$\begin{aligned} \mathbf{L}_n \begin{bmatrix} c_n \\ e_n \end{bmatrix} - \mathbf{L'}_n \begin{bmatrix} c'_n \\ e'_n \end{bmatrix} &= i^{n+1} \frac{2n+1}{\beta_{\mathrm{eff}} n(n+1)} \begin{bmatrix} f_2^1(\beta_{\mathrm{eff}} a) \\ f_4^1(\beta_{\mathrm{eff}} a) \end{bmatrix} \\ \mathbf{M}_n \begin{bmatrix} c_n \\ e_n \end{bmatrix} - \frac{\mu_{\mathrm{I}}}{\mu_{\mathrm{eff}}} \mathbf{M'}_n \begin{bmatrix} c'_n \\ e'_n \end{bmatrix} &= i^{n+1} \frac{2n+1}{\beta_{\mathrm{eff}} n(n+1)} \begin{bmatrix} f_6^1(\beta_{\mathrm{eff}} a) \\ f_8^1(\beta_{\mathrm{eff}} a) \end{bmatrix} \\ \mathbf{N}_n \begin{bmatrix} d_n \\ d'_n \end{bmatrix} &= -\frac{i^n(2n+1)}{n(n+1)} \begin{bmatrix} f_9^1(\beta_{\mathrm{eff}} a) \\ f_{11}^1(\beta_{\mathrm{eff}} a) \end{bmatrix}. \end{aligned} \tag{3.64}$$

The matrices $\mathbf{L_n}, \mathbf{M_n}, \mathbf{L'_n}$ and $\mathbf{M'_n}$ are defined in Equation 3.53. The radial functions $f_m^i(qr), (m = 1, 2, ..., 8; i = 1, 2)$ are given in Equation 3.54 and the same rules as defined above still hold. The matrix $\mathbf{N}_n$ is defined as

$$\mathbf{N}_n = \begin{bmatrix} f_9^2(\beta_{\mathrm{eff}} a) & f_{10}^1(\beta_{\mathrm{I}} a) \\ f_{11}^2(\beta_{\mathrm{eff}} a) & f_{12}^1(\beta_{\mathrm{I}} a) \end{bmatrix} \tag{3.65}$$

and the radial functions $f_m^i(qr), (m = 9, ..., 12; i = 1, 2)$ are given by

$$\begin{aligned} f_9^i(\beta_{\rm I} r) &= y_n^i(\beta_{\rm I} r), \\ f_{10}^i(\beta_{\rm I} r) &= -y_n^i(\beta_{\rm I} r), \\ f_{11}^i(\beta_{\rm I} r) &= (n-1)y_n^i(\beta_{\rm I} r) - \beta_{\rm I} r y_{n+1}^i(\beta_{\rm I} r), \\ f_{12}^i(\beta_{\rm I} r) &= -\frac{\mu_{\rm I}}{\mu_{\rm eff}}\left((n-1)y_n^i(\beta_{\rm I} r) - \beta_{\rm I} r y_{n+1}^i(\beta_{\rm I} r)\right). \end{aligned} \tag{3.66}$$

A numerical problem arises in the calculation of the scattering coefficients. To solve for a_n, b_n, c_n, d_n and e_n and the corresponding coefficients for the transmitted wave fields, the inverse of the matrix $\mathbf{D}$

$$\mathbf{D} = \begin{bmatrix} \mathbf{L}_n & -\mathbf{L}'_n \\ \mathbf{M}_n & -\frac{\mu_{\rm I}}{\mu_{\rm eff}}\mathbf{M}'_n \end{bmatrix}$$

and the inverse of the matrix $\mathbf{N}_n$ are calculated. Taking the inverse of these matrices is numerically critical due to numerical ill-conditioning, since they contain numbers with the numerical value approaching infinity and numbers with the numerical value approaching zero at once. The big difference in these numbers is caused by the simultaneous appearance of spherical Bessel and Hankel functions of order n and $n+1$ in $\mathbf{D}$ and $\mathbf{N}_n$. To overcome this numerical difficulty, the matrices $\mathbf{D}$ and $\mathbf{N}_n$ are normalized. The normalized system of equations for the calculation of the scattering coefficients is given in the Appendix.

3.3.2 Scattered power

The scattered power on the surface of a sphere with radius $r \geq a$ is determined as (Achenbach [2])

$$P^{\rm s} = \frac{1}{2}{\rm Im}\left(\omega \int_A \sigma_{ij}^{\rm s} n_j \bar{u}_i^{\rm s} {\rm d}S\right) \tag{3.67}$$

where $\sigma_{ij}^{\rm s}$ is the scattered stress field, $\bar{u}_i^{\rm s}$ is the scattered displacement field and n_j is the unit vector normal to the sphere. The overbar in the scattered displacement field

denotes the conjugate-complex value.

In a spherical coordinate system (r, θ, ϕ), the unit vector normal to the surface of a sphere in Equation 3.67 is given as $n_j = (1, 0, 0)$. Thus, the expression $\sigma^{\mathrm{s}}_{ij} n_j \bar{u}^{\mathrm{s}}_i$ is simplified to $\sigma^{\mathrm{s}}_{rr}\bar{u}^{\mathrm{s}}_r + \sigma^{\mathrm{s}}_{\phi r}\bar{u}^{\mathrm{s}}_\phi + \sigma^{\mathrm{s}}_{\theta r}\bar{u}^{\mathrm{s}}_\theta$.

The derivation of the scattered power at the surface of the spherical inclusion is shown for the case of the incident longitudinal wave. From Equations 3.48 and 3.49 it is possible to write the components of the scattered displacement field as

$$\begin{aligned} u^{\mathrm{s}} &= u^{\mathrm{L}}_n(r) P_n(\cos\theta) \\ v^{\mathrm{s}} &= v^{\mathrm{L}}_n(r) \frac{\mathrm{d}P_n(\cos\theta)}{\mathrm{d}\theta} \\ w^{\mathrm{s}} &= 0 \end{aligned} \tag{3.68}$$

with the functions

$$\begin{aligned} u^{\mathrm{L}}_n &= \frac{1}{r}\left[n h_n(\alpha_{\mathrm{eff}} r) - \alpha_{\mathrm{eff}} r h_{n+1}(\alpha_{\mathrm{eff}} r)\right] a_n + \frac{1}{r} n(n+1) h_n(\beta_{\mathrm{eff}} r) b_n \\ v^{\mathrm{L}}_n &= \frac{1}{r} h_n(\alpha_{\mathrm{eff}} r) a_n + \frac{1}{r}\left[(n+1) h_n(\beta_{\mathrm{eff}} r) - \beta_{\mathrm{eff}} r h_{n+1}(\beta_{\mathrm{eff}} r)\right] b_n. \end{aligned} \tag{3.69}$$

By using Equations 3.60 and the differential equation for the Legendre polynomials (compare with Equation 3.62), the required components of the scattered stress field take the form

$$\begin{aligned} \sigma^{\mathrm{s}}_{rr} &= \sum_{n=0}^{\infty} A^{\mathrm{L}}_{rrn}(r) P_n(\cos\theta) \\ \sigma^{\mathrm{s}}_{\theta r} &= \sum_{n=0}^{\infty} A^{\mathrm{L}}_{\theta rn}(r) \frac{\mathrm{d}P_n(\cos\theta)}{\mathrm{d}\theta} \end{aligned} \tag{3.70}$$

with the abbreviations

$$\begin{aligned} A^{\mathrm{L}}_{rrn} &= \mu_{\mathrm{eff}} \left[-\beta^2_{\mathrm{eff}} h_n(\alpha_{\mathrm{eff}} r) + \frac{2}{r^2}(n^2 - n) h_n(\alpha_{\mathrm{eff}} r) + \frac{4}{r}\alpha_{\mathrm{eff}} h_{n+1}(\alpha_{\mathrm{eff}} r)\right] a_n \\ &\quad + \left[\frac{2\mu_{\mathrm{eff}}}{r^2} n(n+1)\left[(n-1) h_n(\beta_{\mathrm{eff}} r) - \beta_{\mathrm{eff}} r h_{n+1}(\beta_{\mathrm{eff}} r)\right]\right] b_n \\ B^{\mathrm{L}}_{rrn} &= \left[\frac{2\mu_{\mathrm{eff}}}{r^2}\left[(n-1) h_n(\alpha_{\mathrm{eff}} r) - \alpha_{\mathrm{eff}} r h_{n+1}(\alpha_{\mathrm{eff}} r)\right]\right] a_n \\ &\quad + \frac{\mu_{\mathrm{eff}}}{r^2}\left[2\beta_{\mathrm{eff}} r h_{n+1}(\beta_{\mathrm{eff}} r) + 2\left(n^2 - 1 - \frac{(\beta_{\mathrm{eff}} r)^2}{2}\right) h_n(\beta_{\mathrm{eff}} r)\right]. \end{aligned} \tag{3.71}$$

Thus, the integrand in Equation 3.67 is obtained as

$$\begin{aligned}\sigma^{\mathrm{s}}_{ij} n_j \bar{u}^{\mathrm{s}}_i &= \sum_{n=0}^{\infty}\sum_{m=0}^{n} A^{\mathrm{L}}_{rrm}(r)\bar{u}^{\mathrm{L}}_{n-m}(r) P_m(\cos\theta) P_{n-m}(\cos\theta) \\ &+ \sum_{n=0}^{\infty}\sum_{m=0}^{n} A^{\mathrm{L}}_{\theta rm}(r)\bar{v}^{\mathrm{L}}_{n-m}(r) \frac{\mathrm{d}P_m(\cos\theta)}{\mathrm{d}\theta}\frac{\mathrm{d}P_{n-m}(\cos\theta)}{\mathrm{d}\theta} \end{aligned} \tag{3.72}$$

by using the identity (Gradshteyn [16])

$$\left(\sum_{n=0}^{\infty} x_n\right)\left(\sum_{n=0}^{\infty} y_n\right) = \sum_{n=0}^{\infty}\left(\sum_{m=0}^{n} x_m y_{n-m}\right).$$

Since the integrand is independent of ϕ, the surface integral is expressed as

$$I = \int_{\phi=0}^{2\pi}\int_{\theta=0}^{\pi} \sigma^{\mathrm{s}}_{ij} n_j \bar{u}^{\mathrm{s}}_i \mathrm{d}S = 2\pi r^2 \int_{\theta=0}^{\pi} \sigma^{\mathrm{s}}_{ij} n_j \bar{u}^{\mathrm{s}}_i \sin\theta \mathrm{d}\theta. \tag{3.73}$$

From Equation 3.72 it is obvious that only the products of the Legendre polynomials and its derivatives depend on θ. Thus, the integration has to be carried out over the products of the Legendre polynomials only. It will be shown that this integration can be simplified by the use of the orthogonality of the Legendre polynomials.

Consider the first term in Equation 3.72. By substituting $y = \cos\theta$, it is possible to write

$$\begin{aligned}&\sum_{n=0}^{\infty}\sum_{m=0}^{n} A^{\mathrm{L}}_{rrm}(r)\bar{u}^{\mathrm{L}}_{n-m}(r) \int_{\theta=0}^{0} P_m(\cos\theta) P_{n-m}(\cos\theta)\sin\theta \mathrm{d}\theta \\ &\quad = \sum_{n=0}^{\infty}\sum_{m=0}^{n} A^{\mathrm{L}}_{rrm}(r)\bar{u}^{\mathrm{L}}_{n-m}(r) \int_{y=-1}^{1} P_m(y) P_{n-m}(y) \mathrm{d}y. \end{aligned} \tag{3.74}$$

The orthogonality of the Legendre polynomials (Gradshteyn [16])

$$\int_{-1}^{1} P_n(x) P_m(x) \mathrm{d}x = \frac{2}{2n+1}\delta_{nm} \tag{3.75}$$

is then applied to simplify Equation 3.74 to

$$\sum_{n=0}^{\infty}\sum_{m=0}^{n} A^{\mathrm{L}}_{rrm}(r)\bar{u}^{\mathrm{L}}_{n-m}(r) \int_{y=-1}^{1} P_m(y) P_{n-m}(y) \mathrm{d}y = \sum_{n=0}^{\infty} A^{\mathrm{L}}_{rrn}(r)\bar{u}^{\mathrm{L}}_{n}(r) \frac{2}{2n+1}. \tag{3.76}$$

It is possible to find orthogonality for the second term in Equation 3.72 by applying a similar substitution as in the previous case. In detail, one obtains the expression

$$\int_0^{\pi} \frac{\mathrm{d}P_m(\cos\theta)}{\mathrm{d}\theta} \frac{\mathrm{d}P_{n-m}(\cos\theta)}{\mathrm{d}\theta} \sin\theta \mathrm{d}\theta = \frac{2m(m+1)}{2m+1}\delta_{(m)(n-m)} \tag{3.77}$$

which is used to simplify

$$\begin{aligned} & \sum_{n=0}^{\infty}\sum_{m=0}^{n} A^{\mathrm{L}}_{\theta rm}(r)\bar{v}^{\mathrm{L}}_{n-m}(r) \int_{\theta=0}^{\pi} \frac{\mathrm{d}P_m(\cos\theta)}{\mathrm{d}\theta} \frac{\mathrm{d}P_{n-m}(\cos\theta)}{\mathrm{d}\theta}\mathrm{d}\theta \\ = & \sum_{n=0}^{\infty} A^{\mathrm{L}}_{\theta rn}(r)\bar{v}^{\mathrm{L}}_{n}(r)\frac{2n(n+1)}{2n+1}. \end{aligned} \tag{3.78}$$

Finally, the scattered power for the incident longitudinal wave is

$$P^{\mathrm{s}}_{\mathrm{L}} = \frac{\omega}{2}\mathrm{Im}\left[2\pi r^2 \sum_{n=0}^{\infty}\left(A^{\mathrm{L}}_{rrn}\bar{u}^{\mathrm{L}}_{n}\frac{2}{2n+1} + A^{\mathrm{L}}_{\theta rn}\bar{v}^{\mathrm{L}}_{n}\frac{2n(n+1)}{2n+1}\right)\right]. \tag{3.79}$$

The derivation of the scattered power for the incident transverse wave follows the same way as for the incident longitudinal wave, but is more complicated since orthogonality for the associated Legendre polynomials cannot be found in all integrals. The resulting equation is

$$P^{\mathrm{s}}_{\mathrm{T}} = \frac{\omega}{2}\mathrm{Im}\left[\pi r^2 \sum_{n=1}^{\infty}\left(A^{\mathrm{T}}_{rrn}\bar{u}^{\mathrm{T}}_{n}\frac{2n(n+1)}{2n+1} + \left(A^{\mathrm{T}}_{\theta rn}\bar{v}^{\mathrm{T}}_{n1} + B^{\mathrm{T}}_{\theta rn}\bar{v}^{\mathrm{T}}_{n2}\right)\frac{2n^2(n+1)^2}{2n+1}\right)\right] \tag{3.80}$$

where $A^{\mathrm{T}}_{rrn}, A^{\mathrm{T}}_{\theta rn}, \bar{u}^{\mathrm{T}}_{n}$ and $\bar{v}^{\mathrm{T}}_{n1}$ are obtained from $A^{\mathrm{L}}_{rrn}, A^{\mathrm{L}}_{\theta rn}, \bar{u}^{\mathrm{L}}_{n}$ and $\bar{v}^{\mathrm{L}}_{n}$ by replacing a_n and b_n with c_n and e_n. The remaining functions in Equation 3.80 are

$$\begin{aligned} B^{\mathrm{T}}_{\theta rn}(r) &= \frac{1}{r}\mu_{\mathrm{eff}}\left[(n-1)h_n(\beta_{\mathrm{eff}}r) - \beta_{\mathrm{eff}}r h_{n+1}(\beta_{\mathrm{eff}}r)\right]d_n \\ v^{\mathrm{T}}_{n2}(r) &= h_n(\beta_{\mathrm{eff}}r)d_n. \end{aligned} \tag{3.81}$$

The scattered power for spherical aluminum inclusions in titanium calculated directly on the surface of the scatterer ($r = a$) is shown in Figure 3.11 for the incident longitudinal and incident transverse wave. The radius of the scatterer is $a = 1 \cdot 10^{-3}$ m. Since the matrix is described as an elastic material, the scattered power is the same

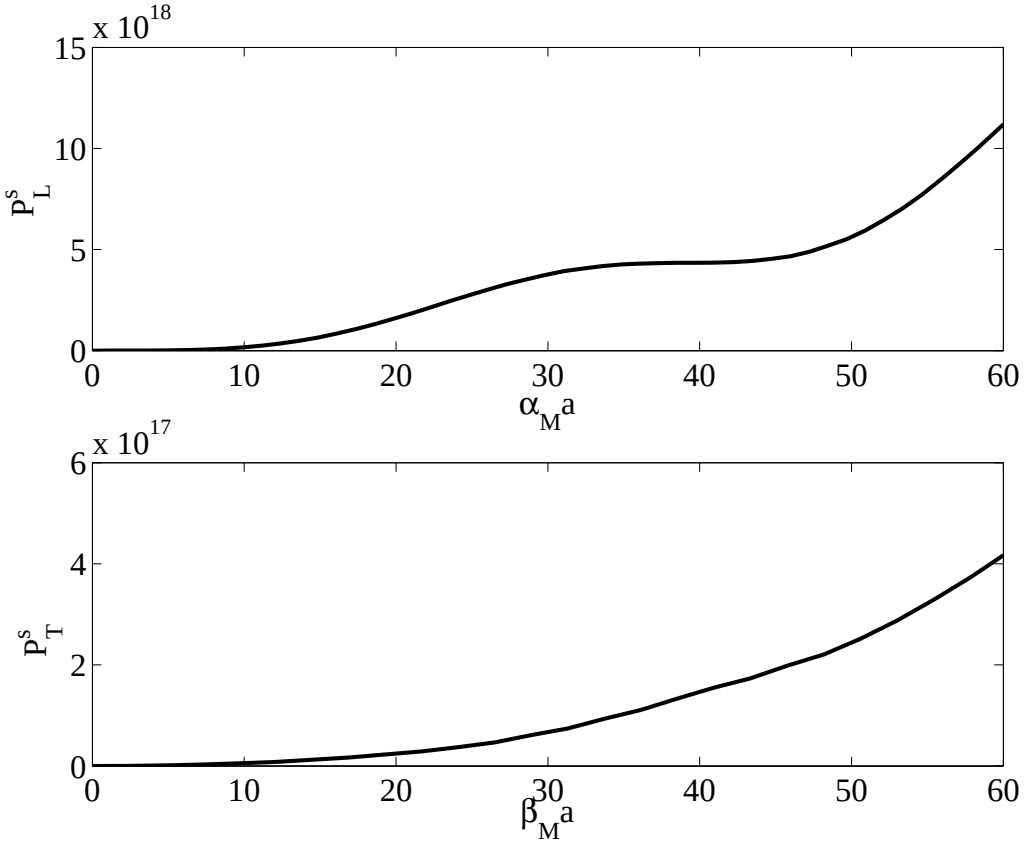

Figure 3.11: Scattered power for an incident longitudinal wave (upper figure) and an incident transverse wave(lower figure).

for all arbitrary values of r with $r \geq a$, or in other words, the scattered power is the same in the near- and far-field.

The scattered power can also be expressed as a far-field approximation. By using the relations

$$h_n(kr)\bar{h}_{n+1}(kr) = \frac{i}{(kr)^2}$$
$$\bar{h}_n(kr)h_{n+1}(kr) = -\frac{i}{(kr)^2} \tag{3.82}$$

where k is any wavenumber, one obtains for the incident longitudinal wave in the far-field

$$P_{\mathrm{L}}^{\mathrm{s}} \sim \pi \mu_{\mathrm{eff}} \omega \sum_{n=0}^{\infty} \left[\frac{2}{2n+1} \frac{\beta_{\mathrm{eff}}^2}{\alpha_{\mathrm{eff}}} a_n \bar{a}_n + \frac{2n(n+1)}{2n+1} \beta_{\mathrm{eff}} b_n \bar{b}_n \right] \equiv P_{\mathrm{L,ff}}^{\mathrm{s}} \tag{3.83}$$

and for the incident transverse wave the far-field approximation

$$P_{\mathrm{T}}^{\mathrm{s}} \sim \frac{1}{2} \pi \mu_{\mathrm{eff}} \omega \sum_{n=1}^{\infty} \left[\frac{2n(n+1}{2n+1} \frac{\beta_{\mathrm{eff}}^2}{\alpha_{\mathrm{eff}}} c_n \bar{c}_n + \frac{2n^2(n+1)^2}{2n+1} \left(\beta_{\mathrm{eff}} e_n \bar{e}_n + \frac{1}{\beta_{\mathrm{eff}}} d_n \bar{d}_n \right) \right] \equiv P_{\mathrm{T,ff}}^{\mathrm{s}}. \tag{3.84}$$

It is again pointed out, that the far-field approximations are very accurate if the matrix material is elastic.

Now consider the case of a viscoelastic matrix material. To this purpose, complex Lamé constants are introduced with $\lambda = \lambda' + i\lambda''$ and $\mu = \mu' + i\mu''$. The resulting matrix has damping effects and the viscoelastic losses in the far-field are illustrated in Figure 3.12. In Figure 3.12, the far-field scattered power calculated with Equations 3.83 and 3.84 are subtracted from the scattered power calculated directly on the surface of the scatterer with Equations 3.79 and 3.80, so that the viscoelastic loss in the scattered power is plotted. The imaginary parts of the Lamé constants are chosen as $\lambda'' = \lambda'/100$ and $\mu'' = \mu'/100$. Note that these values of imaginary parts of the Lamé constants lead to high viscoelastic attenuation coefficients. These values are chosen to amplify the effect of the viscoelastic attenuation and to make clear that care has to be taken in the calculation of the scattered power in the far-field. This point is of specific importance for the multiple scattering approach with the self-consistent scheme, which will be explained in Section 4.3.

3.3.3 Scattering amplitudes

The forward and backward scattering amplitudes are the amplitudes of the scattered wave in the forward and backward direction, i.e. for the incident wave propagating in $+\mathbf{z}$ direction, the forward direction is defined by $\theta = 0$, and the backward direction by $\theta = \pi$. The forward scattering theorem (Varatharajulu [46]) states that for an incident longitudinal wave, the total rate at which energy is transmitted across

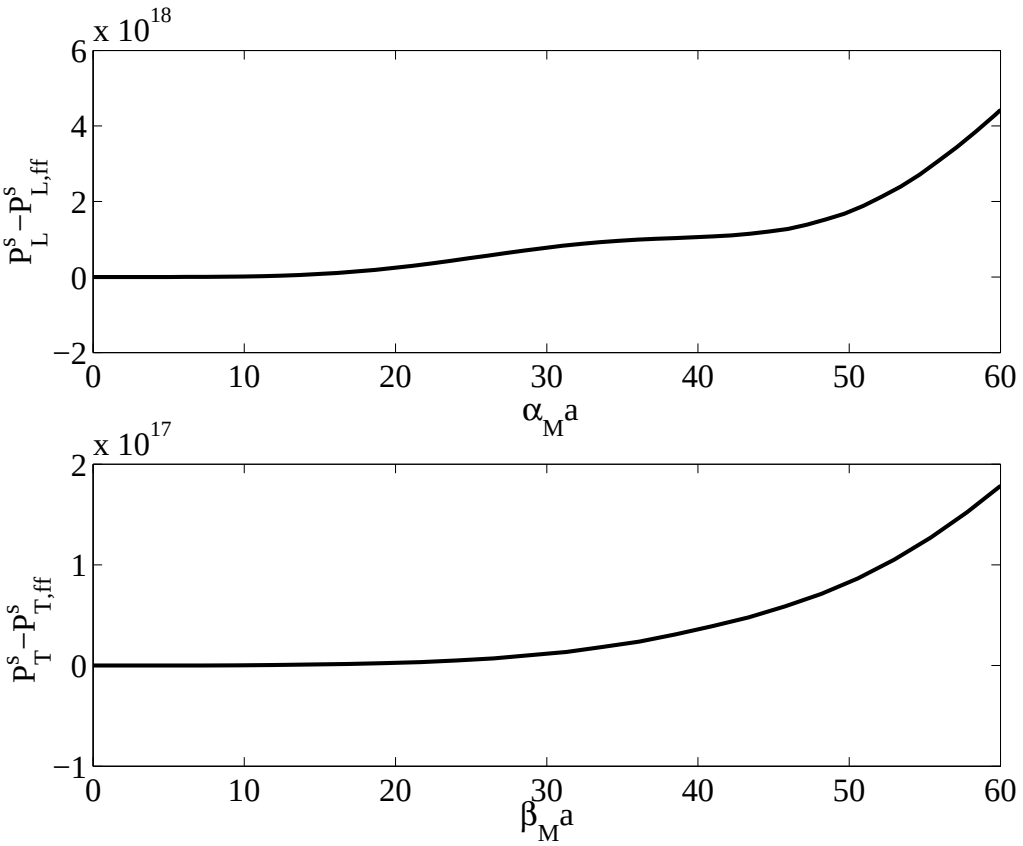

Figure 3.12: Viscoelastic loss of the scattered power in the far-field for an incident longitudinal wave (upper figure) and an incident transverse wave(lower figure).

a closed surface by both scattered longitudinal and shear waves, is directly proportional to the real part of the far-field amplitude of the scattered longitudinal wave in the forward direction. For the case of an incident transverse wave, the total scattered power is proportional to the far-field amplitude of the scattered transverse wave in the forward direction. Based on the forward scattering theorem, the far-field scattering amplitudes are used to describe the rate of the scattered energy.

Consider an incident longitudinal wave propagating in $\mathbf{z}-$direction with unit amplitude as defined in Equation 3.45. The scattered displacement field is then described by Equation 3.47. At a large distance from the scatterer, the displacement is approximated by $\mathbf{u}^{\mathrm{s}} \approx f(\theta)\mathrm{e}^{i\alpha_{\mathrm{eff}}r}\mathbf{e}^{r}/r$. The term $f(\theta)$ is denoted as the far-field scattering

amplitude of the longitudinal wave. It is obtained from the exact solution in Equation 3.47 by considering the component of the displacement field propagating in $\mathbf{e}^r$ direction and by neglecting terms containing the expression $1/r$. In the far-field, the spherical Hankel functions are approximated as (Kim [28])

$$h_n(kr) \sim (-i)^{n+1} \frac{e^{ikr}}{kr} \tag{3.85}$$

where k is either the longitudinal or transverse wavenumber. By applying the recurrence equation given in Abramowitz et al. [1]

$$\frac{\mathrm{d}}{\mathrm{d}z} h_n(z) = \frac{n+1}{z} h_n(z) - h_{n-1}(z) \tag{3.86}$$

with $z = kr$, it is possible to replace the derivative of the spherical Hankel function by the function itself and the spherical Hankel function of reduced order. The far-field scattering amplitude is then determined as

$$f(\theta) = \sum_{n=0}^{\infty} (-i)^n a_n P_n(\cos\theta) \tag{3.87}$$

and for the special cases of the forward ($\theta = 0$) and backward ($\theta = \pi$) directions one obtains

$$f(0) = \sum_{n=0}^{\infty} (-i)^n a_n, \qquad f(\pi) = \sum_{n=0}^{\infty} (i)^n a_n \tag{3.88}$$

by using $P_n(1) = 1$ and $P_n(-1) = (-1)^n$.

For the case of an incident transverse wave propagating in $\mathbf{z}-$direction and polarized in $\mathbf{x}-$direction as given in Equation 3.55, the exact scattered displacement is defined in Equation 3.57, which can be approximated in the far-field by

$$\mathbf{u}^{\mathrm{s}} \approx g_1(\theta,\phi) \frac{\mathrm{e}^{i\beta_{\mathrm{eff}} r}}{r} \mathbf{e}^{\theta} + g_2(\theta,\phi) \frac{\mathrm{e}^{i\beta_{\mathrm{eff}} r}}{r} \mathbf{e}^{\phi} \tag{3.89}$$

where the functions $g_1(\theta,\phi)$ and $g_2(\theta,\phi)$ are the far-field scattering amplitudes of the shear waves in directions of $\mathbf{e}^{\theta}$ and $\mathbf{e}^{\phi}$. By applying Equations 3.86 and 3.85 to Equation 3.57, the far-field scattering amplitudes are found to be

$$\begin{aligned} g_1(\theta,\phi) &= \sum_{n=1}^{\infty} d_n \frac{(-i)^{n+1}}{\beta_{\mathrm{eff}}} \frac{P_n^1(\cos\theta)}{\sin\theta} \cos\phi + e_n (-i)^n \frac{\mathrm{d}P_n^1(\cos\theta)}{\mathrm{d}\theta} \cos\phi \\ g_2(\theta,\phi) &= \sum_{n=1}^{\infty} -d_n \frac{(-i)^{n+1}}{\beta_{\mathrm{eff}}} \frac{\mathrm{d}P_n^1(\cos\theta)}{\mathrm{d}\theta} \sin\phi - e_n (-i)^n \frac{P_n^1(\cos\theta)}{\sin\theta} \sin\phi. \end{aligned} \tag{3.90}$$

The forward and backward scattering amplitudes of the transverse wave are defined as

$$g(0) = \cos\phi g_1(0,\phi) - \sin\phi g_2(0,\phi), \qquad g(\pi) = -\cos\phi g_1(\pi,\phi) - \sin\phi g_2(\pi,\phi). \quad (3.91)$$

Useful equations for the determination of the associated Legendre polynomials and their derivatives at $\theta = 0$ and $\theta = \pi$ are found in Arfken [6] and Morse [33]. For the forward scattering amplitude ($\theta = 0$), the relationships

$$\lim_{\theta\to 0} \frac{P_n^1(\cos\theta)}{\sin\theta} = \lim_{\theta\to 0} \frac{\mathrm{d}P_n^1(\cos\theta)}{\mathrm{d}\theta} = \frac{n(n+1)}{2} \quad (3.92)$$

are used to obtain

$$g(0) = \sum_{n=0}^{\infty} \frac{n(n+1)}{2} \left[d_n (-i)^{n+1} \frac{1}{\beta_{\text{eff}}} + e_n (-i)^n \right]. \quad (3.93)$$

Similarly, the limiting cases for the associated Legendre polynomials in the backward direction ($\theta = \pi$) are

$$\lim_{\theta\to \pi} \frac{P_n^1(\cos\theta)}{\sin\theta} = -\lim_{\theta\to \pi} \frac{\mathrm{d}P_n^1(\cos\theta)}{\mathrm{d}\theta} = -(-1)^n \frac{n(n+1)}{2} \quad (3.94)$$

and give the transverse backward scattering amplitude

$$g(\pi) = \sum_{n=0}^{\infty} \frac{n(n+1)}{2} \left[d_n i^{n+1} \frac{1}{\beta_{\text{eff}}} - e_n i^n \right]. \quad (3.95)$$

In general, it is sufficient to calculate the first few terms in the infinite sum, for the calculation of the scattered power as well as for the calculation of the scattering amplitudes. As a rule of thumb, the sum up to the order $n \approx ka+5$ gives already high accuracy. This can be explained by the fact that the scattering coefficients converge quickly to zero for $n > 2$.

3.4 Comparison of the Born approximation and the exact solution

The results of both single scatterer solutions are compared in terms of the scattering cross section. For the exact solution, the scattering cross sections are obtained from the forward scattering amplitude as

$$\gamma_{\mathrm{L}}(\omega) = \frac{4}{\alpha_{\mathrm{M}} a^2} \mathrm{Im}\{f(0)\} \tag{3.96}$$

for the incident longitudinal wave and

$$\gamma_{\mathrm{T}}(\omega) = \frac{4}{\beta_{\mathrm{M}} a^2} \mathrm{Im}\{g(0)\} \tag{3.97}$$

for the incident transverse wave. These equations are found in Kanaun et al. [24] in accordance to Kim's [28] equations for the extinction cross section. This is due to the fact that the scattering cross section is equal to the extinction cross section for elastic materials without damping effects. In this context, the subscripts $_L$ and $_T$ characterize the incident wave and not the scattered waves as before, and thus γ_{L} and γ_{T} are both total scattering cross sections.

Note that the scattering cross section following from the exact solution approach can also be calculated from the scattered power. The time rate at which energy is scattered by an obstacle is defined by Ying et al. [52] as $\dot{Q}_k^{\mathrm{s}} = P_k^{\mathrm{s}}/2$, where k is either L or T. The energy per unit area carried per unit time by the incident wave is

$$\dot{F}_{\mathrm{L}}^{\mathrm{i}} = \frac{\rho_{\mathrm{M}} \omega^3}{\alpha_{\mathrm{M}}}, \quad \dot{F}_{\mathrm{T}}^{\mathrm{i}} = \frac{\rho_{\mathrm{M}} \omega^3}{\beta_{\mathrm{M}}} \tag{3.98}$$

and the scattering cross sections are

$$\gamma_k = \frac{\dot{Q}_k^{\mathrm{s}}}{\dot{F}_k^{\mathrm{i}}}. \tag{3.99}$$

The results obtained from Equation 3.99 are exactly the same as the ones obtained from Equations 3.96 and 3.97.

Figure 3.13 shows the normalized scattering cross sections for an incident longitudinal wave (upper figure) and an incident transverse wave (lower figure) calculated with the

scattering amplitude of the exact solution (solid lines) and with Equation 3.37 for the Born approximation (dashed lines). The results are plotted for spherical aluminum inclusions in titanium with the material properties as given in Table 3.1. From Fig-

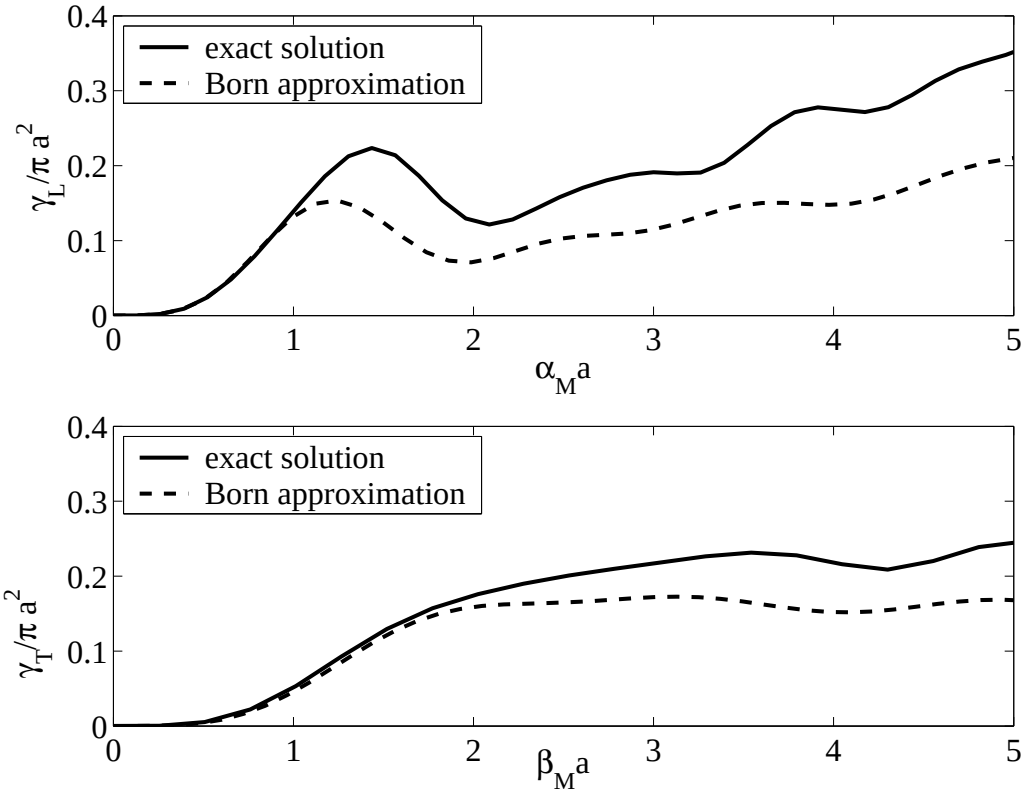

Figure 3.13: Scattering cross sections for an incident longitudinal wave (upper figure) and an incident transverse wave(lower figure).

ure 3.13, it is obvious that the Born approximation gives accurate results for the low frequencies in the Rayleigh domain. For the incident longitudinal wave, the Born approximation gives satisfactory results up to $\alpha_{\mathrm{M}}a \approx 1$, and for the incident transverse wave up to $\beta_{\mathrm{M}}a \approx 1.5$. For higher frequencies, the scattering cross sections calculated with the Born approximation are too low.

In summary, the exact solution is the only possibility to solve the single scattering problem accurately in the high frequency domain. For low frequencies, the Born approximation has some advantages compared to the exact solution. These advantages are especially the simple application of the Born approximation to different scatterer

shapes and the treatment of oblique incidence on the scatterer which corresponds to the scattering at inclusions in different orientations. Note that the Born approximation gives rather poor results for all frequencies, if the material properties of the matrix and the inclusion show big differences, as it is the case for cracks or voids in the matrix material.

CHAPTER 4

Multiple Scattering

Multiple scattering is important for materials containing many inclusions or obstacles, where the volume fraction of the inclusions is higher than approximately 20%. In one sense, multiple scattering means that the interactions between the single scatterers can no longer be neglected. The individual, single inclusions influence each other because the scattered wave is scattered again at its neighboring scatterers (obstacles).

For polycrystalline materials, each grain boundary acts as a scatterer. Thus, the volume fraction of the scatterers is 100%, making it extremely important to include the multiple scattering effect.

There are several approaches for treating multiple scattering, for example the differential self-consistent approach for multiple scattering at cracks in Littles [31] or the self-consistent scheme for multiple scattering in composites in Kim [25] and Kanaun et al. [24]. Treatments of scattering in polycrystalline materials can be found in Ahmed [3] and Turner [45].

4.1 The model of Waterman and Truell

The treatment of multiple scattering in composite materials is developed by Waterman et al. [47]. This theory is referred to as the Waterman and Truell theory. Multiple scattering in cubic polycrystalline materials is treated by Rose [37].

The theory developed in Waterman et al. [47] is valid for spherical inclusions in isotropic materials. It is further restricted to low volume fractions of the inclusions,

i.e. for concentrations of inclusions $f_\mathrm{I} < 20\%$. The volume fraction of the inclusions is defined as $f_\mathrm{I} = V_\mathrm{I}/V$, where V_I is the volume of all the scatterers (inclusions) and V is the total volume under consideration (inclusions and matrix material). An extension of the theory of Waterman and Truell that is applicable for higher volume fractions has been developed by Sayers [40].

For the case of an incident longitudinal wave, Waterman and Truell find for the complex effective wavenumber $\alpha^*_\mathrm{eff} = \alpha'_\mathrm{eff} + i\alpha''_\mathrm{eff}$ the relation

$$\left(\frac{\alpha^*_\mathrm{eff}}{\alpha_\mathrm{M}}\right) = \left(1 + \frac{2\pi n_0 f(0)}{\alpha^2_\mathrm{M}}\right)^2 - \left(\frac{2\pi n_0 f(\pi)}{\alpha^2_\mathrm{M}}\right)^2 \tag{4.1}$$

where $f(0)$ and $f(\pi)$ are the forward and backward scattering amplitudes for the scattered longitudinal wave of a single scatterer. For spherical inclusions, the number of scatterers per unit volume n_0 is related to the concentration or volume fraction f_I of the scatterers by

$$n_0 = \frac{3f_\mathrm{I}}{4\pi a^3}.$$

For an incident transverse wave, the effective transverse wavenumber $\beta^*_\mathrm{eff} = \beta'_\mathrm{eff} + \beta''_\mathrm{eff}$ is given by

$$\left(\frac{\beta^*_\mathrm{eff}}{\beta_\mathrm{M}}\right) = \left(1 + \frac{2\pi n_0 g(0)}{\beta^2_\mathrm{M}}\right)^2 - \left(\frac{2\pi n_0 g(\pi)}{\beta^2_\mathrm{M}}\right)^2 \tag{4.2}$$

with $g(0)$ and $g(\pi)$ denoting the forward and backward scattering amplitudes for the scattered shear wave.

The longitudinal and transverse scattering coefficients, $\alpha_\mathrm{L} = \alpha''_\mathrm{eff}$ and $\alpha_\mathrm{T} = \beta''_\mathrm{eff}$ are directly determined from Equations 4.1 and 4.2 by calculating α^*_eff and β^*_eff and taking the imaginary part of the according effective wavenumber. Figure 4.1 shows the longitudinal and transverse attenuation coefficients for spherical aluminum inclusions in titanium normalized to the (purely real) wavenumbers of the matrix material, α_M or β_M, plotted over the normalized frequency $\alpha_\mathrm{M} a$. The material properties of titanium and aluminum are defined in Table 3.1. Both attenuation coefficients are plotted for 5% and 15% volume fraction of the inclusions. The forward and backward scattering

amplitudes in Equation 4.1 and 4.2 are determined from the exact solution approach for the single scatterer, i.e. with Equations 3.88, 3.93 and 3.95.

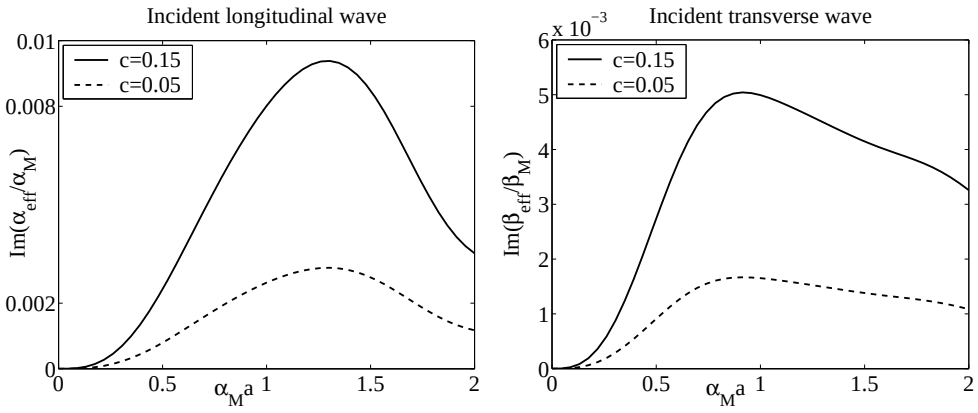

(a) Longitudinal attenuation coefficient. (b) Transverse attenuation coefficient.

Figure 4.1: Attenuation coefficients obtained from the model of Waterman and Truell.

4.2 Differential self-consistent scheme

The differential self-consistent scheme is based on the theory of effective elastic constants. By this, the elastic properties of a material with inclusions are calculated. In the next step, a differential or an algebraic equation describing the scattering cross section in terms of the volume fraction of the inclusions is derived.

4.2.1 Effective elastic moduli using the Mori-Tanaka method

There exist some micromechanical models which treat the determination of the effective elastic constants in a medium containing inclusions with different material properties. In this context, the surrounding material is referred to as the matrix material. Micromechanical models appropriate for the application in the differential self-consistent scheme include Eshelby's theory derived in Eshelby [15], a micromechanical self-consistent model for static effective material properties in Gubernatis et al. [21] and the Mori-Tanaka method, which will be used in this study. Overviews and comparisons between these models can be found in Mura [34].

This description of the Mori-Tanaka method follows Mura [34]. The formal structure of a composite material with volume D is shown in Figure 4.2. The stiffness tensor of the matrix material is denoted with $\mathbf{C}^{(0)}$, the stiffness tensors of the inclusions are $\mathbf{C}^{(1)}$, $\mathbf{C}^{(2)}$, $\mathbf{C}^{(3)}$,$\cdots$,$\mathbf{C}^{(N)}$.

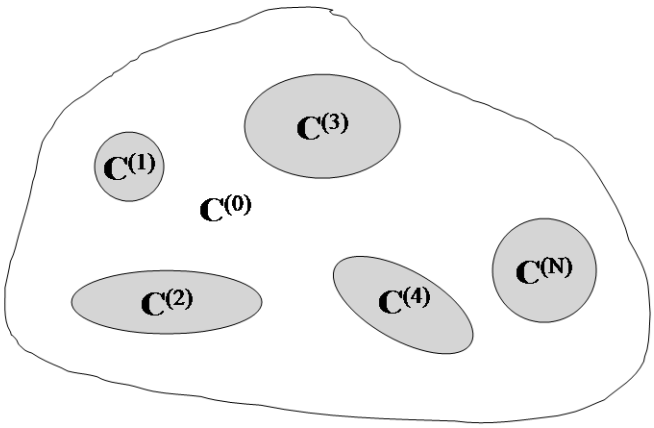

Figure 4.2: Structure of the composite material

Consider a traction σ prescribed on the boundary S of the composite with

$$\sigma \cdot \mathbf{n} = \sigma^0 \cdot \mathbf{n}. \tag{4.3}$$

By the average stress theorem, the average stress is then given by

$$\bar{\sigma} = \sigma^0 = \frac{1}{D} \int_D \sigma \mathrm{d}V = \sum_{r=0}^{N} f_r \bar{\sigma}_r \tag{4.4}$$

where f_r is the volume fraction of the single inclusion depicted with the subscript $_r$. The average stress in the r^{th} phase is

$$\bar{\sigma}_r = \frac{1}{\Omega_r} \int_{\Omega_r} \sigma \mathrm{d}V, \qquad r = 0, 1, \cdots, N \tag{4.5}$$

with Ω_r being the volume of the r^{th} inhomogeneity. The average strain in the r^{th} phase is defined as

$$\bar{\varepsilon}_r = \frac{1}{\Omega_r} \int_{\Omega_r} \varepsilon \mathrm{d}V, \qquad r = 0, 1, \cdots, N. \tag{4.6}$$

Hooke's law relates the average strain and the average stress in each inhomogeneity

$$\bar{\sigma}_r = \mathbf{C}^{(r)} \cdot \bar{\varepsilon}_r, \qquad \bar{\varepsilon}_r = \mathbf{M}^{(r)} \cdot \bar{\sigma}_r \tag{4.7}$$

where $\mathbf{M}$ is the compliance tensor. If ε_r^{pt} is the strain perturbation from $\bar{\varepsilon}_0$, which is the average strain in the matrix, then

$$\bar{\varepsilon}_r = \bar{\varepsilon}_0 + \varepsilon_r^{pt}. \tag{4.8}$$

The equivalent inclusion method leads to

$$\bar{\sigma}_r = \mathbf{L}^{(r)} \cdot \bar{\varepsilon}_r = \mathbf{L}^{(0)} \cdot (\bar{\varepsilon}_0 + \varepsilon_r^{pt}) = \mathbf{L}^{(0)} \cdot (\bar{\varepsilon}_0 + \varepsilon_r^{pt} - \varepsilon^*). \tag{4.9}$$

The Mori-Tanaka method assumes that

$$\varepsilon_r^{pt} = \mathbf{S}^{(0)} \cdot \varepsilon_r^* \tag{4.10}$$

where $\mathbf{S}^{(0)}$ is the Eshelby tensor for the matrix material $\mathbf{M}^{(0)}$ and ε^* is the eigenstrain in the r^{th} inhomogeneity. By substituting Equation 4.10 in Equation 4.9 one obtains an equation for ε^*, which can be solved to obtain

$$\bar{\sigma}_r = \mathbf{B}_r \cdot \bar{\sigma}_0 \qquad \text{in} \quad \Omega_r \tag{4.11}$$

where $\mathbf{B}$ is called the stress concentration tensor of a single inhomogeneity with stiffness tensor $\mathbf{L}^{(r)}$ which is embedded in the matrix with the stiffness tensor $\mathbf{L}^{(0)}$ subjected to a uniform stress $\bar{\sigma}_0$. $\mathbf{B}$ is defined as

$$\mathbf{B}_r = \left[\mathbf{I} + \mathbf{L}^0 \cdot (\mathbf{I} - \mathbf{S}^{(0)}) \cdot (\mathbf{M}^{(r)} - \mathbf{M}^{(0)})\right]^{-1}. \tag{4.12}$$

Substitution of Equation 4.11 into Equation 4.4 yields

$$\bar{\sigma} = \sum_{r=0}^{N} f_r \mathbf{B}_r \cdot \bar{\sigma}_0. \tag{4.13}$$

Using Equation 4.11 in Equation 4.8 gives

$$\bar{\sigma}_r = \mathbf{B}_r \cdot \left[\sum_{r=0}^{N} f_r \mathbf{B}_r\right]^{-1} \cdot \bar{\sigma}. \tag{4.14}$$

Substituting Equation 4.15 into Equation 4.7 leads to

$$\bar{\varepsilon}_r = \mathbf{M}^{(r)} \cdot \mathbf{B}_r \cdot \left[\sum_{r=0}^{N} f_r \mathbf{B}_r\right]^{-1} \cdot \bar{\sigma}. \tag{4.15}$$

Replacing $\bar{\varepsilon}_r$ in Equation 4.6 by Equation 4.15 gives

$$\bar{\varepsilon}_r = \sum_{r=0}^{N} f_r \mathbf{M}^{(r)} \cdot \mathbf{B}_r \cdot \left[\sum_{n=0}^{N} f_n \mathbf{B}_n\right]^{-1} \cdot \bar{\sigma}. \tag{4.16}$$

Finally, the the effective compliance tensor follows as

$$\bar{\mathbf{M}} = \sum_{r=0}^{N} f_r \mathbf{M}^{(r)} \cdot \mathbf{B}_r \cdot \left[\sum_{n=0}^{N} f_n \mathbf{B}_n\right]^{-1}. \tag{4.17}$$

The effective stiffness tensor for a prescribed displacement is defined as

$$\bar{\mathbf{L}} = \left[\sum_{r=0}^{N} f_r (\mathbf{L}_0^* + \mathbf{L}^{(r)})^{-1}\right]^{-1} - \mathbf{L}_0^* \tag{4.18}$$

where

$$\mathbf{L}_0^* = \mathbf{L}^{(0)} \cdot \left(\mathbf{S}^{(0)}\right)^{-1} - \mathbf{L}^{(0)}. \tag{4.19}$$

For the case of spherical inhomogeneities in isotropic matrix material, the effective elastic moduli are defined as

$$\bar{\mu} = \mu_{\mathrm{M}} \left[1 + \frac{f_{\mathrm{I}}(\mu_{\mathrm{I}} - \mu_{\mathrm{M}})}{\mu_{\mathrm{M}} + 2\delta_{\mathrm{M}}(1 - f_{\mathrm{I}})(\mu_{\mathrm{I}} - \mu_{\mathrm{M}})}\right] \tag{4.20}$$

$$\bar{\kappa} = \kappa_{\mathrm{M}} \left[1 + \frac{f_{\mathrm{I}}(\kappa_{\mathrm{I}} - \kappa_{\mathrm{M}})}{\kappa_{\mathrm{M}} + 3\gamma_{\mathrm{M}}(1 - f_{\mathrm{I}})(\kappa_{\mathrm{I}} - \kappa_{\mathrm{M}})}\right] \tag{4.21}$$

with

$$\delta_{\mathrm{M}} = \frac{3k_{\mathrm{M}} + 6\mu_{\mathrm{M}}}{15k_{\mathrm{M}} + 20\mu_{\mathrm{M}}} \quad , \quad \gamma_{\mathrm{M}} = \frac{k_{\mathrm{M}}}{3k_{\mathrm{M}} + 4\mu_{\mathrm{M}}}. \tag{4.22}$$

In Equation 4.21, κ denotes the bulk modulus, which is related to the Lamé constants by

$$\kappa = \lambda + \frac{2}{3}\mu. \tag{4.23}$$

Figure 4.3 shows the effective Lamé constants calculated with the Mori-Tanaka method for titanium as the matrix material and aluminum inhomogeneities. Note that this model gives the exact result for the elastic moduli when the volume fraction of the inclusions equals 100%.

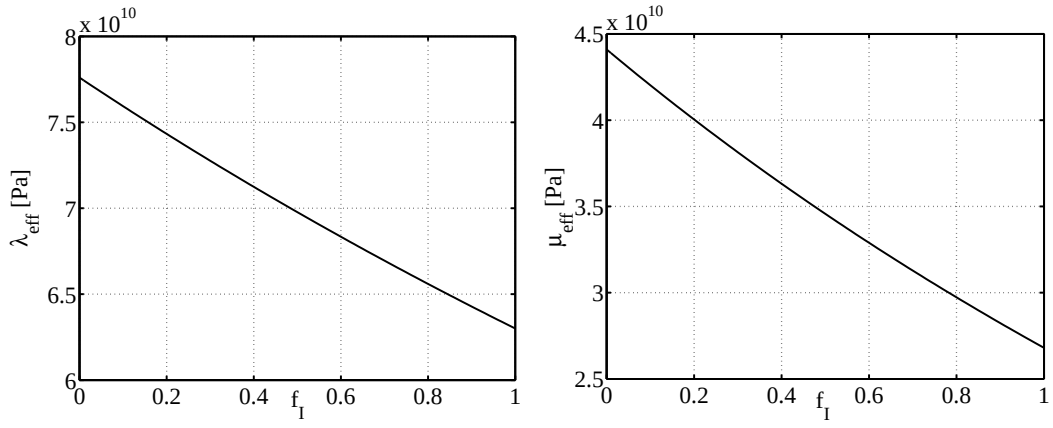

(a) Effective λ (b) Effective μ

Figure 4.3: Effective Lamé constants for aluminum inclusions in titanium

4.2.2 Dependence of the scattering cross section on the volume fraction of the inclusions

The goal of the differential self-consistent scheme is to find a differential equation or any other equation which describes the scattering cross section of the composite material with respect to the volume fraction of the inclusions in the matrix material. The basic idea is to calculate the scattering cross section of a single scatterer in an effective medium and to derive the equation by repeating the single scatterer problem for different volume fractions of the inclusion. For polycrystalline materials, the volume fraction of the inclusions is supposed to be 100 %, since every grain is regarded as a scatterer, which makes it impossible to apply the differential self-consistent scheme to grain boundary scattering. The fundamental procedure in deriving equations for the determination of the scattering cross section in terms of the concentration of the

inclusions is described in this section.

The derivation starts with the situation of N scatterers in an elastic medium (the matrix) with the stiffness tensor C_{M}, see Figure 4.4(a). It is of interest to calculate the scattering cross section of only the last scatterer added, which is characterized by its stiffness tensor C_{SS}^{N}, in the presence of the other $N-1$ inclusions already embedded in the matrix. Therefore, the situation of Figure 4.4(a) is transferred to the equivalent model in Figure 4.4(b). Clearly, the scattering cross section of the single inclusion with the elastic properties C_{SS}^{N} in the effective medium with C_{eff}^{N} determined with the Mori-Tanaka method, can be calculated by the methods provided in Chapter 3.

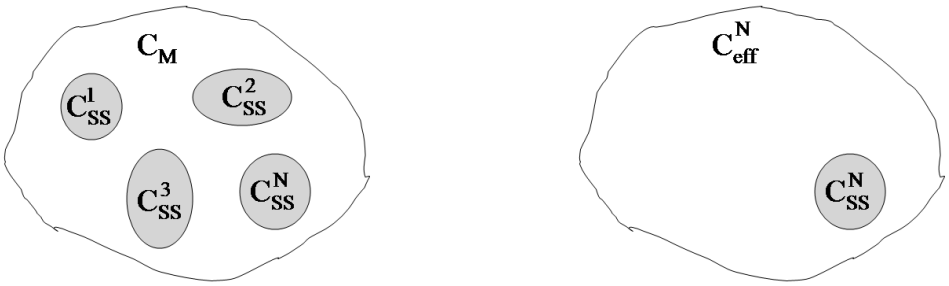

(a) N scatterers in the matrix material (b) Single scatterer in effective medium

Figure 4.4: Equivalent scattering problem for N inclusions.

With this assumption, it is possible to solve the single scattering case for an arbitrary concentration of the inclusions. The scattering cross section caused by the single scatterer in Figure 4.4(b) is denoted with γ_{SS}^{N} and clearly depends on the elastic moduli of the matrix C_{eff}^{N}, the elastic properties of that single inclusion C_{SS}^{N} and furthermore on the volume and shape of the inclusion, that is $\gamma_{\mathrm{SS}}^{N} = \gamma_{\mathrm{SS}}^{N}(C_{\mathrm{eff}}^{N}, C_{\mathrm{SS}}^{N}, V_{\mathrm{SS}}, S_{\mathrm{SS}})$. The subscript $_{\mathrm{SS}}$ stands hereby for single scatterer. Now, by first assuming all the inclusions having the same shape, size and elastic constants, and by expressing the average elastic properties as a function of the volume fraction of the scatterers, it is possible

to express γ_{SS}^{N} as a function of the volume fraction only, i.e. $\gamma_{\mathrm{SS}}^{N} = \gamma_{\mathrm{SS}}^{N}(f_{\mathrm{I}}^{N})$.

In the next step, one more inclusion, characterized by its stiffness tensor C_{SS}^{N+1} is added to the configuration in Figure 4.4. It is possible to capture this new situation in two different models, which are shown in Figure 4.5.

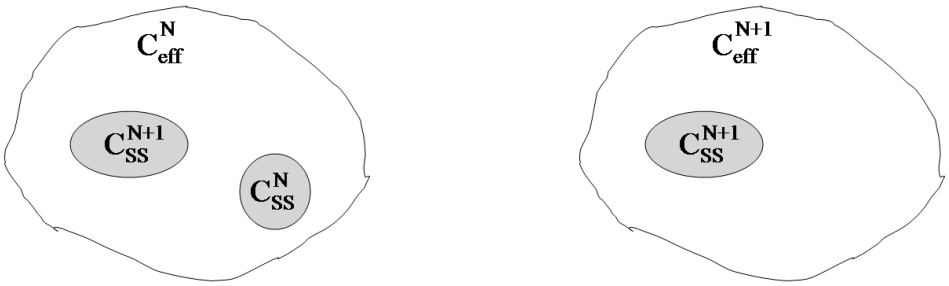

(a) 2 scatterers in the effective medium containing $N-1$ inclusions

(b) Single scatterer in effective medium containing N inclusions

Figure 4.5: Equivalent scattering problem for $N+1$ inclusions.

In Figure 4.5(a), the additional scatterer is included in the effective medium composed of the matrix material and $N-1$ inhomogeneities. Assuming that the two scatterers in the host material do not influence each other, i.e. applying the single scatterer theorem, it is possible to calculate the scattering cross section of the inclusion C_{SS}^{N+1} again with the methods described in Chapter 3. This leads to the scattering cross section

$$\gamma_{\mathrm{SS}}^{N+1} = \gamma_{\mathrm{SS}}^{N+1}(C_{\mathrm{eff}}^{N}, C_{\mathrm{SS}}^{N+1}, V_{\mathrm{SS}}^{N+1}, S_{\mathrm{SS}}^{N+1}) = \gamma_{\mathrm{SS}}^{N+1}(f_{\mathrm{I}}^{N}), \tag{4.24}$$

where f_{I}^{N} is the volume fraction of the N inclusions in the matrix material.

In contrast, the additional scatterer is embedded in an effective medium composed of the matrix material and N inclusions with the stiffness tensor C_{eff}^{N+1} in Figure 4.5(b). The scattering cross section of the single scatterer is now dependent on C_{eff}^{N+1} and it

is denoted by

$$\gamma_{\mathrm{SS}}^{N+1} = \gamma_{\mathrm{SS}}^{N+1}(C_{\mathrm{eff}}^{N+1}, C_{\mathrm{SS}}^{N+1}, V_{\mathrm{SS}}^{N+1}, S_{\mathrm{SS}}^{N+1}) = \gamma_{\mathrm{SS}}^{N+1}(f_{\mathrm{I}}^{N+1}), \tag{4.25}$$

with f_{I}^{N+1} being the volume fraction of the $N+1$ inhomogeneities in the matrix material.

Consider now the scattering cross section obtained from the multiple scatterer situation and denoted with γ_{MS}. In the situation depicted in Figure 4.4, the total scattering cross section based on N scatterers is γ_{MS}^{N}, in Figure 4.5 it is $\gamma_{\mathrm{MS}}^{N+1}$ due to the $N+1$ scatterers. If the multiple scattering cross section $\gamma_{\mathrm{MS}}^{N+1}$ is expressed in terms of the situation in Figure 4.5(a), it can be written as

$$\gamma_{\mathrm{MS}}^{N+1}(f_{\mathrm{I}}^{N+1}) = \gamma_{\mathrm{MS}}^{N}(f_{\mathrm{I}}^{N}) + \gamma_{\mathrm{SS}}^{N+1}(f_{\mathrm{I}}^{N}) \tag{4.26}$$

so the one additional scattering cross section of the one inclusion added in comparison to Figure 4.4 is simply added to the total scattering cross section corresponding to N inclusions. This procedure is repeated for every single scatterer added into the effective medium and finally one obtains for the multiple scattering cross section of M scatterers

$$\gamma_{\mathrm{MS}}^{M} = \sum_{i=0}^{M} \gamma_{\mathrm{SS}}^{i}(f_{\mathrm{I}}^{i}). \tag{4.27}$$

The differential self-consistent scheme derived so far and described by Equation 4.27 is compared to the Waterman and Truell model presented in Section 4.1. To that purpose, the attenuation coefficient has to be determined from the scattering cross section. A differential equation describing the attenuation in terms of the scattering cross section is (Kim [27])

$$\frac{\mathrm{d}\alpha_k}{\mathrm{d}f_{\mathrm{I}}} = \frac{1}{2}\frac{\gamma_k(f_{\mathrm{I}})}{V_{\mathrm{I}}} \tag{4.28}$$

where V_{I} is the volume of a single inclusion and k stands either for L or T, denoting the scattering cross section and the attenuation coefficient for the incident longitudinal and transverse wave, respectively. If the scattering cross section does not depend on

the concentration of the inclusions, Equation 4.28 is simplified to

$$\alpha_k = \frac{1}{2}\frac{3\gamma_k}{4\pi a^3} f_{\mathrm{I}} \tag{4.29}$$

for spherical inclusions.

In Figure 4.6, the normalized attenuation coefficients resulting from Equation 4.27 and Equation 4.29 are compared to the normalized attenuation coefficients found with the model of Waterman and Truell. The matrix and the scatterers are the same as before, i.e. spherical aluminum inclusions in titanium with a concentration of $f_{\mathrm{I}} = 0.15$. Figure 4.6 shows that the attenuation coefficients obtained from Equation 4.27 are

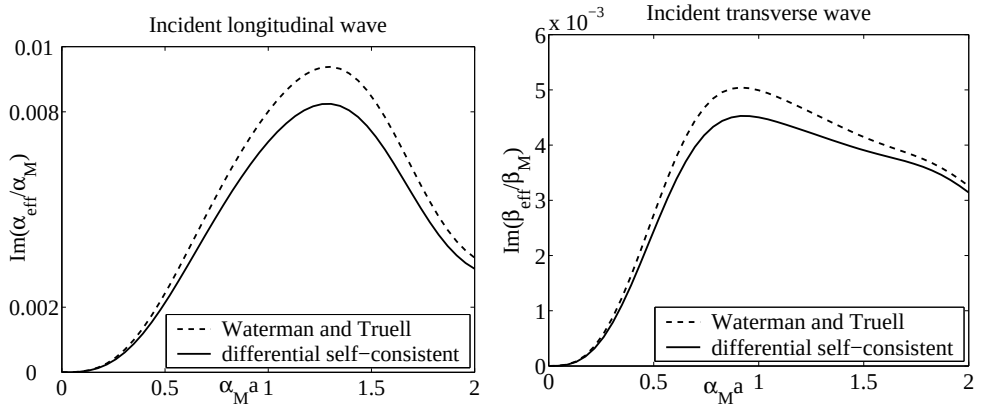

(a) Longitudinal attenuation coefficient. (b) Transverse attenuation coefficient.

Figure 4.6: Attenuation coefficients obtained from the differential self-consistent scheme compared to the model of Waterman and Truell.

lower than the ones calculated by Waterman and Truell for the incident longitudinal wave and for the incident transverse wave. This observation agrees with the models used, because in the differential self-consistent scheme, the scattering cross section of the single scatter decreases with increasing volume fraction of the inclusions since the effective elastic constants are used, and thus the material properties of the inclusions have a higher similarity to the ones of the surrounding material. On the other hand, each single scatterer has the same scattering cross section independent of the volume fraction in the model of Waterman and Truell. This explains why the curves in Figure 4.6 just show a shift in the amplitude, but no change in shape.

Note that the single scattering cross sections appearing in Equation 4.27 are determined with the exact solution approach and Equations 3.96 and 3.97 to make the differential self-consistent approach comparable to the model of Waterman and Truell. The exact solution uses the wavenumbers of the effective medium, this makes it necessary to calculate the effective density with

$$\rho_{\text{eff}} = f_{\text{I}}\rho_{\text{I}} + (1 - f_{\text{I}})\rho_{\text{M}}. \tag{4.30}$$

The calculation of the sum in Equation 4.27 is very tedious since the single scattering problem has to be solved for every inclusion with the new effective material properties. To save calculation time, several inclusions are added at once to the differential self-consistent scheme and their single scattering cross sections are calculated with the same effective stiffness.

Other approaches are made to describe the multiple scattering cross section depending on the concentration of the inclusions. For the first approach, assume that $\gamma_{\text{MS}}^{N+1}(f_{\text{I}}^{N+1}) \approx \gamma_{\text{MS}}^{N+1}(f_{\text{I}}^{N})$, i.e. both multiple scattering cross sections in Figure 4.5 are approximately the same. Now subtract $\gamma_{MS}^{N}(f_{\text{I}}^{N})$ on both sides and divide after this both sides by $\Delta f_{\text{I}} = f_{\text{I}}^{N+1} - f_{\text{I}}^{N}$. This gives

$$\frac{\gamma_{\text{MS}}^{N+1}(f_{\text{I}}^{N+1}) - \gamma_{\text{MS}}^{N}(f_{\text{I}}^{N})}{f_{\text{I}}^{N+1} - f_{\text{I}}^{N}} = \frac{\gamma_{\text{MS}}^{N+1}(f_{\text{I}}^{N}) - \gamma_{\text{MS}}^{N}(f_{\text{I}}^{N})}{f_{\text{I}}^{N+1} - f_{\text{I}}^{N}}, \tag{4.31}$$

and with $f_{\text{I}}^{N+1} - f_{\text{I}}^{N} = V_{\text{I}}/V_0$ and by taking the limiting case $f_{\text{I}}^{N+1} - f_{\text{I}}^{N} \to \mathrm{d}f_{\text{I}}$ on the right side one obtains

$$\frac{\mathrm{d}\gamma_{\text{MS}}(f_{\text{I}})}{\mathrm{d}f_{\text{I}}} = \frac{V_0}{V_{\text{I}}}\gamma_{\text{SS}}^{N+1}(f_{\text{I}}^{N}) \tag{4.32}$$

since $\gamma_{\text{MS}}^{N+1}(f_{\text{I}}^{N}) - \gamma_{\text{MS}}^{N}(f_{\text{I}}^{N}) = \gamma_{\text{SS}}^{N}$, see Figure 4.5(a) and Equation 4.26. Here, V_{I} is the volume of the single inclusion and V_0 is the unit volume. The multiple scattering cross section is then

$$\gamma_{\text{MS}}^{M}(f_{\text{I}}^{M}) = \int_0^{f_{\text{I}}^{M}} \gamma_{\text{SS}}^{N}(f_{\text{I}}^{N})\mathrm{d}f_{\text{I}}^{N}. \tag{4.33}$$

This multiple scattering cross section is in fact the same as the one in Equation 4.27 for the following reasons. The integral in Equation 4.33 can only be solved numerically. By adding one scatterer after the other, f_{I}^N does not increase steadily, but stepwise. Thus the integral is replaced by a sum, again from 0 to M. In this sum, each element has to be multiplied with $\Delta f_{\mathrm{I}} = V_{\mathrm{I}}/V_0$ to account for the integration, so the V_0/V_{I} in Equation 4.33 is cancelled out and Equation 4.27 is obtained.

The second approach uses the Taylor series expansion

$$\gamma_{\mathrm{MS}}^{N+1}(f_{\mathrm{I}}^{N+1}) = \gamma_{\mathrm{MS}}^{N+1}(f_{\mathrm{I}}^{N}) + (f_{\mathrm{I}}^{N+1} - f_{\mathrm{I}}^{N})\frac{\mathrm{d}\gamma_{\mathrm{MS}}^{N+1}(f_{\mathrm{I}}^{N})}{\mathrm{d}f_{\mathrm{I}}^{N}} \tag{4.34}$$

for the multiple scattering cross section. Now use $\gamma_{\mathrm{MS}}^{N+1}(f_{\mathrm{I}}^{N+1}) = \gamma_{\mathrm{MS}}^{N+1}(f_{\mathrm{I}}^{N}) = \gamma_{\mathrm{MS}}^{N}(f_{\mathrm{I}}^{N}) + \gamma_{\mathrm{SS}}^{N}(f_{\mathrm{I}}^{N})$, saying that the multiple scattering cross sections in Figure 4.5(a) and 4.5(b) are the same and that the multiple scattering cross section in Figure 4.5(a) is obtained by adding one single scattering cross section to Figure 4.4(b). Assume furthermore that $\gamma_{\mathrm{MS}}^{N}(f_{\mathrm{I}}^{N}) \approx \gamma_{\mathrm{MS}}^{N+1}(f_{\mathrm{I}}^{N})$ to obtain again

$$\frac{\mathrm{d}\gamma_{\mathrm{MS}}(f_{\mathrm{I}})}{\mathrm{d}f_{\mathrm{I}}} = \frac{V_0}{V}\gamma_{\mathrm{SS}}^{N+1}(f_{\mathrm{I}}^{N}) \tag{4.35}$$

and from that Equation 4.33.

In summary, several approaches to the differential self-consistent scheme all lead to the same equation for the multiple scattering cross section in terms of the volume fraction of the inclusions (Equation 4.27). The single scatterers are treated independently of each other and their scattering cross sections are summed over the number of scatterers. This approach is also known as the independent scattering model.

4.2.3 Causal differential method

A further development of the differential self-consistent scheme is the causal differential method. The governing equation for the description of the multiple scattering effects is similar as for the differential self-consistent scheme in Equation 4.27. In

terms of the attenuation coefficient, it is given as

$$\alpha_k(f_\mathrm{I} + \Delta f_\mathrm{I}) = \alpha_k(f_\mathrm{I}) + \frac{\Delta f_\mathrm{I}}{2V_\mathrm{I}}\gamma_k(f_\mathrm{I}) \tag{4.36}$$

where the subscript $_k$ is either $_L$ for the incident longitudinal wave or $_T$ for the incident transverse wave. The volume of the single scatterer is again denoted as V_I. In Equation 4.36, $\gamma_k(f_\mathrm{I})$ is the scattering cross section for all scatterers added to the effective medium by increasing the volume fraction of the scatterers by Δf_I. The scattering cross section is calculated in the effective medium with the volume fraction of the scatterers being f_I. In the next step, the effective medium is again homogenized with the volume fraction of the inclusions being now $f_\mathrm{I} + \Delta f_\mathrm{I}$. In contrast to the differential self-consistent scheme, the homogenization is carried out in a dynamic way by using the Kramers-Krönig relations (Beltzer et al. [9]) instead of the static Mori-Tanaka method. The Kramers-Krönig relations given by Weaver et al. [48]

$$\frac{1}{c_k(\omega)} - \frac{1}{c_k(0)} = \frac{2\omega^2}{\pi} P \int_0^\infty \frac{\alpha_k(\Omega)}{\Omega^2(\Omega^2 - \omega^2)} \mathrm{d}\Omega \tag{4.37}$$

yield the frequency-dependent wave speeds in the new medium. In Equation 4.37, $c_k(0)$ denotes the longitudinal or transverse wave speed in the static limit. The iterative process of calculating the attenuation and the corresponding wave speeds is repeated until the desired volume fraction of the scatterers is reached.

A method for the calculation of the principal value integral in Equation 4.37 is given by Kim [26]. The integral is split into three parts

$$P \int_0^\infty \frac{\alpha_k(\Omega)}{\Omega^2(\Omega^2 - \omega^2)} \mathrm{d}\Omega = \left[\int_\varepsilon^{\omega-\bar{\omega}} + \int_{\omega-\bar{\omega}}^{\omega+\bar{\omega}} + \int_{\omega+\bar{\omega}}^\infty \right] \frac{\alpha_k(\Omega)}{\Omega^2(\Omega^2 - \omega^2)} \mathrm{d}\Omega \tag{4.38}$$

where $\varepsilon, \bar{\omega} \to 0$. The first integral in Equation 4.38 can be evaluated if the singularity is removed by assuming that the attenuation and its derivative vanish at $\omega = 0$. With that assumption and a substitution of the variable, the second integral in Equation 4.38 is transformed into the form

$$\int_{\omega-\bar{\omega}}^{\omega+\bar{\omega}} \frac{\alpha_k(\Omega)}{\Omega^2(\Omega^2 - \omega^2)} \mathrm{d}\Omega = \int_0^{\bar{\omega}} \frac{1}{z} \left(\frac{\alpha_k(\omega + z)}{(\omega + z)^2(2\omega + z)} - \frac{\alpha_k(\omega - z)}{(\omega - z)^2(2\omega - z)} \right) \mathrm{d}z \tag{4.39}$$

which can be integrated. By assuming a large number K_k such that $\alpha_k(\omega)$ is approximately constant for all $\omega > K_k$, the third integral in Equation 4.38 is approximated as

$$\int_{\omega+\bar{\omega}}^{\infty} \frac{\alpha_k(\Omega)}{\Omega^2(\Omega^2-\omega^2)}\mathrm{d}\Omega \approx \int_{\omega+\bar{\omega}}^{K} \frac{\alpha_k(\Omega)}{\Omega^2(\Omega^2-\omega^2)}\mathrm{d}\Omega - \frac{\alpha_k(K)}{\omega^2}\left(\frac{1}{K}+\frac{1}{2\omega}\log\frac{K-\omega}{K+\omega}\right). \quad (4.40)$$

With the three integrals defined now, one avoids the singularity in the integral in Equation 4.37 at $\Omega = \omega$ and the frequency-dependent wave speeds can be calculated.

Figure 4.7 shows the attenuation coefficients for an incident longitudinal wave (upper figure) and an incident transverse wave (lower figure) of the causal differential method compared to the model of Waterman and Truell. The attenuation coefficients are normalized to the wave speeds of the matrix material and they are plotted dependent on the normalized frequency $\alpha_{\mathrm{M}}a$. The volume fraction of the spherical aluminum inclusions in the titanium matrix is $f_{\mathrm{I}} = 0.15$. The causal differential method is plotted for the increments of the volume fraction of the scatterers being $\Delta f_{\mathrm{I}} = 0.005$ and $\Delta f_{\mathrm{I}} = 0.075$. The scattering cross sections are calculated with the exact solution approach, thus the attenuation coefficients are valid for all frequencies. It is obvious that the attenuation coefficients obtained from the causal differential method decrease with decreasing increment in the volume fraction of the scatterers, Δf_{I}. This behavior is identical to the results of Kim [26]. For low frequencies, the model of Waterman and Truell and the causal differential method show good agreement in the attenuation coefficients for the incident longitudinal and the incident transverse wave. In contrast, there exists a significant difference between the attenuation coefficients of Waterman and Truell and the ones of the causal differential method for high frequencies.

One would obtain the most accurate solution of the causal differential method by taking the limit $\Delta f_{\mathrm{I}} \to V_{\mathrm{I}}$. Due to the calculational time, this limiting case is not practical. Note that the calculational cost for the causal differential method is high anyway, since the attenuation and the corresponding dynamic effective properties have to be determined up to very high frequencies for the integration of the Kramers-Krönig relations.

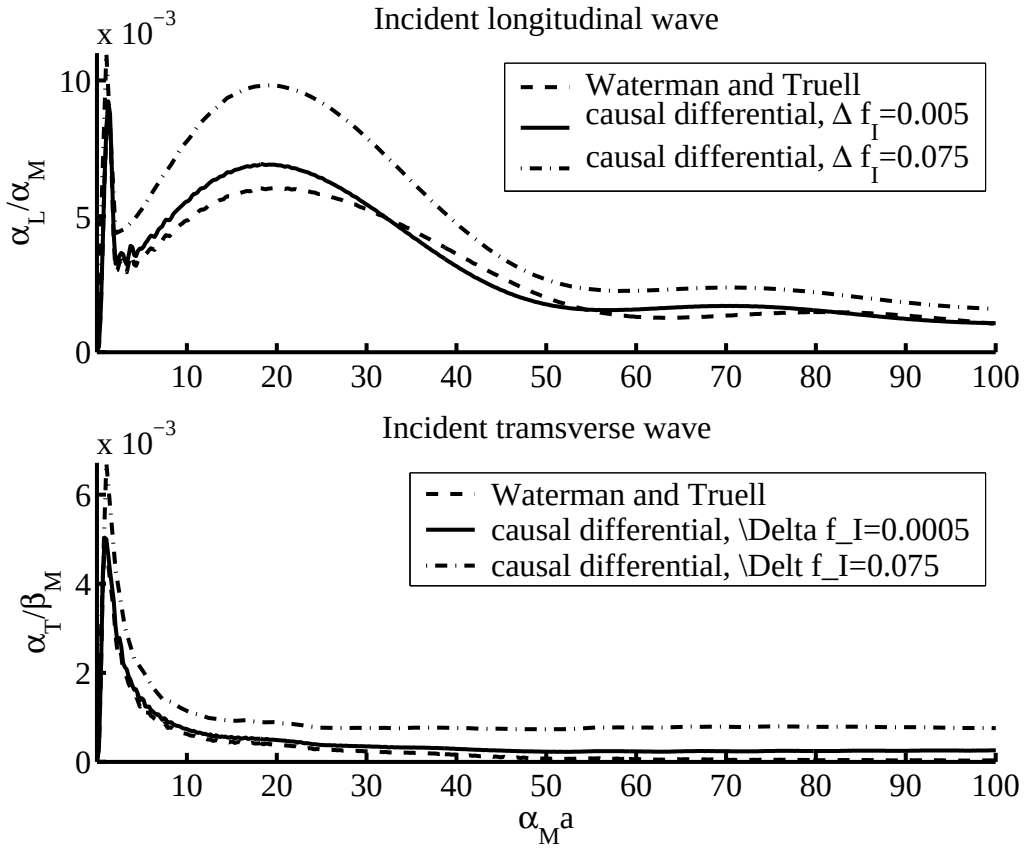

Figure 4.7: Attenuation coefficients of the causal differential method compared to the model of Waterman and Truell.

4.3 Self-consistent scheme

The self-consistent scheme offers the possibility of considering multiple scattering by averaging the single scattering cross section of a single scatterer over its size, shape and orientation. First, some necessary notations and methods for the application of the self-consistent scheme are introduced, before its basic idea and procedure are presented.

4.3.1 Numerical and averaging methods

There are two fundamental methods which are used in the self-consistent scheme. The one is the Newton-Raphson method, which is used to find the zeros of a system of nonlinear equations. The other one is the Voigt method, which gives the average

elastic properties of polycrystalline materials with anisotropic behavior of the single grains.

4.3.1.1 Newton-Raphson method

A more detailed presentation of the Newton-Raphson method can be found in Press [36]. Consider a system of N nonlinear equations

$$F_i(x_1, x_2, \ldots, x_N) = 0, \qquad i = 1, 2, \ldots, N \tag{4.41}$$

for which a simultaneous solution is searched. Let $\mathbf{x}$ be the vector of the values x_i and $\mathbf{F}$ the vector of the functions F_i. The Taylor series expansion of the functions F_i in the neighborhood of $\mathbf{x}$ is

$$F_i(\mathbf{x} + \delta\mathbf{x}) = F_i(\mathbf{x}) + \sum_{j=1}^{N} \frac{\partial F_i}{\partial x_j} \delta x_j + O(\delta\mathbf{x}^2) \tag{4.42}$$

where the matrix of partial derivatives is the Jacobian matrix $\mathbf{J}$ defined as

$$J_{ij} = \frac{\partial F_i}{\partial x_j}. \tag{4.43}$$

In matrix notation, Equation 4.42 is written as

$$\mathbf{F}(\mathbf{x} + \delta\mathbf{x}) = \mathbf{F}(\mathbf{x}) + \mathbf{J} \cdot \delta\mathbf{x} + O(\delta\mathbf{x}^2). \tag{4.44}$$

If the terms of order $\delta\mathbf{x}^2$ and higher order are neglected, a set of linear equations is obtained by setting $\mathbf{F}(\mathbf{x} + \delta\mathbf{x}) = 0$. These linear equations are given by

$$\mathbf{J} \cdot \delta\mathbf{x} = -\mathbf{F} \tag{4.45}$$

so that the corrections $\delta\mathbf{x}$ move each function closer to zero simultaneously. The corrections are added to the solution vector

$$\mathbf{x}_{\text{new}} = \mathbf{x}_{\text{old}} + \delta\mathbf{x} \tag{4.46}$$

and the procedure is repeated until the result is converging. The iteration is stopped if either the sum of the magnitudes of the functions F_i is less than some tolerance, or if the absolute values of the corrections δx_i are less than some other tolerance.

In the case of the self-consistent scheme, the functions F_i can not be obtained analytically, so it is not possible to compute J analytically. Instead, finite differences are used to calculate the partial derivatives numerically.

4.3.1.2 The Voigt method

An overview of the methods of averaging elastic constants is given in Musgrave [35]. In this study, the Voigt method is used to determine the average elastic constants of polycrystalline materials.

If a uniform stress σ_{RS} is applied to the surface of an aggregate, the macroscopic strain in the specimen is defined as

$$\varepsilon_{MN} = S_{MNRS}\sigma_{RS} \tag{4.47}$$

where S_{MNRS} is the compliance tensor of the aggregate. The strain of any crystallite referred to the local coordinate system of the crystal is given by

$$\varepsilon_{ij} = s_{ijkl}\sigma_{kl} \tag{4.48}$$

with s_{ijkl} denoting the tensor of compliances for the crystallite.

An assumption for the calculation of the average elastic constants is that each grain experiences the stress field σ_{RS} when

$$a_{Mi}a_{Ni}\varepsilon_{ij} = \varepsilon_{MN} + \Delta\varepsilon_{MN} = (a_{Mi}a_{Nj}a_{Rk}a_{Sl}s_{ijkl}) \tag{4.49}$$

where a_{Mi} are the direction cosines between the local crystal coordinate system $X_i,\ i = 1, 2,3$ and the reference coordinate system $X_{\mathrm{M}}, M = 1, 2, 3$. Taking the sum over all the grains of the aggregate gives

$$\sum_{\text{agg}} (\varepsilon_{MN} + \Delta\varepsilon_{MN}) = \varepsilon_{MN} = \sigma_{RS} \sum_{\text{agg}} a_{Mi}a_{Nj}a_{Rk}a_{Sl}s_{ijkl} f(\psi_q) \tag{4.50}$$

where the normalized distribution function $f(\psi_q)$ expresses the probability that a particular grain has its crystal axes x_i related to X_{M} by $a_{Mi}(\psi_q)$.

The Voigt average elastic constants are calculated under the assumption of a constant strain field ε_{RS} in all crystals. The mean isotropic stiffness averaging the stresses $\sigma_{MN} + \Delta\sigma_{MN}$ on each grain is then defined as

$$\bar{c}_{MNRS} = \mathcal{N}^{-1} \int a_{Mi}a_{Nj}a_{Rk}a_{Sl}c_{ijkl}\mathrm{d}\psi_q \tag{4.51}$$

with $\mathcal{N}$ denoting the number of the grains.

For an aggregate of cubic crystals, the Voigt averages are

$$\begin{aligned} \bar{c}_{11} &= c_{11} - 2c/5 \\ \bar{c}_{12} &= c_{12} + c/5 \\ \bar{c}_{44} &= c_{11} + c/5 \\ c &= c_{11} - c_{12} - 2c_{44} \end{aligned} \tag{4.52}$$

where the small letters denote reference of the elastic properties to the local crystal axes, whereas capitol letters stand for the macroscopic material properties.

The reduced stiffness tensor $c_{ij} = c_{ji}$ consists generally of 21 independent elastic constants. These reduce to fewer independent terms, if the crystal obeys certain symmetries. In a cubic crystal, see Kino [30], there are only three independent constants, namely c_{11}, c_{44} and c_{12}, and the symmetries are

$$\begin{aligned} &c_{11} = c_{22} = c_{33} \\ &c_{12} = c_{21} = c_{31} = c_{13} = c_{23} = c_{32} \\ &c_{14} = c_{15} = c_{16} = c_{24} = c_{25} = c_{26} = c_{34} = c_{35} = c_{36} = 0 \end{aligned} \tag{4.53}$$

Similar to cubic crystals, the Voigt averages for aggregates of hexagonal crystals are

$$\begin{aligned} \bar{c}_{11} &= \frac{1}{15}\left(8c_{11} + 3c_{33} + 4c_{13} + 8c_{44}\right) \\ \bar{c}_{12} &= \frac{1}{15}\left(c_{11} + c_{33} + 5c_{12} + 8c_{13} - 4c_{44}\right) \\ \bar{c}_{11} &= \frac{1}{30}\left(7c_{11} + 2c_{33} - 5c_{12} - 4c_{13} + 6c_{44}\right) \end{aligned} \tag{4.54}$$

The reduced 6×6 stiffness tensor c_{ij} for a hexagonal system is (see Anastassakis [5])

$$c_{ij} = \begin{pmatrix} c_{11} & c_{12} & c_{13} & \cdot & \cdot & \cdot \\ & c_{11} & c_{13} & \cdot & \cdot & \cdot \\ & & c_{33} & \cdot & \cdot & \cdot \\ & & & c_{44} & \cdot & \cdot \\ & & & & c_{44} & \cdot \\ & & & & & c_{66} \end{pmatrix} \tag{4.55}$$

with $c_{66} = (c_{11} - c_{12})/2$.

Note that the tensor c_{mn} is written in the reduced notation, while the scattering equations, for example Equation 3.10, employ the 4th order tensor C_{ijkl}. The relationship between the indices in the 2-suffix elements and the 4-suffix elements is given in Table 4.1.

Table 4.1: Relationship between the 4th order stiffness tensor and the reduced notation.

Suffix in c_{mn}	1	2	3	4	5	6
Suffix in C_{ijkl}	11	22	33	23, 32	31, 13	12, 21

If the self-consistent scheme is applied to grain boundary scattering, the scatterers are treated as anisotropic material, so their stiffness tensor depends on the direction of the incident wave. The relationship for the transformation of the stiffness tensor from the coordinate system of the incident wave, x^i_{M}, in the coordinate system fixed to the scatterer, x'_m is given by

$$C_{mnrs} = a_{mM} a_{nN} a_{rR} a_{sS} C_{MNRS} \tag{4.56}$$

where the a_{ij} are the direction cosines. They are found by rotating the coordinate system of the scatterer into the one of the incident wave. As a result, the rotation

matrix is obtained as

$$\mathbf{R}^T = a_{ij} = \begin{pmatrix} -\cos\theta^{\mathrm{i}}\cos\phi^{\mathrm{i}} & -\sin\phi^{\mathrm{i}} & \sin\theta^{\mathrm{i}}\cos\phi^{\mathrm{i}} \\ -\cos\theta^{\mathrm{i}}\sin\phi^{\mathrm{i}} & \cos\phi^{\mathrm{i}} & \sin\theta^{\mathrm{i}}\sin\phi^{\mathrm{i}} \\ \sin\theta^{\mathrm{i}} & 0 & \cos\theta^{\mathrm{i}} \end{pmatrix} \tag{4.57}$$

in terms of the incident angles θ^{i} and ϕ^{i}.

4.3.2 Basic procedure of the self-consistent scheme

The most important concept in the self-consistent scheme is the introduction of complex elastic moduli for the matrix material. The Lamé constants are then expressed as $\lambda^* = \lambda' + i\lambda''$ and $\mu^* = \mu' + i\mu''$. The scattering cross section of a single scatterer, averaged over different scattering situations, vanishes for certain values of the imaginary parts of the Lamé constants. For these imaginary parts, complex wave speeds $\alpha^* = \alpha' + i\alpha''$ and $\beta^* = \beta' + i\beta''$ are calculated, whose imaginary parts in turn yield the attenuation coefficients.

Consider the general scattering situation illustrated in Figure 4.8. The incident wave is propagating in an arbitrary direction, which is determined by the incident angles θ^i and ϕ^i. The inclusion is an ellipsoid with two axes having the same length, for example $a_2 = a_3$, so its geometry is completely described by the axis $a_1 = a$ and $a_2 = a_3 = b$. It is also possible to describe the ellipsoidal shape by the variables a and the ratio $r = b/a$.

With the methods described in Section 3.1.2, the scattering cross section can be determined for all situations covered in Figure 4.8, that is for all directions of the incident wave and all arbitrary values of a and b. The scattering cross section can be calculated for the incident longitudinal wave as well as for the incident transverse wave.

The multiple scattering and the resulting averaging procedure is demonstrated in Figure 4.9. For each inclusion in the matrix material, the total scattering cross sections,

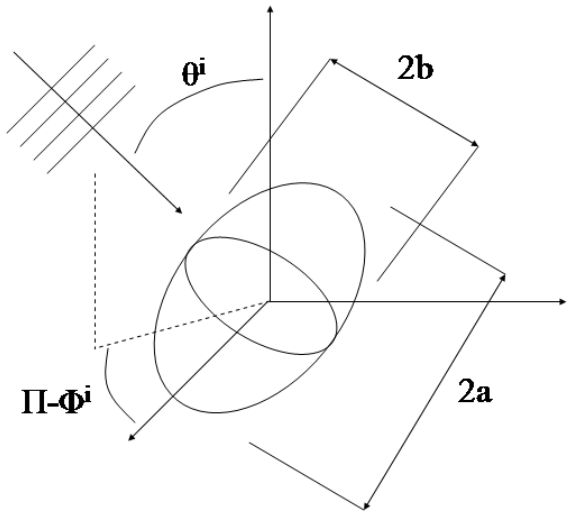

Figure 4.8: Geometry of the single scattering problem.

for both cases, i.e. the incident longitudinal and the incident transverse wave, are calculated. These values are denoted as γ_i^{L} and γ_i^{T}, respectively. These values are both functions of the angles θ^{i} and ϕ^{i} defining the direction of the incident wave, as well as the size and the shape of the inclusions, which are determined by a and b. Note that the dependence on the direction of the incident wave is not only due to the changing orientation of the inclusion, but also to the fact, that the crystallographic elastic properties are used for the scatterer as described in Section 4.3.1.2. In contrast, the averaged medium calculated with the Voigt method is applied for the surrounding material in the case of grain boundary scattering. To apply the self-consistent scheme to composite materials with isotropic inclusions and isotropic matrix material, an effective medium approach like the Mori-Tanaka method (Section 4.2.1) has to be used for the calculation of the material properties of the surrounding material. The averaging methods (Voigt or Mori-Tanaka) yield the real parts of the Lamé constants, λ' and μ'.

Finally, it is possible to state that

$$\begin{aligned}\gamma_i^{\mathrm{L}} &= \gamma_i^{\mathrm{L}}\left(\theta^{\mathrm{i}}, \phi^{\mathrm{i}}, a, b, C_{ijkl}^{\mathrm{M}}, c_{mnrs}^{\mathrm{I}}\right)\\ \gamma_i^{\mathrm{T}} &= \gamma_i^{\mathrm{T}}\left(\theta^{\mathrm{i}}, \phi^{\mathrm{i}}, a, b, C_{ijkl}^{\mathrm{M}}, c_{mnrs}^{\mathrm{I}}\right)\end{aligned} \tag{4.58}$$

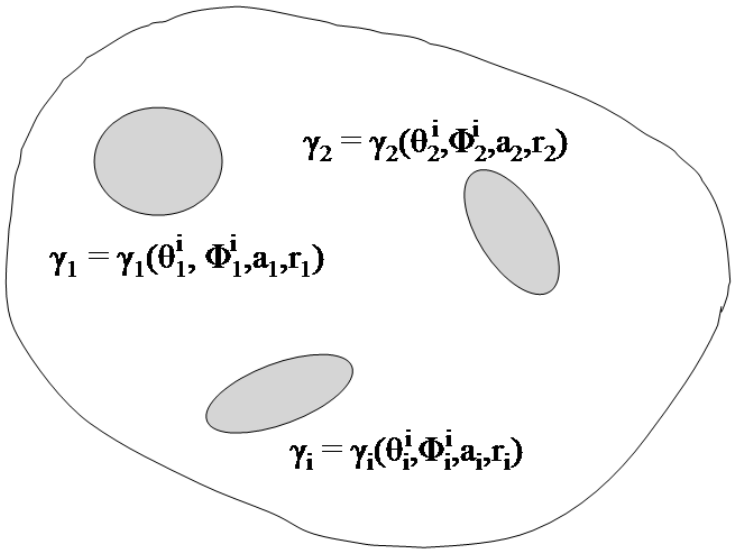

Figure 4.9: General multiple scattering situation.

where C^{M}_{ijkl} is the effective stiffness tensor of the matrix and c^{I}_{mnrs} is the stiffness tensor of the particular inclusion. Note that each scattering cross section is just a real number.

The scattering cross sections of all inclusions are then averaged. The result is expressed as

$$\langle \gamma^k \rangle = \frac{1}{N} \sum_{i=1}^{N} \gamma_i^k \tag{4.59}$$

where N is the total number of the considered inclusions and the superscript ^{k} is either $^{\mathrm{L}}$ for the incident longitudinal or $^{\mathrm{T}}$ for the incident transverse wave.

Setting the averaged scattering cross sections to zero, i.e.

$$\langle \gamma^{\mathrm{L}} \rangle = 0, \qquad \langle \gamma^{\mathrm{T}} \rangle = 0, \tag{4.60}$$

one obtains two equations for the two unknowns $\mathrm{Im}\{\lambda^*\} = \lambda''$ and $\mathrm{Im}\{\mu^*\} = \mu''$ which are solved with the Newton-Raphson method. The complex wave speeds are then given by $c^*_{\mathrm{L}} = ((\lambda^* + 2\mu^*)/\rho)^{1/2}$ and $c^*_{\mathrm{T}} = (\mu^*/\rho)^{1/2}$, and the attenuation coefficients

α_L and α_T are the real parts of the complex wave numbers, precisely

$$\alpha_{\mathrm{L}} = \mathrm{Re}\left\{\frac{\omega}{c_{\mathrm{L}}^*}\right\}, \qquad \alpha_{\mathrm{T}} = \mathrm{Re}\left\{\frac{\omega}{c_{\mathrm{T}}^*}\right\}. \tag{4.61}$$

4.3.3 Applications, restrictions and further developments of the self-consistent scheme

The self-consistent scheme as described in Section 4.3.2 is first tested for the case of spherical, isotropic inclusions in an isotropic matrix material, where the Born approximation approach of Section 3.1 is used to calculate the longitudinal and transverse scattering cross sections of the single scatterer in Equation 4.60. The two unknowns are the imaginary parts of the Lamé constants of the effective, isotropic medium. The real parts of the Lamé constants of the effective medium are determined with the Mori-Tanaka method (Section 4.2.1). Figure 4.10 illustrates the problems arising during the solution of the self-consistent scheme with the methods mentioned above. In Figure 4.10, the averaged longitudinal and transverse scattering cross sections are plotted in terms of the imaginary parts of the Lamé constants, λ'' and μ'', normalized with the corresponding real parts, λ' and μ'.

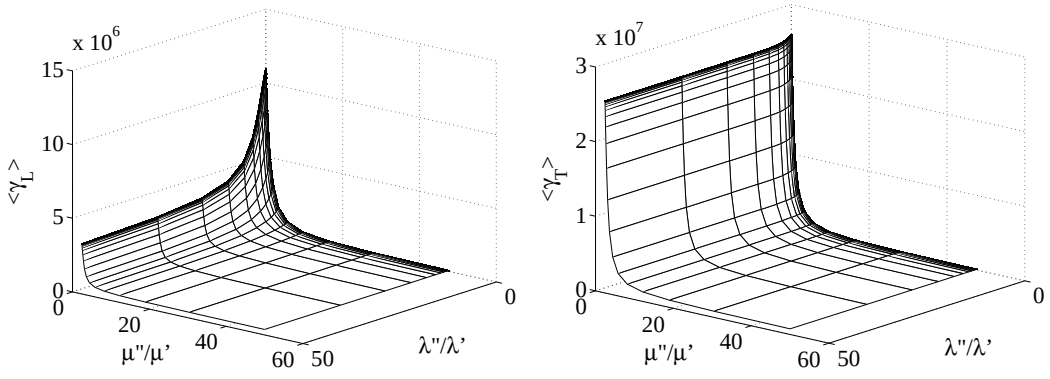

(a) Averaged longitudinal scattering cross section.

(b) Averaged transverse scattering cross section.

Figure 4.10: Averaged scattering cross sections dependent on the imaginary parts of the Lamé constants.

A reasonable result for the attenuation coefficients would require the averaged longitudinal and transverse scattering cross sections to have zeros in the order of $0 < \lambda''/\lambda' < 1$ and $0 < \mu''/\mu' < 1$. As it is obvious from Figure 4.10, these zeros do not occur. The averaged longitudinal and transverse scattering cross sections are furthermore just converging to zero for $\lambda''/\lambda' \to \infty$ and $\mu''/\mu' \to \infty$. Thus, the self-consistent scheme gives the solution that the imaginary parts of the Lamé constants have to be infinite. This leads to unreasonably high imaginary parts of the longitudinal and transverse wavenumbers, and therefore leads to attenuation coefficients whose values are far too high. In a physical sense, this result (which makes no sense at a first glance) can be explained and point the way to make improvements to the self-consistent scheme.

To explain this behavior, note that the goal of the self-consistent scheme is to make the scattering cross sections of an averaged scatterer to be zero by describing the effective material as a viscoelastic material. This means that the attenuation caused by the scattering is taken over by the damping effects of the viscoelastic material. In the self-consistent scheme carried out so far, the real parts of the effective Lamé constants are calculated by the Mori-Tanaka method and are treated as constant values throughout the determination of the imaginary parts. The drawback of the Mori-Tanaka method in this application is that it is just an approximation, but not the exact solution to the effective material properties. Thus, a mismatch in the real parts of the Lamé constants between the used value (the Mori-Tanaka model) and the actual value is inherent in the self-consistent scheme. This makes it clear that the scattering cross section of the averaged scatterer can never be zero for reasonable values of the imaginary parts of the Lamé constants. The solution obtained with infinite values for λ'' and μ'' is due to the fact that the resulting viscoelastic material has a very high — or infinitely high — damping effect. The scattered wave is therefore simply attenuated so strongly, that the scattering cross sections are zero at the observation point. Note that in this context the scattering cross section is the ratio of the incident power to the scattered power, and the scattered power is zero at the observation point due to the extreme attenuation in the viscoelastic material. This effect is enforced by the far-field approximation used together with the Born approximation.

The two major drawbacks of the self-consistent scheme as it is described in Section 4.3.2 are therefore the use of the far-field scattering cross section and the use of the Mori-Tanaka method for the determination of the real parts of the effective Lamé constants. A further developed self-consistent scheme is determining λ' and μ' together with λ'' and μ'' for the effective material. The effective material is completely described by introducing the complex density $\rho^* = \rho' + i\rho''$. Thus the new self-consistent scheme is determining six unknowns, which are the real and imaginary parts of the effective Lamé constants and the effective density.

One possibility to solve for the six unknowns is to use the forward far-field scattering amplitudes for the incident longitudinal and incident transverse wave calculated with the exact solution and given in Equations 3.88 and 3.93 instead of the longitudinal and transverse scattering cross sections. The real and imaginary parts of the far-field scattering amplitudes are set to zero, yielding four equations which are

$$\begin{aligned} \mathrm{Re}\{< f(0) >\} = 0, \qquad \mathrm{Im}\{< f(0) >\} = 0 \\ \mathrm{Re}\{< g(0) >\} = 0, \qquad \mathrm{Im}\{< g(0) >\} = 0. \end{aligned} \tag{4.62}$$

From these four equations, it is possible to determine the real and imaginary parts of the effective Lamé constants. Sabina et al. [39] derived an equation for the calculation of the effective density, which is

$$\rho^* = \rho_\mathrm{M} + \frac{f_\mathrm{I} h_1(-k)(\rho_\mathrm{I} - \rho_\mathrm{M})}{1 + (\rho_\mathrm{I} - \rho_\mathrm{M})(3 - \varepsilon_\alpha - 2\varepsilon_\beta)/(3\rho^*)} \tag{4.63}$$

where k is either the longitudinal or the transverse wavenumber. Note that Equation 4.63 leads to the real and the imaginary part of the effective density at once. The quantities ε_k with k being either α or β are given by

$$\varepsilon_k = \frac{3(1 - ika)}{(ka)^3} \left[\sin(ka) - ka\cos(ka)\right] e^{ika} \tag{4.64}$$

and the function $h_1(k)$ is

$$h_1(k) = \frac{3(\sin(ka) - ka\cos(ka)}{(ka)^3}. \tag{4.65}$$

The solution of the self-consistent scheme requires an iteration. First, the effective Lamé constants are determined from Equation 4.62 and then the effecive density is calculated with Equation 4.63. The iteration is repeated until all unknowns are converging.

To overcome the problem of using a far-field quantity like the far-field scattering amplitudes, it is proposed that instead of using Equation 4.62, the scattered longitudinal and transverse power are set to zero, i.e.

$$< P_{\mathrm{L}}^{\mathrm{s}} >= 0, \quad < P_{\mathrm{T}}^{\mathrm{s}} >= 0 \tag{4.66}$$

where the scattered powers are calculated with the exact solution approach in Section 3.3.2 in the near-field — or in the optimal case directly on the surface of the scatterer. The near-field solution ensures that the scattered power cannot be zero just because of the damping in the viscoelastic medium. Equation 4.63 is used for the calculation of the effective density. The two missing equations are the Kramers-Krönig relations, given by Kim [27] and expressed in terms of the attenuation coefficients as

$$\frac{\alpha_{\mathrm{L}}^2(\omega) + (\alpha'(\omega))^2}{\omega\alpha'(\omega)} - \frac{\alpha_{\mathrm{L}}^2(0) + (\alpha'(0))^2}{\omega\alpha_{\mathrm{L}}(0)} = \frac{2\omega^2}{\pi} \int_0^\infty \frac{\alpha_{\mathrm{L}}(\Omega)}{\Omega^2(\Omega^2 - \omega^2)} \mathrm{d}\Omega \tag{4.67}$$

for the longitudinal wave and by

$$\frac{\alpha_{\mathrm{T}}^2(\omega) + (\beta'(\omega))^2}{\omega\beta'(\omega)} - \frac{\alpha_{\mathrm{T}}^2(0) + (\beta'(0))^2}{\omega\alpha_{\mathrm{T}}(0)} = \frac{2\omega^2}{\pi} \int_0^\infty \frac{\alpha_{\mathrm{T}}(\Omega)}{\Omega^2(\Omega^2 - \omega^2)} \mathrm{d}\Omega \tag{4.68}$$

for the transverse wave. The numerical calculation of the integrals in the Kramers-Krönig relations is described in Section 4.2.3.

CHAPTER 5

Conclusions and future work

This research provides a complete solution for the problem of a single scatterer subjected to incident transverse and longitudinal waves. The single scatterer problem is solved in two ways — with the Born approximation, and an exact solution. The advantages and preferred applications for both approaches are emphasized. The simplicity of the Born approximation in the treatment of scatterers of different shapes is clearly demonstrated. Explicit solutions are given for the scattering by spherical and ellipsoidal inclusions. Section 3.1 describes the applicability of the Born approximation to the case of oblique incidence of the incident wave, which is shown to correspond to scattering at inhomogeneities in different orientations. This result is a critical advantage of the Born approximation — the possibility to solve the single scattering problem for anisotropic inclusions by averaging over the cases with the incident wave travelling in arbitrary directions. However, the Born approximation has three major drawbacks. First, it is restricted to low frequencies in the Rayleigh domain, which makes it hard to precisely treat scattering at inclusions of varying size. Second, the Born approximation is coupled with a far-field approximation. Since the far-field approximation has some disadvantages for scattering problems in viscoelastic matrix materials (which is shown in Section 3.3.2), the Born approximation is further restricted to elastic matrix materials. The third drawback of the Born approximation is its poor accuracy for scatterers with material properties that are very different from the material properties of the matrix. To overcome these problems, an exact solution approach is taken. The exact solution can be used for all frequency domains, as well as for elastic and viscoelastic matrix materials, and gives accurate solutions for any combination of matrix and inclusion properties. Several quantities are derived to describe the scattering effects, especially the scattered power and the scattering

amplitudes. The scattering cross section can be easily obtained from the scattered power and the scattering amplitudes. To complete the single scattering treatment, far-field expressions for the scattered power and the scattering amplitudes are derived from the exact solution approach. Note that all exact solutions are presented for the case of spherical scatterers.

Chapter 4 considers three different multiple scattering approaches. First, the model of Waterman and Truell yields results for the attenuation coefficients of incident longitudinal and transverse waves. It should be noted that the Waterman and Truell model can only be used for low volume fractions of the inclusions. The second multiple scattering approach is the differential self-consistent scheme. The differential self-consistent scheme gives an equation which describes the scattering cross section of multiple scatterers dependent on the volume fraction of the scatterers. Formulae for the calculation of the attenuation coefficient from the scattering cross section are developed. It is shown that the differential self-consistent scheme approach can be transferred into the independent scattering model, and that its results are very similar to the results obtained from the Waterman and Truell model. Note that the differential self-consistent scheme is also restricted to a low scatterer concentration, such that the mutual influence of the single scatterers must be neglected. The advantage of both the Waterman and Truell model and the differential self-consistent scheme is their applicability to an elastic or viscoelastic matrix material. Therefore these two multiple scattering approaches can be used in connection with the Born approximation approach for the single scattering problem. The last multiple scattering approach treated in this study is the self-consistent scheme. The self-consistent scheme requires the use of a viscoelastic matrix material, because the attenuation due to scattering at multiple inclusions is described by the viscoelastic loss in the surrounding material. It is shown in Section 4.3.3 that the far-field approximation and as a consequence, the Born approximation, do not give reasonable results if they are used in the self-consistent scheme. A modified self-consistent scheme is proposed which is based on the exact solution approach for the single scattering problem.

Characterizing the damage state of a material depends on the properties and the structure of the specific material used. All materials have a reference "state" of the undamaged material, that is needed for accurate comparison to a model containing defects and flaws. Knowing this, it is possible to distinguish between the attenuation inherent to the material, and the additional attenuation caused by the damage. To account for the scattering at cracks, the single scatterer problem has to be extended to crack-like inclusions. These crack-like inclusions might be modeled using ellipsoidal inclusions, and choosing extreme values for the axes of the ellipsoid in the single scatterer solution with the Born approximation. To cover scattering at inhomogeneities of different sizes, shapes and orientation, the use of a probability function is recommended.

For composite materials, especially with low volume fractions of inclusions, a single attenuation model is sufficient. Single in this context means that the same type of multiple attenuation model is used to create the reference model and the model containing damage. If the interactions between all scatterers are weak, the model of Waterman and Truell or the differential self-consistent scheme can be applied.

The treatment of polycrystalline materials is more complicated because of the grain boundary scattering. The only multiple scattering approach taken in this research that can account for grain boundary scattering is the self-consistent scheme. The scattering at defects and flaws is then overlaid on the grain boundary scattering. Clearly, the interactions between the flaws and the grains are lost in this way, because the two sources of the scattering — grains and defects — are treated independently, but in general it is possible to solve the grain boundary scattering by the self-consistent scheme and the scattering at defects by any other multiple scattering approach.

AppendixA

Normalized systems of equations for the calculation of the scattering coefficients

The system of equations resulting from the continuity conditions at the boundary of the scatterer which is used for the determination of the scattering coefficients is given here in its normalized form to avoid numerical problems by inverting the matrices.

For the case of an incident longitudinal wave, the normalized system of equations is written as

$$\begin{bmatrix} d_{11} & d_{12} & d_{13} & d_{14} \\ d_{21} & d_{22} & d_{23} & d_{24} \\ d_{31} & d_{32} & d_{33} & d_{34} \\ d_{41} & d_{42} & d_{43} & d_{44} \end{bmatrix} \begin{bmatrix} a_n^{\mathrm{N}} \\ b_n^{\mathrm{N}} \\ a_n'^{\mathrm{N}} \\ b_n'^{\mathrm{N}} \end{bmatrix} = \begin{bmatrix} l_1 \\ l_2 \\ l_3 \\ l_4 \end{bmatrix} \tag{A.1}$$

where the superscript $^{\mathrm{N}}$ denotes the normalized coefficients. The elements of the vector on the right hand side are given as

$$l_1 = i^{n+1}\frac{2n+1}{\alpha_{\mathrm{eff}}}\left(n - \alpha_{\mathrm{eff}}a\frac{j_{n+1}(\alpha_{\mathrm{eff}}a)}{j_n(\alpha_{\mathrm{eff}}a)}\right) \tag{A.2}$$

$$l_2 = i^{n+1}\frac{2n+1}{\alpha_{\mathrm{eff}}} \tag{A.3}$$

$$l_3 = i^{n+1}\frac{2n+1}{\alpha_{\mathrm{eff}}}\left[\left(n^2 - n - \frac{(\beta_{\mathrm{eff}}a)^2}{2}\right) + 2\alpha_{\mathrm{eff}}a\frac{j_{n+1}(\alpha_{\mathrm{eff}}a)}{j_n(\alpha_{\mathrm{eff}}a)}\right] \tag{A.4}$$

$$l_4 = i^{n+1}\frac{2n+1}{\alpha_{\mathrm{eff}}}\left((n-1) - \alpha_{\mathrm{eff}}a\frac{h_{n+1}(\alpha_{\mathrm{eff}}a)}{h_n(\alpha_{\mathrm{eff}}a)}\right). \tag{A.5}$$

The components of the matrix are then

$$
\begin{aligned}
d_{11} &= n - \alpha_{\text{eff}} a \frac{h_{n+1}(\alpha_{\text{eff}} a)}{h_n(\alpha_{\text{eff}} a)} && \text{(A.6)}\\
d_{12} &= n(n+1) && \text{(A.7)}\\
d_{13} &= -n + \alpha_{\text{I}} a \frac{j_{n+1}(\alpha_{\text{I}})}{j_n(\alpha_{\text{I}})} && \text{(A.8)}\\
d_{14} &= -n(n+1) && \text{(A.9)}\\
d_{21} &= 1 && \text{(A.10)}\\
d_{22} &= (n+1) - \beta_{\text{eff}} a \frac{h_{n+1}(\beta_{\text{eff}} a)}{h_n(\beta_{\text{eff}} a)} && \text{(A.11)}\\
d_{23} &= -1 && \text{(A.12)}\\
d_{24} &= -(n+1) + \beta_{\text{I}} a \frac{j_{n+1}(\beta_{\text{I}} a)}{j_n(\beta_{\text{I}} a)} && \text{(A.13)}\\
d_{31} &= \left(n^2 - n - \frac{(\beta_{\text{eff}} a)^2}{2} \right) + 2\alpha_{\text{eff}} a \frac{h_{n+1}(\alpha_{\text{eff}} a)}{h_n(\alpha_{\text{eff}} a)} && \text{(A.14)}\\
d_{32} &= n(n+1) \left[(n-1) - \beta_{\text{eff}} a \frac{h_{n+1}(\beta_{\text{eff}} a)}{h_n(\beta_{\text{eff}} a)} \right] && \text{(A.15)}\\
d_{33} &= -\frac{\mu_{\text{I}}}{\mu_{\text{eff}}} \left[\left(n^2 - n - \frac{(\beta_{\text{I}} a)^2}{2} \right) + 2\alpha_{\text{I}} a \frac{j_{n+1}(\alpha_{\text{I}} a)}{j_n(\alpha_{\text{I}} a)} \right] && \text{(A.16)}\\
d_{34} &= -\frac{\mu_{\text{I}}}{\mu_{\text{eff}}} n(n+1) \left[(n-1) - \beta_{\text{I}} a \frac{j_{n+1}(\beta_{\text{I}} a)}{j_n(\beta_{\text{I}} a)} \right] && \text{(A.17)}\\
d_{41} &= (n-1) - \alpha_{\text{eff}} a \frac{h_{n+1}(\alpha_{\text{eff}} a)}{h_n(\alpha_{\text{eff}} a)} && \text{(A.18)}\\
d_{42} &= \left(n^2 - 1 - \frac{(\beta_{\text{eff}} a)^2}{2} \right) + \beta_{\text{eff}} a \frac{h_{n+1}(\beta_{\text{eff}} a)}{h_n(\beta_{\text{eff}} a)} && \text{(A.19)}\\
d_{43} &= -\frac{\mu_{\text{I}}}{\mu_{\text{eff}}} \left[(n-1) - \alpha_{\text{I}} a \frac{j_{n+1}(\alpha_{\text{I}} a)}{j_n(\alpha_{\text{I}} a)} \right] && \text{(A.20)}\\
d_{44} &= -\frac{\mu_{\text{I}}}{\mu_{\text{eff}}} \left[\left(n^2 - 1 - \frac{(\beta_{\text{I}} a)^2}{2} \right) + \beta_{\text{I}} a \frac{j_{n+1}(\beta_{\text{I}} a)}{j_n(\beta_{\text{I}} a)} \right]. && \text{(A.21)}
\end{aligned}
$$

The original scattering coefficients are recovered from the normalized scattering coefficients by

$$
\begin{aligned}
a_n &= a_n^{\text{N}} \frac{j_n(\alpha_{\text{eff}} a)}{h_n(\alpha_{\text{eff}} a)} && \text{(A.22)}\\
b_n &= b_n^{\text{N}} \frac{j_n(\alpha_{\text{eff}} a)}{h_n(\beta_{\text{eff}} a)}. && \text{(A.23)}
\end{aligned}
$$

Similar relationships hold for the coefficients a'_n and b'_n determining the transmitted wave.

If the incident wave is a transverse wave, the two normalized systems of equations necessary for the calculation of the scattering coefficients are

$$\begin{bmatrix} d_{11} & d_{12} & d_{13} & d_{14} \\ d_{21} & d_{22} & d_{23} & d_{24} \\ d_{31} & d_{32} & d_{33} & d_{34} \\ d_{41} & d_{42} & d_{43} & d_{44} \end{bmatrix} \begin{bmatrix} c_n^{\mathrm{N}} \\ e_n^{\mathrm{N}} \\ c_n'^{\mathrm{N}} \\ e_n'^{\mathrm{N}} \end{bmatrix} = \begin{bmatrix} t_1 \\ t_2 \\ t_3 \\ t_4 \end{bmatrix} \tag{A.24}$$

$$\begin{bmatrix} d_{55} & d_{56} \\ d_{65} & d_{66} \end{bmatrix} \begin{bmatrix} d_n^{\mathrm{N}} \\ d_n'^{\mathrm{N}} \end{bmatrix} = \begin{bmatrix} t_5 \\ t_6 \end{bmatrix}. \tag{A.25}$$

The yet undefined components are found to be

$$t_1 = i^{n+1}\frac{2n+1}{\beta_{\mathrm{eff}}} \tag{A.26}$$

$$t_2 = i^{n+1}\frac{2n+1}{n(n+1)\beta_{\mathrm{eff}}}\left[(n+1) - \beta_{\mathrm{eff}}a\frac{j_{n+1}(\beta_{\mathrm{eff}}a)}{j_n(\beta_{\mathrm{eff}}a)}\right] \tag{A.27}$$

$$t_3 = i^{n+1}\frac{2n+1}{\beta_{\mathrm{eff}}}\left[(n-1) - \beta_{\mathrm{eff}}a\frac{j_{n+1}(\beta_{\mathrm{eff}}a)}{j_n(\beta_{\mathrm{eff}}a)}\right] \tag{A.28}$$

$$t_4 = i^{n+1}\frac{2n+1}{n(n+1)\beta_{\mathrm{eff}}}\left[\left(n^2 - 1 - \frac{(\beta_{\mathrm{eff}}a)^2}{2}\right) + \beta_{\mathrm{eff}}a\frac{j_{n+1}(\beta_{\mathrm{eff}}a)}{j_n(\beta_{\mathrm{eff}}a)}\right] \tag{A.29}$$

$$t_5 = -i^n\frac{2n+1}{n(n+1)} \tag{A.30}$$

$$t_6 = -i^n\frac{2n+1}{n(n+1)}\left[(n-1) - \beta_{\mathrm{eff}}a\frac{j_{n+1}(\beta_{\mathrm{eff}}a)}{j_n(\beta_{\mathrm{eff}}a)}\right] \tag{A.31}$$

for the vectors on the right side and

$$d_{55} = 1 \tag{A.32}$$

$$d_{56} = -1 \tag{A.33}$$

$$d_{65} = (n-1) - \beta_{\mathrm{eff}}a\frac{h_{n+1}(\beta_{\mathrm{eff}}a)}{h_n(\beta_{\mathrm{eff}}a)} \tag{A.34}$$

$$d_{66} = -\frac{\mu_{\mathrm{I}}}{\mu_{\mathrm{eff}}}\left[(n-1) - \beta_{\mathrm{I}}a\frac{j_{n+1}(\beta_{\mathrm{I}}a)}{j_n(\beta_{\mathrm{I}}a)}\right] \tag{A.35}$$

for the remaining matrix elements on the left side. The elements d_{11} to d_{44} are the same as for the incident longitudinal wave. The sought attenuation coefficients are

obtained from the normalized coefficients through

$$c_n = c_n^{\mathrm{N}} \frac{j_n(\beta_{\mathrm{eff}} a)}{h_n(\alpha_{\mathrm{eff}} a)} \tag{A.36}$$

$$d_n = d_n^{\mathrm{N}} \frac{j_n(\beta_{\mathrm{eff}} a)}{h_n(\beta_{\mathrm{eff}} a)} \tag{A.37}$$

$$e_n = e_n^{\mathrm{N}} \frac{j_n(\beta_{\mathrm{eff}} a)}{h_n(\beta_{\mathrm{eff}} a)}. \tag{A.38}$$

Bibliography

[1] M. Abramowitz and I. A. Stegun. *Handbook of Mathematical Functions*. Dover Publications, 1970.

[2] J. D. Achenbach. *Wave Propagation in Elastic Solids*. North-Holland, 1975.

[3] S. Ahmed and R. B. Thompson. Propagation of elastic waves in equiaxed stainless-steel polycrystals with aligned [001] axes. *Journal of the Acoustial Society of America*, 99(4):2086–2096, 1996.

[4] S. Ahmed, R. B. Thompson, and P. D. Panetta. Ultrasonic attenuation as influenced by elongated grains. In D. O. Thompson and D. E. Chimenti, editors, *Review of Progress in Quantitative Nondestructive Evaluation*, volume 22A, pages 109–116. Plenum Press, 2002.

[5] E. Anastassakis and M. Siakavellas. Elastic properties of textured diamond and silicon. *Journal of Applied Physics*, 90:144–152, 2001.

[6] G. Arfken. *Mathematical Equations for Physicists*. Academic Press, 1970.

[7] J. Becker. Investigation of the microstructure of heterogenous materials using ultrasonic waves. Msc, Georgia Institute of Technology, School of Civil and Environmental Eng., 2003.

[8] A. Bedford and D. S. Drumheller. *Introduction to Elastic Wave Propagation*. Wiley, 1994.

[9] A. I. Beltzer and N. Brauner. The dynamic response of random composites by a causal differential method. *Mechanics of Materials*, 6:337–345, 1987.

[10] D. Brill and G. Gaunard. Resonance theory of elastic waves ultrasonically scattered from an elastic sphere. *Journal of the Acoustical Society of America*, 81:1–21, 1987.

[11] S. K. Datta, S. K. Ledbetter, and Y. Shindo. Phase velocity and attenuation of plane elastic waves in a particle-reinforced composite medium. *Wave Motion*, 10:171–182, 1988.

[12] N. G. Einspruch and R. Truell. Scattering of a plane longitudinal wave by a spherical fluid obstacle in an elastic medium. *Journal of the Acoustical Society of America*, 32(2):214–220, 1960.

[13] N. G. Einspruch, E. J. Witterholt, and R. Truell. Scattering of a plane transverse wave by a spherical obstacle in an elastic medium. *Journal of Applied Physics*, 31(5):806–818, 1960.

[14] A. C. Eringen and E. S. Suhubi. *Elastodynamics, Vol.2*. Academic Press, 1975.

[15] J. D. Eshelby. The determination of the elastic field of an ellipsoidal inclusion, and related problems. *Proceedings of the Royal Society*, 36:376–396, 1957.

[16] I. S. Gradshteyn and I. M. Ryzhik. *Table of Integrals, Series, and Products*. Academic Press, 1980.

[17] K. F. Graff. *Wave Motion in Elastic Solids*. Dover publications, 1975.

[18] J. E. Gubernatis. Long-wave approximations for the scattering of elastic waves from flaws with applications to ellipsoidal voids and inclusions. *Journal of Applied Physics*, 50(6):4046–4058, 1979.

[19] J. E. Gubernatis, E. Domany, and J. A. Krumhansl. Formal aspects of the theory of scattering of ultrasound by flaws in elastic materials. *Journal of Applied Physics*, 48:2804–2811, 1977.

[20] J. E. Gubernatis, E. Domany, J.A. Krumhansl, and M. Huberman. The Born approximation in the theory of the scattering of elastic waves by flaws. *Journal of Applied Physics*, 48:2812–2819, 1977.

[21] J. E. Gubernatis and J. A. Krumhansl. Macroscopic engineering properties of polycrystalline materials: Elastic properties. *Journal of Applied Physics*, 46(5):1875–1883, 1975.

[22] J. E. Gubernatis, J. A. Krumhansl, and R. M. Thomson. Interpretation of elastic wave scattering theory for analysis and design of flaw-characterization experiments: The long-wavelength limit. *Journal of Applied Physics*, 50:3338–3345, 1979.

[23] J.O.Owino and L.J.Jacobs. Attenuation measurements in cement-based materials using laser ultrasonics. *Journal of Engineering Mechanics*, 125(6):637–647, 1999.

[24] S. K. Kanaun, V. M. Levin, and F. J. Sabina. Propagation of elastic waves in composites with random set of spherical inclusions (effective medium approach). *Wave Motion*, 40:69–88, 2004.

[25] J.-Y. Kim. Dynamic self-consistent analysis for elastic wave propagation in fiber reinfirced composites. *Journal of the Acoustical Society of America*, 100(4):2002–2010, 1996.

[26] J.-Y. Kim. Attenuation and speed of antiplane shear wave in fiber-reinforced composites with random interfacial cracks. *International Journal of Solids and Structures*, 38:7121–7137, 2001.

[27] J.-Y. Kim. Extinction and propagation of elastic waves in inhomogeneous media. *Mechanics of Materials*, 35:877–884, 2003.

[28] J.-Y. Kim. Extinction of elastic wave energy due to scattering in a viscoelastic medium. *International Journal of Solids and Structures*, 40:4319–4329, 2003.

[29] J.-Y. Kim, J.-G. Ih, and B.-H. Lee. Dispersion of elastic waves in random particulate composites. *Journal of the Acoustical Society of America*, 97(3):1380–1388, 1995.

[30] G. S. Kino. *Acoustic Waves*. Prentice Hall, 1987.

[31] J. W. Littles, J. Qu, and L. J. Jacobs. Experimental and theoretical investigation of scattering from a distribution of cracks. *Ultrasonics*, 33(1):37–43, 1995.

[32] J. B. Molyneux and D. R. Schmitt. Compressional-wave velocities in attenuating media: A laboratory physical model study. *Geophysics*, 65(4):1162–1167, 2000.

[33] P. M. Morse and H. Feshbach. *Methods of Theoretical Physics*. McGraw-Hill, 1953.

[34] T. Mura. *Micromechanics of Defects in Solids*. Kluwer Academic Publishers, 1987.

[35] M. J. P. Musgrave. *Crystal Acoustics*. Holden Day, 1970.

[36] W. H. Press, S. A. Teukolsky, W. T. Vetterling, and B. P. Flannery. *Numerical Recipes in C*. Cambridge Umiversity Press, 1992.

[37] J. H. Rose. Ultrasonic backscatter from microstrucure. In D. O. Thompson and D.E. Chimenti, editors, *Review of Progress in Quantitative Nondestructive Evaluation*, volume 11B, pages 1677–1684. Plenum Press, 1992.

[38] J. L. Rose. *Ultrasonic Waves in Solid Media*. Cambridge University Press, 1999.

[39] F. J. Sabina and J. R. Willis. A simple self consistent analysis of wave propagation in particulate composites. *Wave Motion*, 10:127–142, 1988.

[40] C. M. Sayers. On the propagation of ultrasound in highly concentrated mixtures and suspensions. *Journal of Physics D: Applied Physics*, 13:179–184, 1980.

[41] C. M. Sayers and R. L. Smith. The propagation of ultrasound in porous media. *Ultrasonics*, 20:201–205, 1982.

[42] F. E. Stanke and G. S. Kino. A unified theory for elastic wave propagation in polycrystalline materials. *Journal of the Acoustical Society of America*, 75(3):665–681, 1984.

[43] R. B. Thompson. A generalized model of the effects of microstructure on ultrasonic backscattering and flaw detection. In D. O. Thompson and D.E. Chimenti, editors, *Review of Progress in Quantitative Nondestructive Evaluation*, volume 15B, pages 1471–1478. Plenum Press, 1996.

[44] J. A. Turner. Elastic wave propagation and scattering in heterogeneous, anisotropic media: Textured polycrystalline materials. *Journal of the Acoustical Society of America*, 106(2):541–552, 1999.

[45] J. A. Turner and R. L. Weaver. Radiative transfer and multiple scattering of diffuse ultrasound in polycrystalline media. *Journal of the Acoustical Society of America*, 96(6):3675–3683, 1994.

[46] V. Varatharajulu. Reciprocity relations and forward amplitude theorems for elastic waves. *Journal of Mathematical Physics*, 18(4):537–543, 1977.

[47] P. C. Waterman and R. Truell. Multiple scattering of waves. *Journal of Mathematical Physics*, 2:512–537, 1961.

[48] R. L. Weaver and Y.-H. Pao. Dispersion relations for linear wave propagation in homogeneous and inhomogeneous media. *Journal of Mathematical Physics*, 22:1909–1918, 1981.

[49] L. Yang and J.A.Turner. Scattering of elastic waves in damaged media. *Journal of the Acoustical Society of America*, 113(6):2992–3000, 2003.

[50] R.-B. Yang. A dynamic generalized self-consistent model for wave propagation in particulate composites. *Journal of Applied Mechanics*, 70:575–582, 2003.

[51] H.-Y. Yeh and J.-H. Cheng. NDE of metal damage: Ultrasonics with a damage mechanics model. *International Journal of Solids and Structures*, 40:7285–7298, 2004.

[52] C. F. Ying and R. Truell. Scattering of a plane longitudinal wave by a spherical obstacle in an isotropically elastic solid. *Journal of Applied Physics*, 27(9):1086–1097, 1956.